DETERMINATION OF ROTOR AND STATOR LOSS COEFFICIENTS FOR AN AXIAL TURBINE WITH SUPERSONIC STATOR EXIT CONDITIONS

Edward Franklin Robbins

NAVAL POSTGRADUATE SCHOOL
Monterey, California

THESIS

DETERMINATION OF ROTOR AND STATOR
LOSS COEFFICIENTS FOR AN AXIAL TURBINE
WITH SUPERSONIC STATOR EXIT CONDITIONS

by

Edward Franklin Robbins

June 1976

Thesis Advisor: R.P. Shreeve

REPORT DOCUMENTATION PAGE		READ INSTRUCTIONS BEFORE COMPLETING FORM
1. REPORT NUMBER	2. GOVT ACCESSION NO.	3. RECIPIENT'S CATALOG NUMBER
4. TITLE (and Subtitle) Determination of Rotor and Stator Loss Coefficients for an Axial Turbine with Supersonic Stator Exit Conditions		5. TYPE OF REPORT & PERIOD COVERED Master's Thesis; June 1976 6. PERFORMING ORG. REPORT NUMBER
7. AUTHOR(s) Edward Franklin Robbins		8. CONTRACT OR GRANT NUMBER(s)
9. PERFORMING ORGANIZATION NAME AND ADDRESS Naval Postgraduate School Monterey, California 93940		10. PROGRAM ELEMENT, PROJECT, TASK AREA & WORK UNIT NUMBERS
11. CONTROLLING OFFICE NAME AND ADDRESS Naval Postgraduate School Monterey, California 93940		12. REPORT DATE June 1976 13. NUMBER OF PAGES 138
14. MONITORING AGENCY NAME & ADDRESS(if different from Controlling Office)		15. SECURITY CLASS. (of this report) Unclassified 15a. DECLASSIFICATION/DOWNGRADING SCHEDULE

16. DISTRIBUTION STATEMENT (of this Report)

Approved for public release; distribution unlimited.

17. DISTRIBUTION STATEMENT (of the abstract entered in Block 20, if different from Report)

18. SUPPLEMENTARY NOTES

19. KEY WORDS (Continue on reverse side if necessary and identify by block number)

Axial turbine

20. ABSTRACT (Continue on reverse side if necessary and identify by block number)

The results of seven different tests of a single stage axial turbine with converging-diverging stator nozzle are reported. From measurements in a special test rig, losses occurring in the stator and rotor blade rows were separately calculated and the performance of the stage was also determined. The rotor speeds varied from 9,500 to 18,600 r.p.m. and the pressure ratios varied from 1.75 to 3.25. The Mach numbers at the stator exit

(20. ABSTRACT Continued)

varied from 0.79 to 1.38. The results for this turbine are appraised and a procedure is demonstrated for smoothing loss coefficient data from the turbine rig. Test rig improvements reported include the design and construction of a new flow nozzle and the revision of the data reduction programs to access a Hewlett-Packard Model 9867B Mass Memory unit.

Determination of Rotor and Stator Loss Coefficients for an Axial Turbine With Supersonic Stator Exit Conditions

by

Edward Franklin Robbins
Lieutenant, United States Navy
B.A., St. Joseph College, 1968

Submitted in partial fulfillment of the
requirements for the degree of

MASTER OF SCIENCE IN AERONAUTICAL ENGINEERING

from the

NAVAL POSTGRADUATE SCHOOL
June 1976

ABSTRACT

The results of seven different tests of a single stage axial turbine with converging-diverging stator nozzle are reported. From measurements in a special test rig, losses occurring in the stator and rotor blade rows were separately calculated and the performance of the stage was also determined. The rotor speeds varied from 9,500 to 18,600 r.p.m. and the pressure ratios varied from 1.75 to 3.25. The Mach numbers at the stator exit varied from 0.79 to 1.38. The results for this turbine are appraised and a procedure is demonstrated for smoothing loss coefficient data from the turbine rig. Test rig improvements reported include the design and construction of a new flow nozzle and the revision of the data reduction programs to access a Hewlett-Packard Model 9867B Mass Memory unit.

TABLE OF CONTENTS

LIST OF TABLES

LIST OF FIGURES

ACKNOWLEDGMENT

For the many hours of counseling and assisting me, I want to thank Professor R. P. Shreeve who showed a genuine interest and concern in my research. Without his analytical brilliance and expertise my research would have been impossible.

Secondly, without the technical assistance and advice of Mr. J. E. Hammer the experimental part of my research work would not have been feasible. His countless hours spent in preparing and running the turbine test rig for my experiments are greatly appreciated.

Lastly, I want to thank my wife, Peg, who spent many hours in typing my original manuscript.

I. INTRODUCTION

The transonic turbine test rig in the Turbopropulsion Laboratory at the Naval Postgraduate School was designed to determine the effect of blading design on turbine efficiency and to allow the separate determination of rotor and stator losses.

Preceding the work of Solms [Ref. 5] in which several different turbine geometries were tested, the separation of the losses in the blade rows was not achieved reliably. Progressive improvements in the hardware and instrumentation of the turbine test rig following each series of tests, and finally the simplification of the data reduction program, resulted in the successful separation of losses for particular configurations reported in Reference 5. However, anomalies remained to be explained, and the values obtained for the stator and rotor loss coefficients were scattered.

The questions raised by the preceding test program mainly involved the results of the turbine configuration designated in Reference 5 as Turbine C. Turbine C had converging-diverging stator passages in an axial entry, single impulse stage which was designed to operate at a pressure ratio of 3.71. Results obtained for this geometry discharging to atmosphere did not agree with results obtained at reduced pressure levels when plotted in terms of similarity variables ("referred" quantities). Furthermore, the values

obtained for flow rate were of questionable accuracy since the existing flow nozzle was too large. Also the correction for a labyrinth leak rate became a more significant fraction of the turbine flow rate.

The goal of the present work was to determine the blade row and stage performances of Turbine C, while resolving the anomalies reported in Reference 5. This would allow the use of the test rig to investigate effects of geometrical changes (stator-rotor separation and tip clearance for example) on the losses. The first step was to design and construct a new flow nozzle for the range of flow rates required by Turbine C. The flow nozzle was carefully calibrated against three different nozzles operating choked. The leakage rate for the labyrinth seal was also measured and a semi-analytic representation of the leakage rate as a function of pressure ratio was obtained which should apply at different temperatures. These developments are reported in Appendix A. The existing data reduction program [Ref. 5] was revised to access a Hewlett-Packard Model 9867B Mass Memory unit. The revised program is described fully in Appendix B.

In the results of the test program given here in Section III, the effect of pressure level reported in Reference 5 was not observed. The scatter in the loss coefficient however was not removed by the improvements in the accuracy of the measurements. In the discussion in Section IV, a method for smoothing the loss coefficient data is demonstrated

which will then allow a useful study of the effect of axial and tip clearances to be carried out.

II. TURBINE TEST RIG INSTALLATION

A. DESCRIPTION

The test installation consists of three major components: an Allis Chalmers twelve stage axial flow compressor, an exhauster assembly, and the turbine test rig (TTR) itself.

The compressor is the source of driving air for the TTR and for the exhauster assembly. Fig. A-1 shows the piping arrangement. Turbine air passes through the first settling tank into an eight-inch pipe containing a flow nozzle, into the second settling tank and into the turbine.

Fig. 1 shows the plenum, the floating stator assembly, the rotor, and the dynamometer [Ref. 5]. Pressure ratios of 6:1 can be achieved when the system is hooded. The hood was needed to achieve near design pressure ratios in the tests reported here. Fig. 2 shows the turbine blading arrangement of the stator and rotor. Ref. 8 contains detailed description of the test rig hardware.

The floating stator assembly depicted in Fig. 3 permits measurements of the stator torque while axial and rotational movements are detected by calibrated force transducers that are heat insensitive. These measurements allow the determination of the axial and tangential velocity components at the stator exit [Appendix A, Ref. 5].

In this report one configuration designated Turbine C was tested, the geometry of which is shown in Fig. 4; Table

1 describes the geometry quantitatively. The stator blade profile is shown in Fig. 5. The blades generate a converging-diverging nozzle shape. Pressure measurements are taken at the locations shown in Fig. 5. The pressures necessary to the analysis of stator forces (Appendix B) are taken at the locations shown in Fig. 6

B. TEST MEASUREMENTS AND ACCURACY

MASS FLOW RATES: Appendix A gives a detailed analysis of the turbine flow rate and the labyrinth seal leak rate, and the results of calibration measurements. The results for the discharge coefficient are given in Fig. A-6. Fig. A-10 shows the Kinetic Energy Factor (Appendix A) obtained in labyrinth seal leak rate calibration and its respective polynomial. The equations used in calculating the flow rate from measurements are summarized in Table A-1 and Table A-2.

FORCES, TORQUES, TEMPERATURES AND PRESSURE: References 8 and 9 give calibration procedures for the TTR. Identical procedures were employed here. Table II of Ref. 5 gives the expected accuracies of these measurements.

C. TESTING AND DATA REDUCTION

The TTR data collection system is described in Ref. 11. Appendix D in Ref. 5 gives a detailed explanation of the turbine test procedures. The data reduction program developed in Ref. 5 was revised to use the mass memory system. The revised program is described in Appendix B.

Seven tests were conducted of Turbine C at pressure ratios from 1.75 to 3.25. The parameters and conditions of the tests are summarized in Table II.

III. RESULTS

A. INTRODUCTION

The reduced data from seven tests of Turbine C are listed in Table V to XI. Table IV gives a listing of the symbols and meanings of the Table headings used in Table V to XI. Plots of the reduced data are presented in Figures 7 to 16. Table III gives an explanation of symbols used in these figures.

Tests 1 and 2 were conducted with the hood off. Tests 3, 4, 5, 6 and 7 were made with the hood installed. Tests 5 and 6 were repeats of tests 3 and 4 respectively. The results are discussed in the following paragraphs.

B. TORQUE

Fig. 7a and 7b give the results of the referred torque versus referred speeds at a constant pressure ratio. A nearly linear dependency exists for all seven runs with consistency in performance for the 1.75 and 2.25 hooded and unhooded pressure ratios.

The results from the unhooded tests (Fig. 7a) agree with the results of the hooded tests (Fig. 7b), at the same pressure ratio, to within 1 percent.

C. EFFICIENCY (TOTAL-TO-STATIC)

Figures 8a and 8b give the results of the total-to-static efficiency versus referred R.P.M. Figures 9a and 9b show plots of efficiency versus isentropic head. The maximum

efficiency occurred at similar values of the isentropic head for all pressure ratios. Ref. 17 relates efficiency to isentropic head. The peak efficiency was achieved at an isentropic head coefficient between 4.0 and 4.5 for both the hooded and unhooded tests.

The efficiency is seen to increase as the pressure ratio is increased, approaching 80 percent at the pressure ratio of 3.25. The efficiency would be expected to increase to the design pressure ratio of 3.71, at which the stator nozzles should be just correctly expanded.

D. THEORETICAL DEGREE OF REACTION

Figures 10a and 10b give the results of theoretical degree of reaction versus isentropic head coefficient at different pressure ratios. Ref. 5 and Ref. 17 give the equation for the theoretical degree of reaction. For all runs the theoretical degree of reaction was negative at lower speeds. For a negative value, P_2/P_{to} must be greater than P_1/P_{to}. The values become positive only at high r.p.m. in both the hooded and unhooded configurations, passing through the design value of zero at a value of the isentropic head coefficient corresponding to the maximum in efficiency. Thus, negative values of the theoretical degree of reaction occur at speeds lower than the design speed at a given pressure ratio. Typically, there is seen to be also a loss of three to five percent in efficiency from the maximum value as the isentropic head coefficient is increased 100 percent above the design value.

Results from hooded and unhooded tests are seen to agree with the exception of Run 3 in Figure 10b for which the values are low. Lack of agreement for the data of this test was found in all but the overall stage performance measurements.

E. EFFECTIVE DEGREE OF REACTION

Figures 11a and 11b give the results for the effective degree of reaction versus isentropic head coefficient. At all pressure ratios, hooded and unhooded, the effective degree of reaction was negative at lower speeds. Ref. 17 states that the effective degree of reaction is a means for judging whether the flow is being accelerated or decelerated in the rotating cascade. The negative degree of reaction in Fig. 11a and 11b show that the flow is decelerated at lower r.p.m. and becomes accelerated as r.p.m. is increased (Isentropic head is decreased). In no case should the design value of the effective degree of reaction be less than zero. As stated above, operation at speeds less than design speed results in a loss in stage efficiency, partially due to the undesirable deceleration in the rotor.

The results for Run 4 (at a pressure ratio of 3.25) in Figure 11b reflect the marked improvement in efficiency at pressure ratios approaching design.

F. STATOR LOSS COEFFICIENT

The results for the stator loss coefficient are shown in Fig. 12a and Fig. 12b. While there is some scatter in

the data, the results from hooded and unhooded tests are seen to be in reasonable agreement. There is a slight increase in the stator loss as speed is increased at any pressure ratio. The stator loss for the highest pressure ratio (3.25) is significantly lower (13-17 percent) than for the lower pressure ratios (18-25 percent). This reflects the poor performance of a converging-diverging nozzle at pressure ratios less than design.

G. ROTOR LOSS COEFFICIENT

The results for rotor loss coefficient are shown in Figure 13a and Figure 13b. For completeness, the results of Run 3 have been included where the rotor loss coefficients were evaluated to be positive. Negative loss coefficients were obtained at higher speeds in Run 3, indicating an error in at least one element of the primary data.

The rotor loss coefficient is the performance parameter most sensitive to small errors (and possibly unsteadiness) in the measurements. The sensitivity arises because it involves most of the parameters (see Ref. 5) previously calculated in the form of a ratio of small differences. In view of this, if the results of Run 3 in Fig. 13b are excluded from consideration, the rotor loss coefficient for the tests are reasonably consistent. The results for hooded and unhooded tests agree to within 20 percent at corresponding pressure ratios. There is also a definite decrease in the rotor loss coefficient as pressure ratio is increased toward

the design value, and a consistent decrease as the speed is increased at a fixed pressure ratio. The simultaneous reduction observed in the rotor and stator loss coefficients at higher pressure ratios is consistent with the increase measured in the stage efficiency (Fig. 8 and Fig. 9).

H. FLOW ANGLES

An example of the variation in the flow angles at the stator and rotor exits as a function of the isentropic head coefficient is shown in Fig. 14. As was found in all cases tested in Ref. 5, the variations in stator exit flow angle and rotor exit relative flow angle are very small. Also, the total variation of the relative flow angle into the rotor is only about 6 degrees for a 50 percent change in r.p.m. The results in Fig. 14 are qualitatively representative of the results for each of the seven tests. The exact variations in the measured angles can be seen in Tables V to XI.

The stator exit flow angle is shown in Fig. 15a and Fig. 15b as a function of isentropic head coefficient for the seven tests. It can be seen that the measurements are in the range of 75 to 77 degrees, with the lower value occurring at the highest pressure ratio (3.25). It can be seen in Fig. 5 that the suction surface of the stator blade is designed to exit at 75 degrees, and the pressure surface at a smaller angle. Thus the measured stator exit angle appears to be slightly larger than would be expected; however,

the measured values when the nozzle passages are nearly correctly expanded approach the geometrical angle.

The large values of stator exit flow angle at lower pressure ratios, and the higher values of stator loss coefficient are probably the results of the presence of flow separation. The effect of flow separation would be reflected in two ways. Firstly, the flow angle of the separated flow could depart significantly from the trailing-edge angle. Secondly, the existence of a region of separated flow could seriously affect the averaging process which is implicit in the data reduction.

I. FLOW RATE

The referred flow rate is shown as a function of the isentropic head coefficient for the seven tests in Fig. 16a and Fig. 16b. The referred flow rate was constant at 1.02 lbs/sec to within the accuracy of the measurements for all speeds and all pressure ratios when operating hooded (Fig. 16b). During unhooded operation (Fig. 16a), the results gave a constant value of 1.01 lbs/sec.

IV. DISCUSSION

A. RESOLUTION OF PREVIOUS ANOMALIES

In the results presented above, the difference in the turbine performance operating hooded compared with unhooded, is seen to be small. This is in contrast to the results presented in Reference 5. Three factors contributed to the resolution of this anomaly; the accurate measurement of the turbine flow rate, installation of temperature insensitive load cells within the hood to measure stator loads, and corrections that were made to the data reduction program. There remains to be explained a difference of 1% in the flow rate between hooded and unhooded operation. More data are needed from unhooded tests to confirm that this difference is repeatable. Because of the sensitivity of the performance parameters to the flow rate, the residual disagreement between hooded and unhooded results might be resolved if the difference in flow rates were explained.

B. FLOW RATE

The use of a choked nozzle to calibrate a large flow nozzle was successful (Appendix A). With the blockage factor correction applied, the results for different sizes of the choked nozzle agreed in the range for which the flow rates overlapped.

The labyrinth leak rate calibration measurements were well represented by the analysis given in Reference 7. The

value obtained for the Kinetic Energy factor was higher than values given in Reference 5; however, the geometry of the turbine testing labyrinth was not known exactly. There was some eccentricity in the alignment of the stator section within the gland, so that the clearance was nonuniform to an unknown degree.

The flow rate through the turbine, when expressed as a referred quantity, was measured to be a constant over the range of pressure ratios tested. (However, there was scatter in the measurements that resulted from unsteadiness in the measurements of nozzle pressure drop.) Since the stator was choked, the constant value was expected. The value of the constant was consistent with the flow rate computed for the stator using a calculated value for the stator throat area. A value of the blockage factor within 1% of unity was required to be applied to the geometrical stator area to obtain total agreement. Since the exact area of the throat where choking occurs in the stator is not known to this accuracy, it is concluded that flow nozzle and stator throat measurements of the flow rate are in agreement.

C. LOSS COEFFICIENTS

The scatter observed in the results for the loss coefficients makes a comparison between predicted and measured values inconclusive. There are trends in the data which are discernible, the rotor losses are consistently higher than the stator losses, for example. However, the scatter does

not allow the effect of parameter changes on the separate loss coefficients to be determined. The scatter is the result of the extreme sensitivity of the loss coefficient to the separate measurements on which they depend. For example, the stator loss coefficient (ζ_s) is given by

$$\zeta_s = 1 - \frac{X_1^2}{1 - P_1^{\frac{\gamma-1}{\gamma}}} \qquad (1)$$

where X_1 is the non-dimensional velocity and p_1 is the calculated pressure ratio (p_1/P_{to}) at station 1. Differentiation of Eq. (1) gives, if X_1 is constant,

$$\frac{d\zeta_s}{\zeta_s} = -\left[\left(\frac{1-\zeta_s}{\zeta_s}\right)\left(\frac{\gamma-1}{\gamma}\right)\left(\frac{P_1^{\frac{\gamma-1}{\gamma}}}{1 - P_1^{\frac{\gamma-1}{\gamma}}}\right)\right] \frac{dP_1}{P_1} \qquad (2)$$

Taking the sonic condition of $P_1 = 0.532$, with $\gamma = 1.4$ and $\zeta_s = 0.2$, the quantity in brackets has the value 5.78. Thus a 1% error in calculating P_1 produces -6% error in the stator loss coefficient. Since P_1 is derived (as is X_1) from measurements scanned over a period of more than a minute, with some variation in operating point (as well as an observable fluctuation in the flow nozzle pressure drop) occurring during the data scan, the scatter in the loss coefficient data is understandable.

Before the loss coefficient can be used as a measure of performance, a method of smoothing the data while retaining accuracy is needed. Two attempts were made here. First, an attempt was made to smooth the calculated values of the interstage pressure (p_1), by comparing p_1 to the pressures measured at the hub and tip. Figure 17 shows the variation p_1 and the measured pressure with isentropic head coefficient for one particular test. Clearly, the calculated average pressure at station 1 must be smoothly behaved if the hub and the tip pressures are smoothly behaved. An attempt to derive a smoothing function for the interstage pressure is shown in Fig. 18, where the data from several tests at the same pressure ratio are plotted in a dimensionless form. The figure clearly shows the degree of scatter in the values of P_1. On the basis of these data above, however, the use of a single polynomial for the quantity $(P_1-P_{hub})/(P_{tip}-P_{hub})$ as a function of isentropic head coefficient cannot be justified. When a polynomial was derived from the data of a single test, and the loss coefficients for the stator and rotor were recomputed, the results shown in Fig. (19a) and (19b) were obtained.

The second attempt to smooth the loss coefficient data involved effectively the elimination of scatter in the input data from which the interstage pressure and velocity were calculated. The referred flow rate was determined to be constant when the stator was choked. By setting the referred flow rate equal to the constant value (1.02 or 1.01,

hooded and unhooded, respectively) and continuing the data reduction as before, the results shown in Fig. 20a and 20b for the loss coefficient were obtained. A considerable reduction in scatter is evident, with the major benefit in the rotor loss coefficient. Further data must be examined to fully appraise the benefit of this smoothing technique.

A third technique, so far not attempted, is to calculate P_1 in the data reduction before calculating the axial velocity component at station 1. The values of P_1 could be smoothed using a polynomial curve fit and the smoothed values of P_1 used to calculate the velocity. An application of all three techniques should produce loss coefficient distributions which are smooth and yet accurate.

V. CONCLUSIONS AND RECOMMENDATIONS

The following conclusions are made for turbine configuration C.

1. The loss coefficients are extremely sensitive to input data, especially the rotor loss coefficient. Repeatability in calculating the loss coefficient directly from measurements was poor.

2. Methods were demonstrated to smooth the loss coefficient data without sacrificing, and possibly improving, the accuracy.

3. For all pressure ratios there was a velocity deceleration through the rotor and a pressure rise across the rotor at lower r.p.m., indicating perhaps a shock wave at or in the rotor.

The following recommendations are made:

1. Apply the three data smoothing techniques described above to all data from Turbine C in sequence: input constant referred flow rate, calculate interstage pressure and smooth using measured hub and tip pressures, then calculate interstage velocity.

2. Determine a more accurate input for K_1, the ratio of the momentum average velocity to the mass-average velocity and examine the effect on the calculated stator exit flow angle.

3. Program the quadratic curves for the theoretical loss coefficient in references 16 and 18 in order to reduce the input error.

Finally, it is concluded that following the recommendations listed here, the effect of parameter variations on the blade row losses could be examined satisfactorily using the turbine test rig.

TABLE I

TURBINE GEOMETRY

	TURBINE	STATOR		ROTOR	
	C	1		1	
	DESCRIPTION	A^* (in^2)	NUMBER OF BLADES	R_M (IN)	h (in.)
STATOR 1	CONVERGING DIVERGING NOZZLES	2.9058	31	4.184	0.5775
ROTOR 1	CIRCULAR ARC	7.119	60	R_{m1}=4.193 R_{m2}=4.250	h_1=0.732 h_2=0.8475

TABLE II TEST PARAMETERS FOR TURBINE C

RUN#	PRESSURE RATIO P_{to}/P_2	AXIAL CLEARANCE (INS)	TIP CLEARANCE (INS)
1.	1.76	0.220	0.010
2.	2.24	0.220	0.010
3.	2.25	0.220	0.010
4.	3.25	0.220	0.010
5.	1.75	0.220	0.010
6.	2.25	0.220	0.010
7.	2.25	0.220	0.010

NOTE:

1. Run 3,4,5,6,7, were conducted with hood installed.
2. Table I gives geometry of Turbine.

TABLE III EXPLANATION OF SYMBOLS IN FIGURES 7 TO 16

SYMBOL	MEANING
P.R.	Pressure Ratio = P_{to}/P_2
T-S	Total-to-Static (Efficiency)

TABLE IV

DEFINITION OF COLUMN HEADINGS IN TABLES V TO XI

SYMBOL	DEFINITION
VI	VELOCITY AT STATOR EXIT PLANE (FT/SEC)
V2	VELOCITY AT ROTOR EXIT PLANE (FT/SEC)
VA1	AXIAL VELOCITY AT STATOR EXIT PLANE (FT/SEC)
VA2	AXIAL VELOCITY AT ROTOR EXIT PLANE (FT/SEC)
VUI	TANGENTIAL VELOCITY AT STATOR EXIT PLANE (FT/SEC)
VU2	TANGENTIAL VELOCITY AT ROTOR EXIT PLANE (FT/SEC)
MI	MACH NUMBER AT STATOR EXIT PLANE
MAI	AXIAL MACH NUMBER AT STATOR EXIT PLANE
M2	MACH NUMBER AT ROTOR EXIT PLANE
MA2	AXIAL MACH NUMBER AT ROTOR EXIT PLANE
A1	FLOW ANGLE AT STATOR EXIT PLANE (DEGREES)
A2	FLOW ANGLE AT THE ROTOR EXIT PLANE (DEGREES)
BI	RELATIVE FLOW ANGLE AT ROTOR INLET PLANE (DEGREES)
B2	RELATIVE FLOW ANGLE AT ROTOR EXIT PLANE (DEGREES)
ZS	STATOR LOSS COEFFICIENT
ZSTH	THEORETICAL STATOR LOSS COEFFICIENT
ZR	ROTOR LOSS COEFFICIENT
ZRTH	THEORETICAL ROTOR LOSS COEFFICIENT
ZR*	ROTOR CARRY OVER LOSS COEFFICIENT
ZI	ROTOR INCIDENCE LOSS COEFFICIENT
P.R.	PRESSURE RATIO P_{to}/P_2
K-IS	ISENTROPIC HEAD COEFFICIENT
NREF	REFERRED RPM (R.P.M.)

WREF	REFERRED FLOW RATE (LBM/SEC)
ETA	TOTAL TO STATIC EFFICIENCY
HPREF	REFERRED HORSEPOWER (H.P.)
RTH	THEORETICAL DEGREE OF REACTION
REFF	EFFECTIVE DEGREE OF REACTION
P1	PRESSURE RATIOS CORRESPONDING TO TAP LOCATIONS
P2	IN FIGURE 5. PRESSURES ARE REFERRED TO STATOR
P3	INLET TOTAL PRESSURE
P4	
P5	
P6	
P7	
P8	
P9	
KBLOCK	STATOR BOCKKAGE FACTOR
STPR	PRESSURE RATIO ACROSS THE STATOR P_{to}/P_1
RPM	ROTOR SPEED (R.P.M.)

RL: 1 TABLE V TURBINE

VELOCITY TRIANGLE

PT.	V1	V2	VA1	VA2	VU1	U2
1	920.8	140.3	213.9	140.2	895.9	-5.7
2	921.7	139.3	210.6	139.7	897.3	8.8
3	921.3	141.3	207.4	137.9	897.7	30.9
4	920.5	150.6	207.1	138.4	895.1	59.8
5	905.7	163.9	204.8	138.0	882.3	88.6
6	897.3	181.8	204.0	138.5	873.6	117.4
7	888.3	205.2	200.8	137.7	865.8	152.2
8	876.9	236.5	200.1	137.9	853.8	192.2

PT.	MACH NUMBERS M1	MA1	M2	MA2	ANLGES A1	A2	B1	B2
1	0.842	0.195	0.130	0.128	75.6	-2.3	67.4	-70.5
2	0.842	0.192	0.130	0.128	76.8	3.3	67.3	-70.5
3	0.841	0.189	0.121	0.118	77.0	12.6	66.8	-70.5
4	0.839	0.189	0.129	0.118	76.8	23.4	65.8	-70.1
5	0.824	0.186	0.140	0.118	76.3	32.7	64.1	-70.0
6	0.816	0.186	0.156	0.119	76.3	40.4	62.4	-69.6
7	0.807	0.182	0.176	0.116	76.9	47.9	60.5	-69.4
8	0.795	0.181	0.203	0.118	76.8	54.3	56.8	-69.3

PT.	LOSSES ZS	ZSTH	ZR	ZRTH	ZR*	II
1	0.2280	0.1071	0.2764	0.4220	0.2786	9.0E-03
2	0.2133	0.1071	0.2933	0.4213	0.3946	8.4E-02
3	0.2030	0.1071	0.2784	0.4066	0.2660	7.1E-03
4	0.2179	0.1071	0.2570	0.3982	0.2607	3.4E-03
5	0.2097	0.1071	0.2506	0.7837	0.2524	1.4E-03
6	0.2138	0.1071	0.2495	0.3691	0.2471	6.1E-05
7	0.2074	0.1071	0.2578	0.6592	0.2469	7.0E-04
8	0.2144	0.1071	0.2168	0.3336	0.1905	6.1E-02

RUN 1 TABLE V TURBINE C

PT.	P.R.	K-IS	NREF	WREF	ETA	HPREF	ETA	ETA
1	1.76	6.75	10027.7	1.016	0.675	18.11	-0.07	-0.13
2	1.76	6.30	10328.1	1.017	0.684	18.31	-0.05	-0.7[illegible]
3	1.76	5.82	10802.7	1.002	0.698	18.47	-0.04	-0.[illegible]
4	1.76	5.27	11350.6	1.006	0.697	18.52	-0.03	-0.52
5	1.76	4.71	12005.0	1.005	0.709	18.01	-0.01	-0.-0
6	1.77	4.29	12606.1	1.007	0.705	18.84	0.01	-0.23
7	1.77	3.81	13350.7	1.005	0.707	18.77	0.03	-0.[illegible]
8	1.77	3.32	14302.6	1.000	0.702	18.69	0.05	0.05

NOZZLE PRESSURE RATIOS

PT.	P1	P2	P3	P4	P5	P6	P7
1	0.712	0.440	0.391	0.530	0.563	0.869	0.673
2	0.712	0.440	0.391	0.533	0.585	0.888	0.67[illegible]
3	0.712	0.440	0.391	0.543	0.589	0.907	0.5[illegible]
4	0.711	0.440	0.392	0.548	0.594	0.886	0.673
5	0.712	0.440	0.393	0.556	0.595	0.858	0.67[illegible]
6	0.712	0.440	0.393	0.561	0.602	0.889	0.67[illegible]
7	0.712	0.440	0.393	0.573	0.609	0.888	0.67[illegible]
8	0.712	0.440	0.394	0.584	0.616	0.887	0.673

PT.	KBLOCK	STPR	RPM	P8	P9
1	0.9979	1.8045	10500.0	0.527	0.508
2	0.9943	1.8307	10820.0	0.527	0.510
3	0.9841	1.8113	11330.0	0.536	0.515
4	0.9878	1.7933	11900.2	0.535	0.521
5	0.9871	1.7729	12590.0	0.537	0.527
6	0.9891	1.7581	13220.0	0.536	0.531
7	0.9867	1.7299	14000.0	0.536	0.541
8	0.9903	1.7113	15000.0	0.526	0.551

RUN 2 TABLE VI TURBINE C

VELOCITY TRIANGLE

PT.	V1	V2	VA1	VA2	VU1	VU2
1	1098.9	167.6	253.8	167.4	1068.7	7
2	1094.4	168.8	256.5	167.8	1064.1	3
3	1091.0	171.6	253.1	167.6	1061.3	36.
4	1088.2	177.6	250.7	166.9	1059.0	61.
5	1080.5	187.7	246.9	166.7	1052.0	96.
6	1071.6	199.6	244.3	166.3	1043.4	115.
7	1058.4	216.0	242.6	166.7	1030.2	140.
8	1034.9	243.3	239.3	166.5	1006.9	177.

MACH NUMBERS ANGLES

PT.	M1	MA1	M2	MA2	A1	A2	B1	B2
1	1.031	0.240	0.143	0.143	76.5	2.7	66.6	-77.
2	1.025	0.240	0.144	0.143	76.5	6.3	66.6	-73.
3	1.022	0.237	0.147	0.143	76.6	12.4	65.5	-73.
4	1.019	0.235	0.152	0.143	76.7	20.2	65.1	-70.
5	1.010	0.231	0.160	0.142	76.3	27.3	64.4	-70.
6	0.999	0.228	0.171	0.142	76.3	33.7	63.3	-69.
7	0.985	0.226	0.186	0.141	76.8	40.1	61.3	-67.
8	0.959	0.222	0.208	0.142	76.6	46.8	58.4	-65.

LOSSES

PT.	ZS	ZSTH	ZR	ZRTH	ZR*	ZI
1	0.1936	0.1071	0.2372	0.4207	0.2472	5.4E-03
2	0.1930	0.1071	0.2051	0.4787	0.2164	4.8E-03
3	0.1920	0.1071	0.2167	0.4709	0.2257	3.6E-03
4	0.1889	0.1071	0.2289	0.4561	0.2369	2.9E-07
5	0.1844	0.1071	0.2544	0.4548	0.2568	1.0E-03
6	0.1857	0.1071	0.2434	0.4962	0.2407	5.2E-03
7	0.1954	0.1071	0.2113	0.4123	0.2010	1.3E-03
8	0.2070	0.1071	0.1950	0.3833	0.1672	3.9E-07

RUN 2 TABLE VI TURBINE C

PT.	P.R.	K-IS	NREF	WREF	ETA	HPREF	ETN	UEN
1	3.24	6.01	12444.5	1.008	0.716	26.12	-0.06	-0.05
2	2.33	5.67	12804.5	1.014	0.727	26.64	-0.05	-0.55
3	2.24	5.40	13156.1	1.010	0.728	26.70	-0.01	-0.50
4	2.24	5.09	13525.9	1.008	0.730	26.66	-0.03	-0.48
5	2.23	4.77	13980.4	1.008	0.731	26.67	-0.01	-0.41
6	2.23	4.41	14516.5	1.008	0.734	26.71	0.00	-0.30
7	2.24	4.01	15267.5	1.007	0.732	26.77	0.02	-0.14
8	2.28	3.59	16077.4	1.012	0.723	26.37	0.04	0.04

NOZZLE PRESSURE RATIOS

PT.	P1	P2	P3	P4	P5	P6	P7
1	0.712	0.442	0.284	0.380	0.495	0.888	0.673
2	0.713	0.442	0.285	0.384	0.499	0.889	0.673
3	0.712	0.442	0.284	0.386	0.498	0.888	0.672
4	0.713	0.442	0.285	0.393	0.494	0.889	0.672
5	0.712	0.442	0.285	0.402	0.488	0.889	0.674
6	0.713	0.443	0.285	0.412	0.502	0.890	0.675
7	0.712	0.442	0.285	0.421	0.508	0.889	0.674
8	0.712	0.442	0.287	0.435	0.515	0.888	0.675

PT.	KBLOCK	STPR	RPM	P8	P9
1	0.9067	2.3513	13050.0	0.517	0.362
2	0.9057	2.3211	13460.0	0.519	0.370
3	0.9017	2.3148	13830.0	0.517	0.374
4	0.9036	2.2948	14220.0	0.519	0.384
5	0.9058	2.2627	14700.0	0.518	0.396
6	0.9088	2.2205	15270.0	0.519	0.406
7	0.9091	2.1957	16060.0	0.517	0.417
8	0.9133	2.1389	16910.0	0.517	0.433

RUN 3 TABLE VII TURBINE C

VELOCITY TRIANGLE

PT.	V1	V2	VA1	VA2	VU1	VU2
1	1136.9	175.5	273.0	168.5	1103.7	-49.2
2	1133.7	171.8	273.9	168.4	1100.1	-33.7
3	1117.6	170.0	273.8	169.2	1083.6	-15.9
4	1105.7	169.0	268.9	166.8	1073.5	6.8
5	1075.7	177.3	262.8	165.0	1043.1	55.4
6	1069.6	192.4	257.3	167.4	1038.2	84.8
7	1052.6	211.0	256.0	167.0	1021.0	123.9
8	1032.1	244.0	248.7	166.7	1001.7	173.1

MACH NUMBERS

PT.	M1	MA1	M2	MA2
1	1.060	0.259	0.151	0.144
2	1.057	0.260	0.147	0.144
3	1.058	0.259	0.146	0.145
4	1.045	0.254	0.145	0.143
5	1.007	0.246	0.152	0.145
6	1.001	0.241	0.165	0.143
7	0.982	0.239	0.181	0.142
8	0.960	0.231	0.209	0.143

ANGLES

PT.	A1	A2	B1	B2
1	76.1	-18.3	67.3	-72.1
2	76.0	-11.3	67.7	-73.5
3	75.8	-5.3	66.2	-73.4
4	75.9	2.3	66.5	-73.7
5	75.9	10.1	66.0	-73.3
6	76.1	29.5	61.2	-73.5
7	75.9	37.7	59.4	-73.4
8	76.1	46.9	56.4	-73.2

LOSSES

PT.	ZS	ZSTH	ZR	ZRTH	ZR*	ZI
1	0.1984	0.1071	0.1718	0.5585	0.1940	1.0E-02
2	0.2047	0.1071	0.1100	0.3517	0.1422	8.4E-06
3	0.2180	0.1071	0.0452	0.3146	0.0863	5.4E-03
4	0.2165	0.1071	0.0449	0.5066	0.0837	3.0E-03
5	0.2347	0.1071	-0.0371	0.4922	0.0001	3.0E-04
6	0.2293	0.1071	-0.0372	0.4536	-0.0064	7.6E-06
7	0.2456	0.1071	-0.1580	0.4207	-0.1361	2.1E-02
8	0.2439	0.1071	-0.0768	0.4604	-0.0910	9.5E-03

RUN 3 TABLE VII TURBINE C

PT.	P.R.	K-IS	NREF	WREF	ETA	HPREF	PTH	HOLE
1	2.25	7.35	11300.6	1.010	0.704	25.96	-0.14	-1.40
2	2.26	6.89	11683.4	1.010	0.714	26.38	-0.11	-0.91
3	2.26	6.43	12092.8	1.010	0.717	26.62	-0.13	-0.77
4	2.25	5.90	12618.1	1.010	0.726	26.94	-0.10	-0.64
5	2.25	4.96	13766.7	1.010	0.731	27.14	-0.06	-0.50
6	2.25	4.42	14559.2	1.010	0.738	27.24	-0.04	-0.63
7	2.25	3.98	15367.3	1.010	0.737	27.17	-0.07	-0.91
8	2.25	3.49	16392.6	1.010	0.727	26.77	0.00	0.10

NOZZLE PRESSURE RATIOS

PT.	P1	P2	P3	P4	P5	P6	P7
1	0.713	0.442	0.262	0.351	0.474	0.889	0.674
2	0.713	0.442	0.263	0.354	0.477	0.888	0.677
3	0.713	0.442	0.263	0.359	0.480	0.888	0.677
4	0.712	0.442	0.263	0.364	0.485	0.889	0.678
5	0.713	0.442	0.262	0.381	0.495	0.889	0.679
6	0.713	0.443	0.262	0.394	0.501	0.889	0.677
7	0.713	0.442	0.265	0.407	0.507	0.888	0.677
8	0.713	0.441	0.273	0.423	0.516	0.888	0.677

PT.	KBLOCK	STPR	RPM	P8	P9
1	0.9921	2.5577	11300.0	0.519	0.313
2	0.9917	2.5639	12238.0	0.518	0.320
3	0.9971	2.5322	12668.0	0.518	0.330
4	0.9973	2.4749	13218.0	0.519	0.341
5	0.9978	2.3885	14450.0	0.518	0.375
6	0.9917	2.3416	15270.0	0.519	0.396
7	0.9914	2.2201	16118.0	0.516	0.413
8	0.9923	2.2337	17190.0	0.510	0.430

RUN 4 TABLE VIII TURBINE C

VELOCITY TRIANGLE

PT.	V1	V2	VA1	VA2	VU1	VU2
1	1384.6	279.5	361.5	227.4	1336.6	-108.1
2	1364.6	273.5	357.4	227.0	1317.0	-152.1
3	1366.8	263.3	361.4	225.8	1318.2	-138.5
4	1359.9	258.4	356.0	233.3	1312.5	-124.1
5	1358.0	248.2	351.4	224.1	1311.7	-106.7
6	1285.7	236.3	323.9	222.4	1235.5	-81.8
7	1319.8	230.8	336.3	220.1	1276.2	-55.6
8	1274.4	228.7	336.6	237.7	1229.2	-21.1
9	1272.9	224.4	323.5	223.9	1231.1	15.1
10	1240.0	230.4	303.6	220.3	1209.2	97.1

MACH NUMBERS AND ANGLES

PT.	M1	MA1	M2	MA2	A1	A2	B1	B2
1	1.382	0.361	0.289	0.194	74.9	-35.2	67.1	-78.1
2	1.354	0.355	0.283	0.194	74.8	-33.8	66.7	-79.5
3	1.356	0.359	0.275	0.193	74.7	-31.6	66.2	-76.3
4	1.346	0.352	0.270	0.191	74.8	-30.0	66.1	-76.1
5	1.344	0.348	0.211	0.191	75.3	-25.5	68.9	-73.7
6	1.301	0.318	0.202	0.189	75.9	-28.2	66.4	-79.7
7	1.292	0.329	0.196	0.190	75.2	-14.0	64.1	-74.1
8	1.234	0.326	0.195	0.194	74.7	-5.4	61.1	-74.1
9	1.232	0.313	0.191	0.190	75.3	0.9	61.2	-78.1
10	1.201	0.297	0.196	0.190	75.7	14.4	59.3	-79.6

LOSSES

PT.	ZS	ZSTH	ZR	ZRTH	ZR+	ZI
1	0.1240	0.1071	0.2763	0.5453	0.2935	7.9E-03
2	0.1339	0.1071	0.2759	0.5518	0.2885	6.6E-03
3	0.1418	0.1071	0.2356	0.5441	0.2553	5.3E-03
4	0.1422	0.1071	0.2156	0.5299	0.2351	5.1E-03
5	0.1379	0.1071	0.2324	0.5417	0.2403	4.6E-03
6	0.1166	0.1071	0.2908	0.5435	0.2897	5.8E-03
7	0.1493	0.1071	0.1766	0.5340	0.1867	1.0E-03
8	0.1332	0.1071	0.1130	0.7242	0.1140	2.4E-03
9	0.1707	0.1071	0.1043	0.4992	0.0909	1.0E-04
10	0.1640	0.1071	0.1391	0.4910	0.0977	1.5E-03

RUN 4 TABLE VIII TURBINE P

PT.	P.R.	N-1R	WREF	WREF	ETA	HPREF		
1	3.20	8.33	12504.4	1.014	0.724	37.19	-0.10	-0.2
2	3.22	8.14	12662.0	1.021	0.722	37.08	-0.09	-0.27
3	3.24	7.73	12947.6	1.014	0.732	37.34	-0.14	-0.15
4	3.23	7.42	13200.6	1.011	0.741	37.63	-0.09	-0.17
5	3.26	6.97	13547.3	1.009	0.750	38.20	-0.07	-0.11
6	3.19	6.41	14139.6	1.017	0.758	38.46	-0.01	-0.46
7	3.25	5.85	14880.1	1.011	0.769	39.15	-0.02	-0.38
8	3.24	5.26	15644.5	1.032	0.761	39.44	-0.04	-0.13
9	3.26	4.68	16662.3	1.016	0.783	40.17	0.01	-0.06
10	3.25	4.17	17513.1	1.020	0.787	40.37	0.05	0.12

NOZZLE PRESSURE RATIOS

PT.	P1	P2	P3	P4	P5	P6	P7
1	0.713	0.440	0.253	0.324	0.256	0.688	0.677
2	0.712	0.440	0.253	0.323	0.292	0.869	0.677
3	0.712	0.440	0.253	0.322	0.300	0.880	0.676
4	0.712	0.440	0.252	0.321	0.309	0.889	0.677
5	0.712	0.440	0.252	0.321	0.311	0.868	0.676
6	0.711	0.440	0.253	0.322	0.305	0.889	0.677
7	0.713	0.440	0.252	0.321	0.321	0.888	0.676
8	0.712	0.440	0.253	0.321	0.345	0.891	0.679
9	0.711	0.439	0.252	0.320	0.358	0.887	0.675
10	0.712	0.440	0.253	0.321	0.375	0.890	0.677

PT.	KBLOCK	STPR	RPM	P8 -	P9
1	0.9958	3.7528	11190.0	0.507	0.226
2	1.0023	3.6424	13000.0	0.510	0.226
3	0.9955	3.7084	13670.0	0.509	0.225
4	0.9924	3.6507	13940.0	0.510	0.224
5	0.9984	3.6082	14410.0	0.509	0.224
6	0.9989	3.5426	14930.0	0.510	0.227
7	0.9980	3.3728	15720.0	0.510	0.227
8	1.0135	3.2339	16530.0	0.522	0.228
9	0.9976	3.1542	17510.0	0.51.	0.229
10	1.0012	2.9643	18610.0	0.509	0.232

RUN 5 TABLE IX TURBINE C

VELOCITY TRIANGLE

PT.	V1	V2	VA1	VA2	VU1	VU
1	920.3	151.6	216.6	141.9	894.4	[illegible]
2	930.7	145.7	212.1	140.2	906.2	[illegible]
3	922.5	140.9	212.2	140.2	897.9	[illegible]
4	913.8	141.5	213.2	142.2	888.6	[illegible]
5	906.4	145.9	206.7	139.5	882.6	[illegible]
6	887.0	157.6	211.4	141.2	862.3	[illegible]
7	893.5	171.5	201.6	137.9	870.4	[illegible]
8	953.9	199.4	207.0	141.4	828.4	[illegible]

MACH NUMBERS

PT.	M1	MA1	M2	MA2
1	0.837	0.197	0.129	0.121
2	0.847	0.193	0.134	0.130
3	0.838	0.193	0.130	0.120
4	0.829	0.193	0.131	0.128
5	0.822	0.187	0.124	0.119
6	0.803	0.191	0.134	0.120
7	0.809	0.182	0.146	0.118
8	0.768	0.186	0.169	0.121

ANLGES

PT.	A1	A2	B1	B2
1	76.4	-20.5	68.8	[illegible]
2	76.8	-15.9	68.9	[illegible]
3	76.7	-5.5	67.8	[illegible]
4	76.3	5.0	66.5	[illegible]
5	76.8	17.0	55.8	[illegible]
6	76.2	26.4	63.0	[illegible]
7	77.0	36.5	60.1	[illegible]
8	76.0	44.5	57.1	[illegible]

LOSSES

PT.	ZS	ZSTH	ZR	ZRTH	ZR+	ZI
1	0.2320	0.1071	0.3044	0.4497	0.3020	1.3E-01
2	0.2065	0.1071	0.3453	0.4522	0.3409	1.4E-02
3	0.2192	0.1071	0.3023	0.8523	0.3021	1.0E-03
4	0.2304	0.1071	0.2562	0.8665	0.2605	6.2E-03
5	0.2059	0.1071	0.3075	0.4227	0.3069	4.5E-03
6	0.2473	0.1071	0.1629	0.4077	0.1690	3.1E-04
7	0.2650	0.1071	0.2841	0.4014	0.2706	3.5E-04
8	0.2593	0.1071	0.1392	0.3607	0.1190	7.4E-03

RUN 5 TABLE IX TURBINE C

PT.	P.R.	K-IS	NREF	WREF	ETA	HPREF	[illegible]	[illegible]
1	1.75	8.26	9089.4	1.027	0.644	17.22	-0.00	[illegible]
2	1.75	7.78	9294.4	1.014	0.660	17.43	-0.07	[illegible]
3	1.75	6.98	9824.5	1.014	0.670	17.81	-0.05	[illegible]
4	1.76	6.31	10346.2	1.020	0.677	18.12	-0.05	[illegible]
5	1.75	5.52	11010.6	1.017	0.696	18.41	-0.01	[illegible]
6	1.75	4.97	11687.6	1.026	0.690	18.52	-0.02	[illegible]
7	1.75	4.43	12325.9	1.006	0.708	18.64	0.02	[illegible]
8	1.75	3.81	13237.9	1.033	0.686	18.42	0.00	[illegible]

NOZZLE PRESSURE RATIOS

PT.	P1	P2	P3	P4	P5	P6	P7
1	0.713	0.441	0.381	0.523	0.583	0.888	[illegible]
2	0.713	0.441	0.383	0.525	0.582	0.889	0.677
3	0.713	0.441	0.386	0.530	0.586	0.888	0.676
4	0.712	0.440	0.388	0.535	0.589	0.888	0.675
5	0.713	0.441	0.396	0.548	0.597	0.889	0.679
6	0.713	0.441	0.400	0.553	0.601	0.889	0.678
7	0.712	0.440	0.407	0.562	0.605	0.887	0.678
8	0.713	0.441	0.419	0.576	0.615	0.888	0.678

PT.	KBLOCK	STPR	RPM	P8	P9
1	1.0082	1.8379	9470.0	0.533	0.506
2	0.9956	1.8259	9780.0	0.534	0.506
3	0.9962	1.8208	10340.0	0.538	0.510
4	1.0012	1.8151	10890.0	0.542	0.514
5	0.9982	1.7613	11590.0	0.550	0.523
6	1.0077	1.7746	12250.0	0.553	0.526
7	0.9876	1.7304	12970.0	0.562	0.535
8	1.0145	1.7103	13930.0	0.582	0.547

RUN 6 TABLE X TURBINE C

VELOCITY TRIANGLE

PT.	V1	V2	VA1	VA2	VU1	VU2
1	1132.6	189.9	273.2	172.9	1099.1	-73.5
2	1136.0	179.2	253.5	166.7	1107.1	-32.7
3	1123.8	175.4	252.0	170.9	1091.4	-30.1
4	1106.4	172.3	266.0	172.0	1073.9	-0.1
5	1083.7	174.2	262.0	171.4	1051.6	0.1
6	1075.1	161.2	253.2	170.7	1044.0	30.1
7	1369.9	198.1	245.1	167.4	1341.4	195.1
8	1007.2	228.8	243.9	169.2	1008.1	143.5

MACH NUMBERS ANGLES

PT.	M1	MA1	M2	MA2	A1	A2	B1	B2
1	1.063	0.252	0.162	0.148	76.0	-24.4	68.0	-73.1
2	1.073	0.249	0.153	0.145	76.6	-13.9	68.0	-70.7
3	1.057	0.246	0.150	0.148	76.5	-13.0	67.8	-70.2
4	1.038	0.252	0.147	0.147	76.1	-3.3	66.8	-70.3
5	1.012	0.245	0.149	0.146	76.0	10.3	64.4	-69.5
6	1.002	0.239	0.154	0.146	76.2	19.6	63.7	-70.1
7	0.907	0.228	0.139	0.148	76.3	32.3	63.1	-70.7
8	0.760	0.226	0.195	0.145	76.4	42.2	58.6	-67.9

LOSSES

PT.	ZS	ZSTH	ZR	ZPTH	ZR+	ZI
1	0.1968	0.1071	0.2704	0.5936	0.2779	1.2E-02
2	0.1725	0.1071	0.3182	0.5638	0.3213	1.4E-02
3	0.1818	0.1071	0.3213	0.5829	0.2971	1.0E-02
4	0.2056	0.1071	0.2038	0.5542	0.2186	5.5E-03
5	0.2163	0.1071	0.1898	0.5256	0.1955	2.5E-03
6	0.2148	0.1071	0.1726	0.5245	0.1823	9.8E-04
7	0.1916	0.1071	0.2382	0.4967	0.2345	3.7E-04
8	0.2137	0.1371	0.1717	0.4579	0.1453	3.5E-03

RUN 6 TABLE X TURBINE D

PT.	P.R.	K-I3	NREF	WREF	ETA	HPREF	MTR	HTR
1	2.26	8.19	10721.1	1.023	0.677	25.36	-0.11	-1.0[illegible]
2	2.25	7.61	11111.5	1.010	0.696	25.65	-0.09	-0.97
3	2.25	6.97	11613.9	1.019	0.706	26.25	-0.08	-0.91
4	2.26	6.34	12301.7	1.023	0.707	26.52	-0.07	-0.[illegible]
5	2.24	5.69	12313.7	1.026	0.706	26.28	-0.05	-0.56
6	2.26	5.06	13629.4	1.020	0.718	26.76	-0.03	-0.37
7	2.25	4.44	14526.4	1.007	0.730	26.78	0.01	-0.26
8	2.25	3.74	15814.9	1.021	0.725	26.95	0.04	0.05

NOZZLE PRESSURE RATIOS

PT.	P1	P2	P3	P4	P5	P6	P7
1	0.713	0.441	0.256	0.332	0.472	0.888	0.675
2	0.713	0.441	0.257	0.336	0.474	0.888	0.676
3	0.713	0.441	0.259	0.340	0.477	0.888	0.676
4	0.713	0.441	0.258	0.342	0.481	0.888	0.676
5	0.713	0.441	0.259	0.348	0.491	0.888	0.675
6	0.713	0.441	0.258	0.373	0.496	0.889	0.676
7	0.712	0.441	0.261	0.389	0.503	0.887	0.675
8	0.713	0.441	0.276	0.418	0.512	0.889	0.676

PT.	NBLOCK	STPR	RPM	P8	P9
1	1.0045	2.5047	11280.0	0.519	0.286
2	0.9916	2.4529	11690.0	0.519	0.293
3	1.0004	2.4109	12220.0	0.519	0.299
4	1.0042	2.4135	12840.0	0.519	0.310
5	1.0075	2.3477	13490.0	0.519	0.335
6	1.0017	2.3062	14350.0	0.519	0.348
7	0.9892	2.2261	15290.0	0.519	0.376
8	1.0027	2.1571	16660.0	0.519	0.403

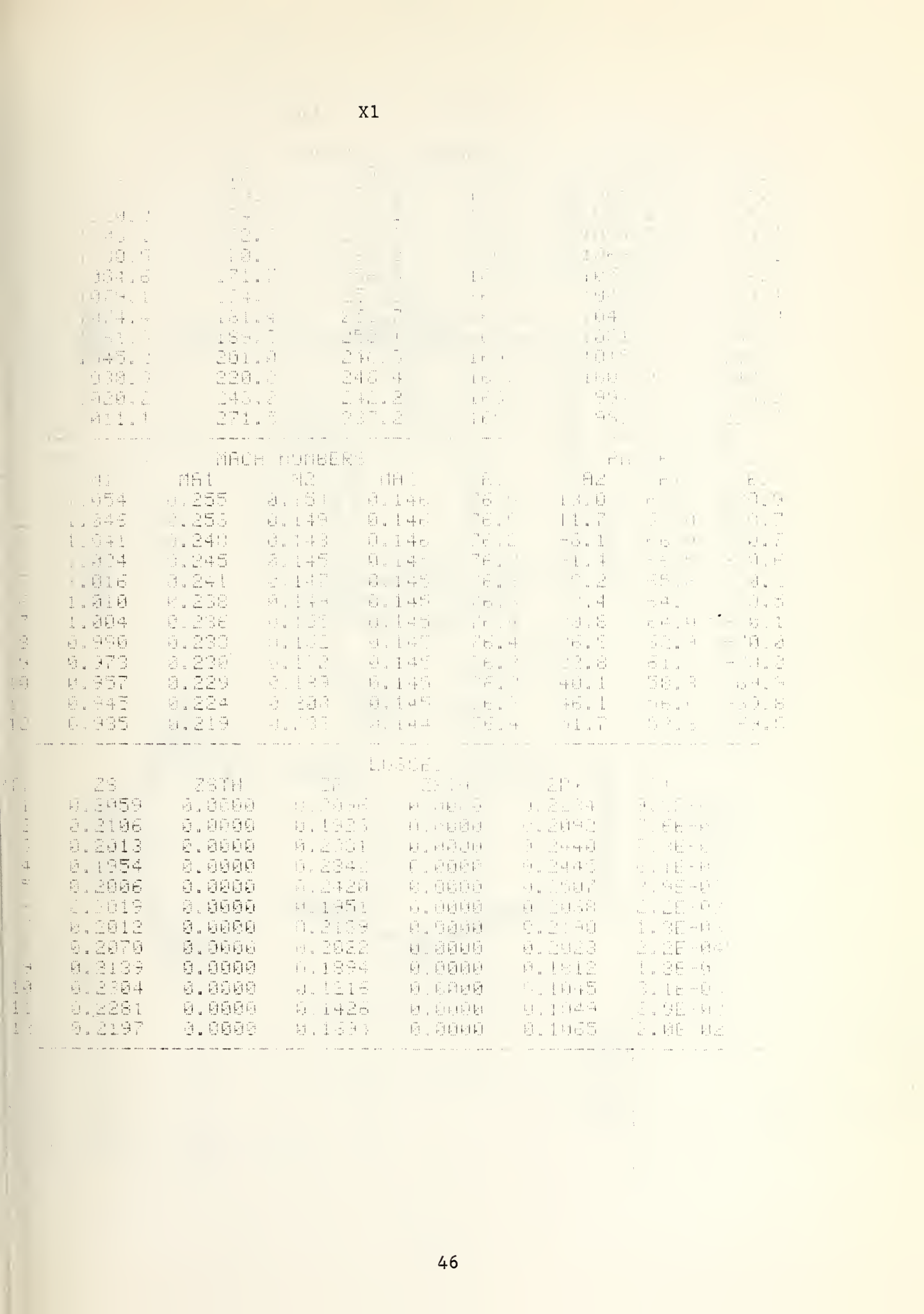

MACH NUMBERS

M	M1	M2	MM				
.954	0.255	0.151	0.146		14.0		
.945	0.253	0.149	0.146		11.7		
1.041	0.240	0.143	0.146		-3.1		
.994	0.245	0.145	0.147		-1.4		
1.016	0.241	0.147	0.145		.2		
1.010	0.238	0.144	0.145		.4		
1.004	0.236	0.139	0.145		-2.8		
0.990	0.230	0.136	0.147		-6.2		
0.973	0.230	0.137	0.145		-3.8		
0.957	0.229	0.143	0.146		+0.1		
0.943	0.224	0.140	0.145		+6.1		
0.935	0.219	0.137	0.144		+1.7		

0.2059	0.0000			0.2134		
0.2106	0.0000	0.1933	0.0000	0.2042		
0.2013	0.0000	0.2301	0.0000	0.2440		
0.1954	0.0000	0.2342	0.0000	0.2443		
0.2006	0.0000	0.2420	0.0000	0.2507		
0.2019	0.0000	0.1951	0.0000	0.2038		
0.2012	0.0000	0.2139	0.0000	0.2240		
0.2070	0.0000	0.2022	0.0000	0.2023		
0.2139	0.0000	0.1994	0.0000	0.1912		
0.2304	0.0000	0.1216	0.0000	0.1045		
0.2281	0.0000	0.1426	0.0000	0.1044		
0.2197	0.0000	0.1697	0.0000	0.1065		

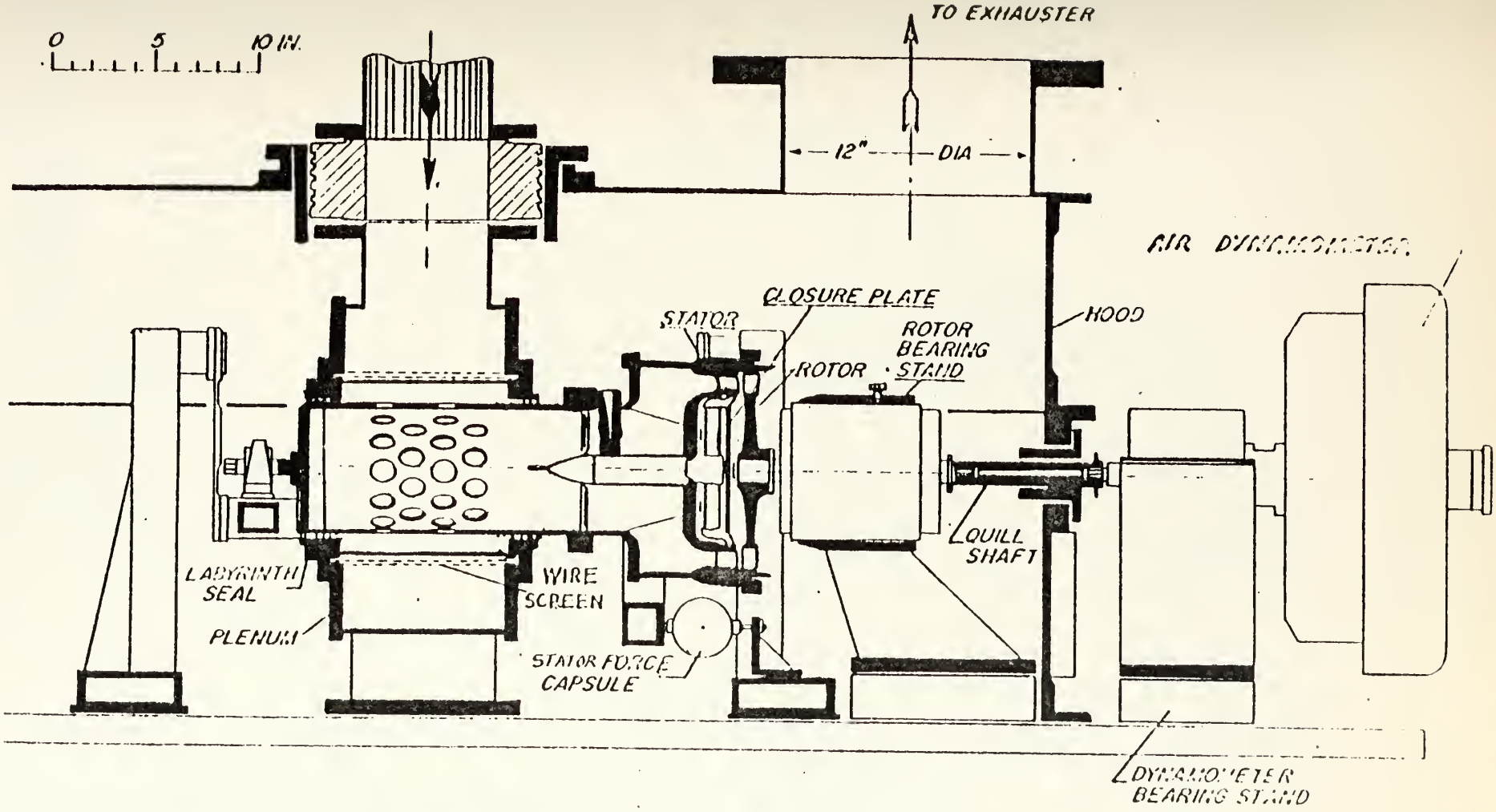

FIGURE 1 TRANSONIC TURBINE TEST RIG

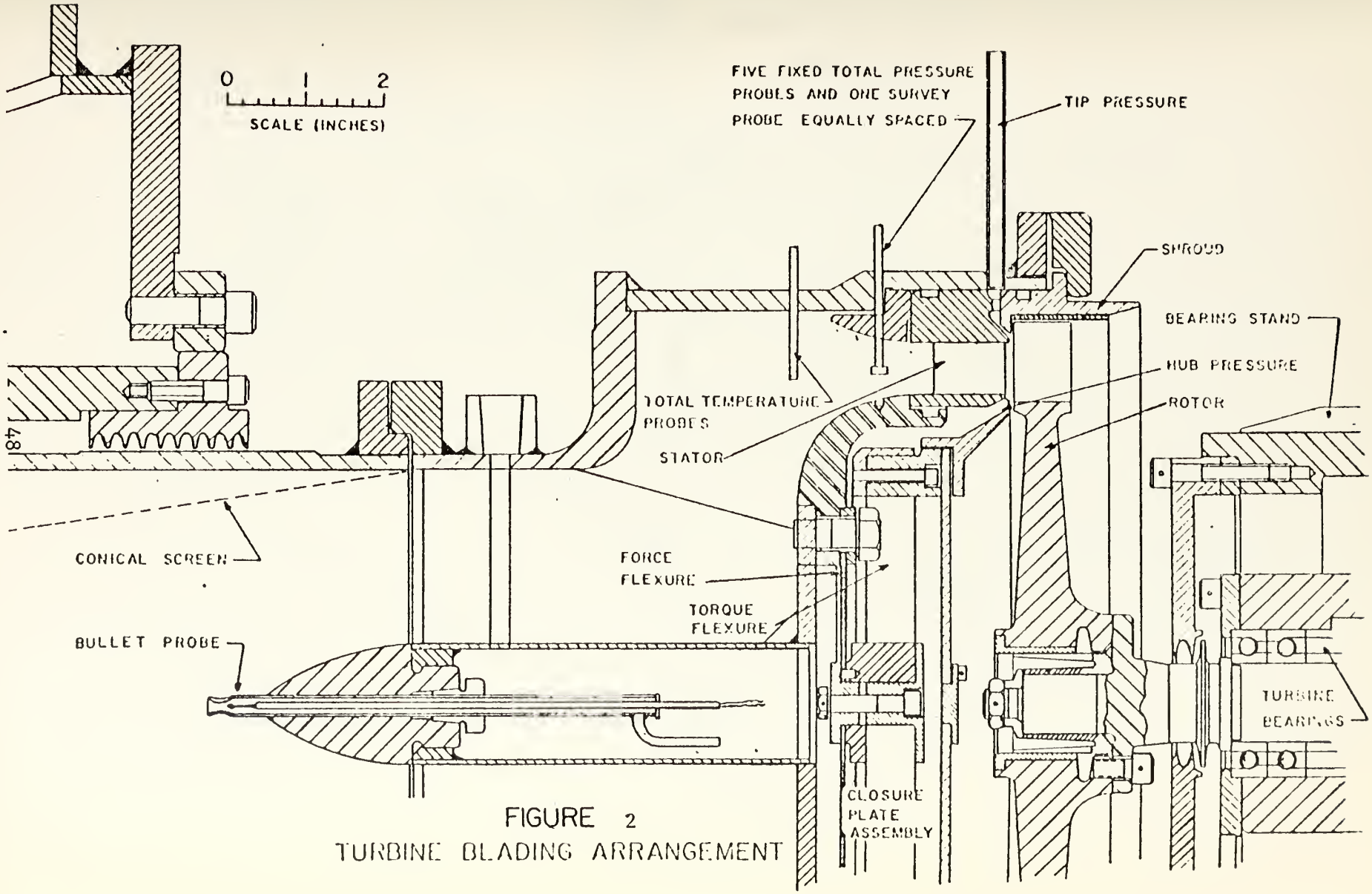

FIGURE 2
TURBINE BLADING ARRANGEMENT

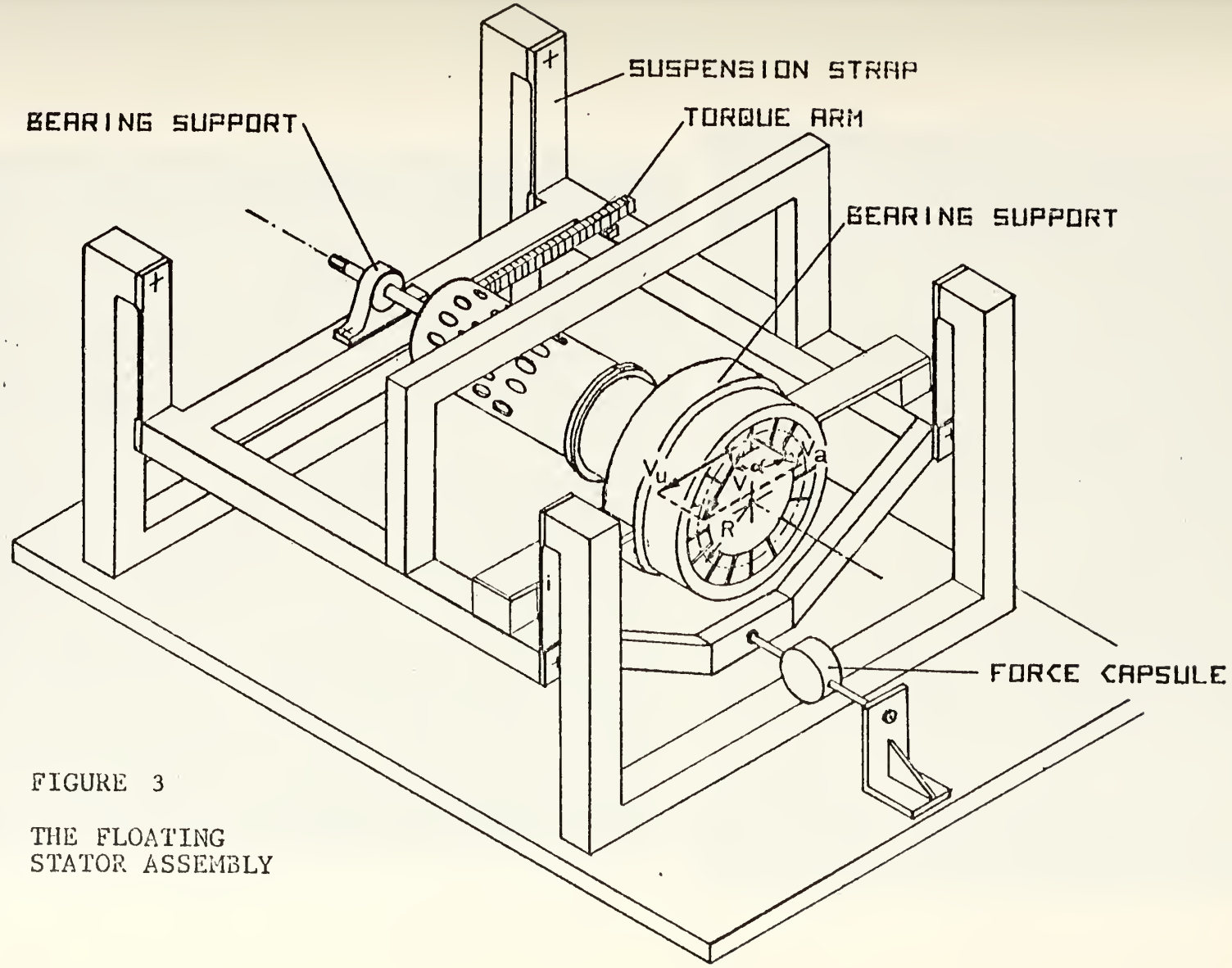

FIGURE 3

THE FLOATING
STATOR ASSEMBLY

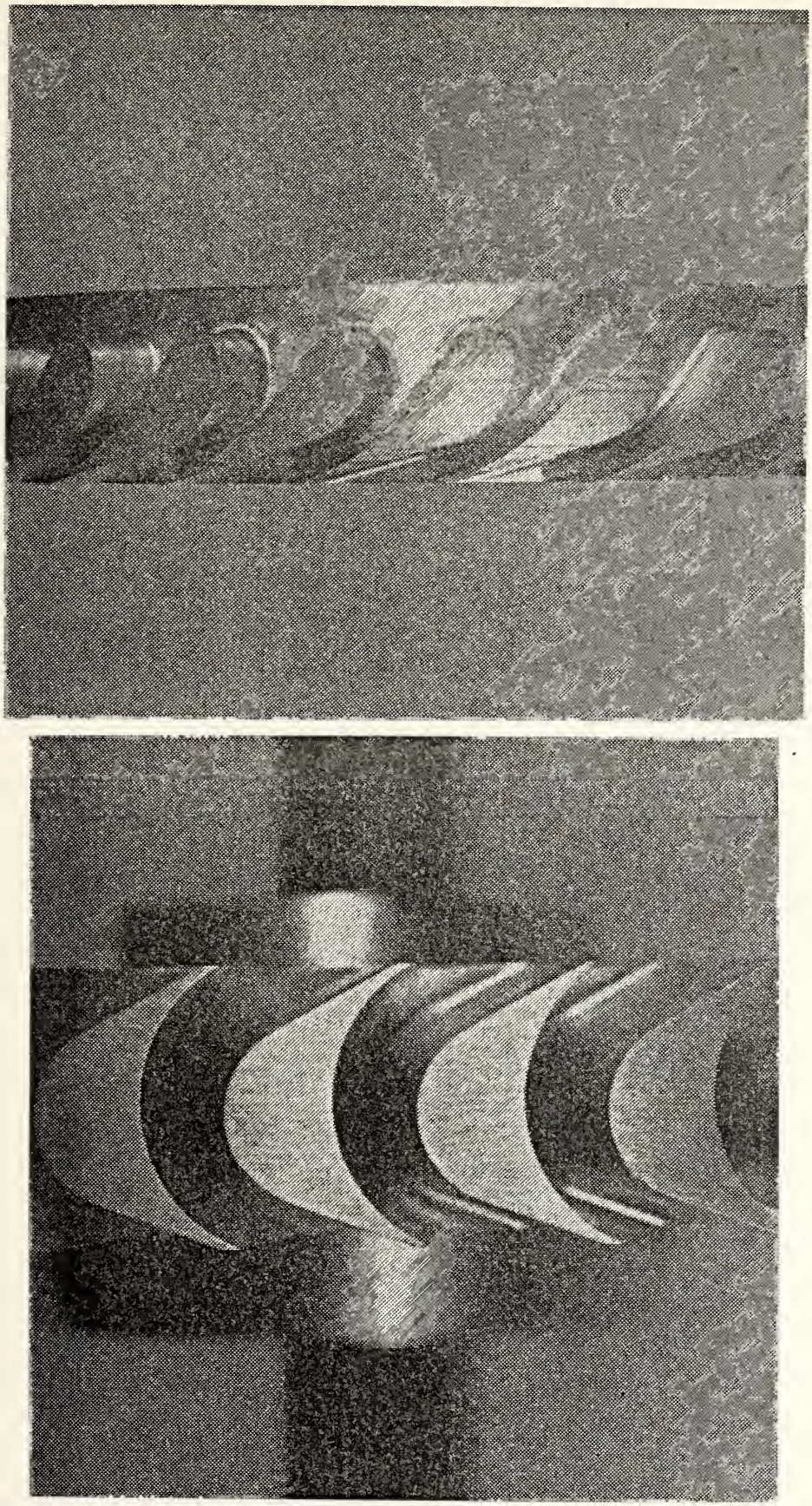

FIGURE 4 TURBINE C

FIGURE 5

PRESSURE TAP LOCATIONS

TURBINE TEST RIG

CONV-DIV. NOZZLES.

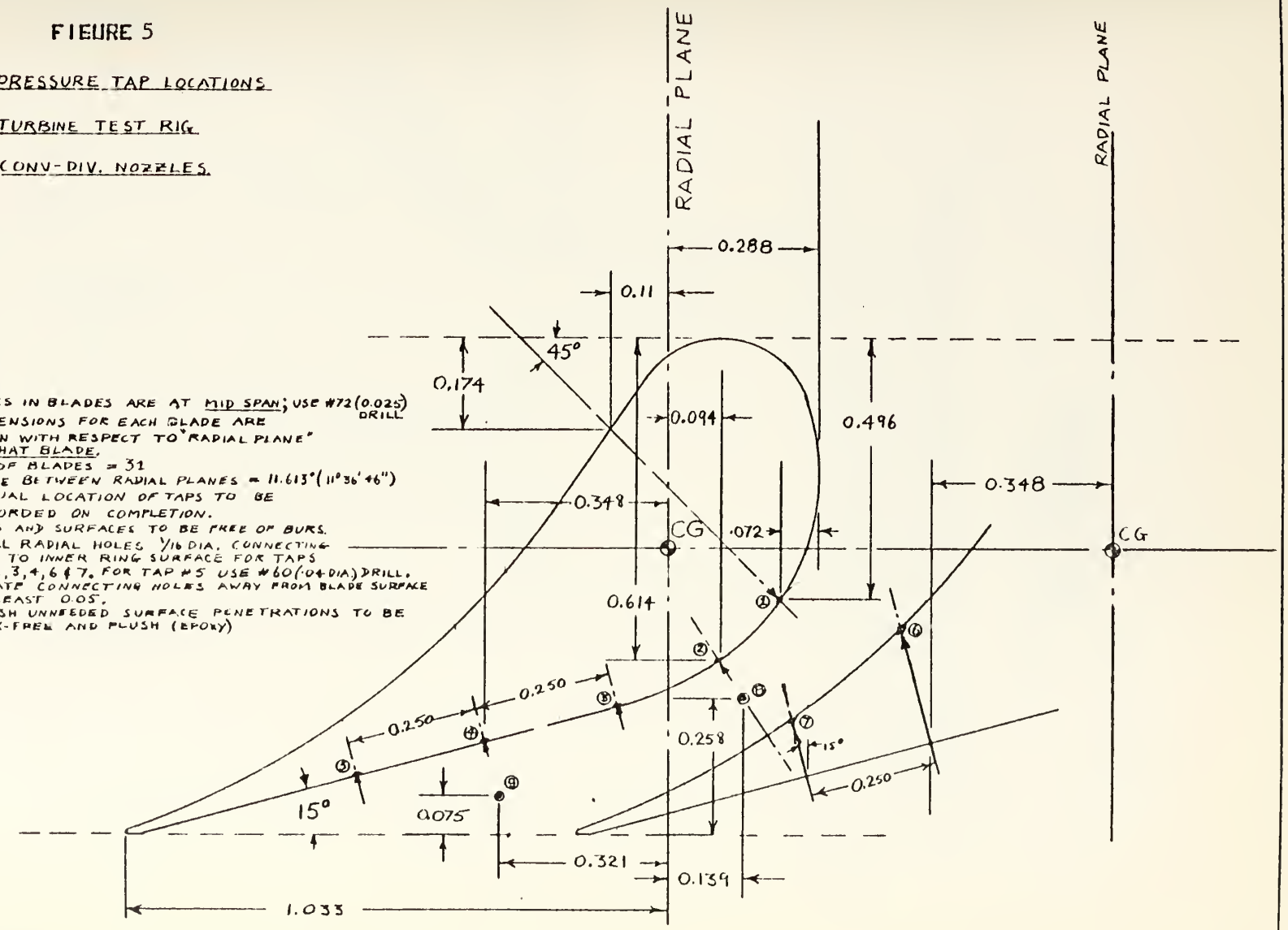

NOTE:

1. HOLES IN BLADES ARE AT MID SPAN; USE #72 (0.025) DRILL
2. DIMENSIONS FOR EACH BLADE ARE GIVEN WITH RESPECT TO "RADIAL PLANE" IN THAT BLADE.
   NO. OF BLADES = 31
   ANGLE BETWEEN RADIAL PLANES = 11.613° (11°36'46")
3. ACTUAL LOCATION OF TAPS TO BE RECORDED ON COMPLETION.
4. TAPS AND SURFACES TO BE FREE OF BURS.
5. DRILL RADIAL HOLES 1/16 DIA. CONNECTING TAPS TO INNER RING SURFACE FOR TAPS #1, 2, 3, 4, 6 & 7. FOR TAP #5 USE #60 (.04 DIA.) DRILL. LOCATE CONNECTING HOLES AWAY FROM BLADE SURFACE AT LEAST 0.05.
6. FINISH UNNEEDED SURFACE PENETRATIONS TO BE LEAK-FREE AND FLUSH (EPOXY)

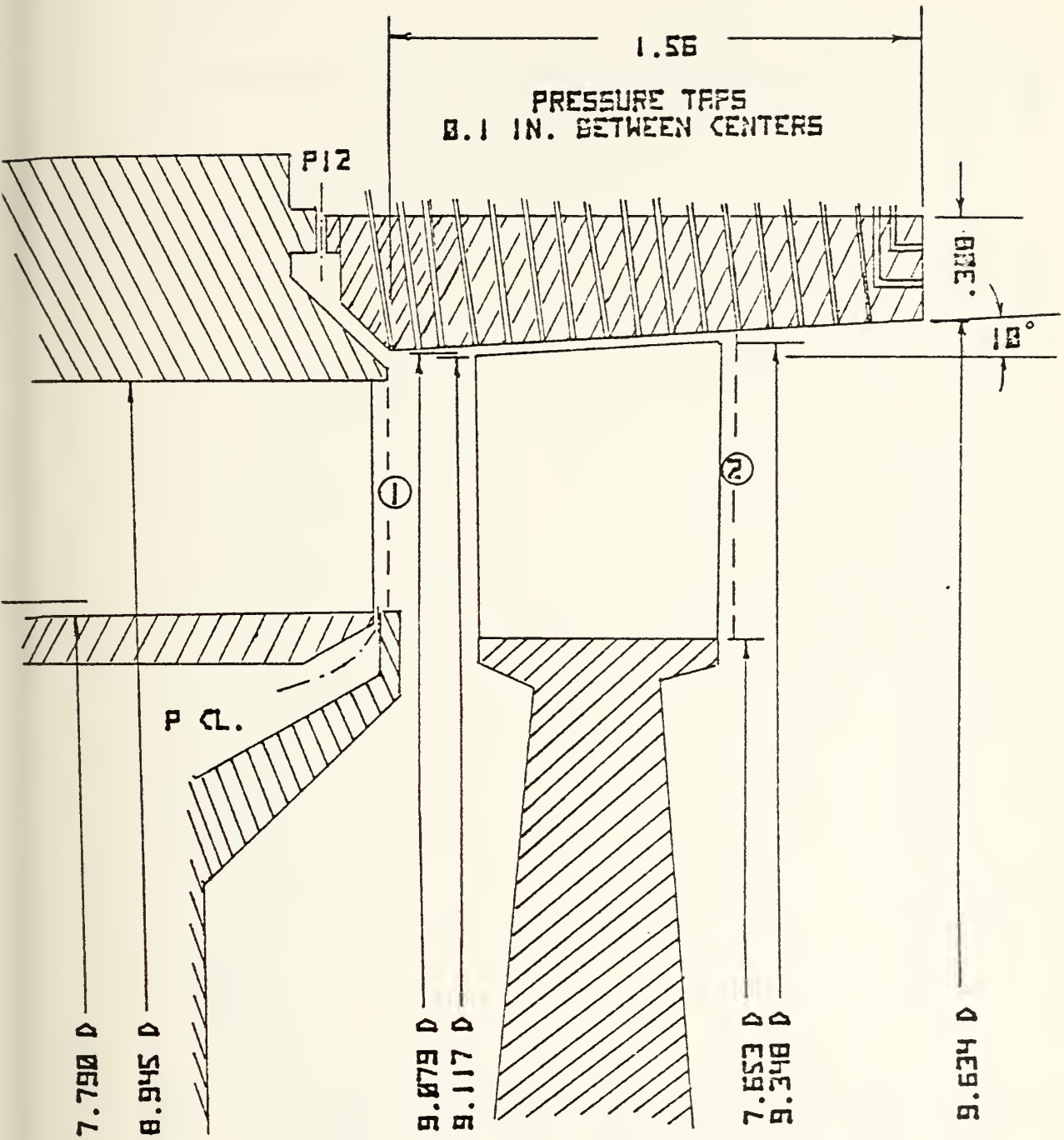

FIGURE 6 TURBINE TEST RIG GEOMETRY FOR TURBINE CONFIGURATION C

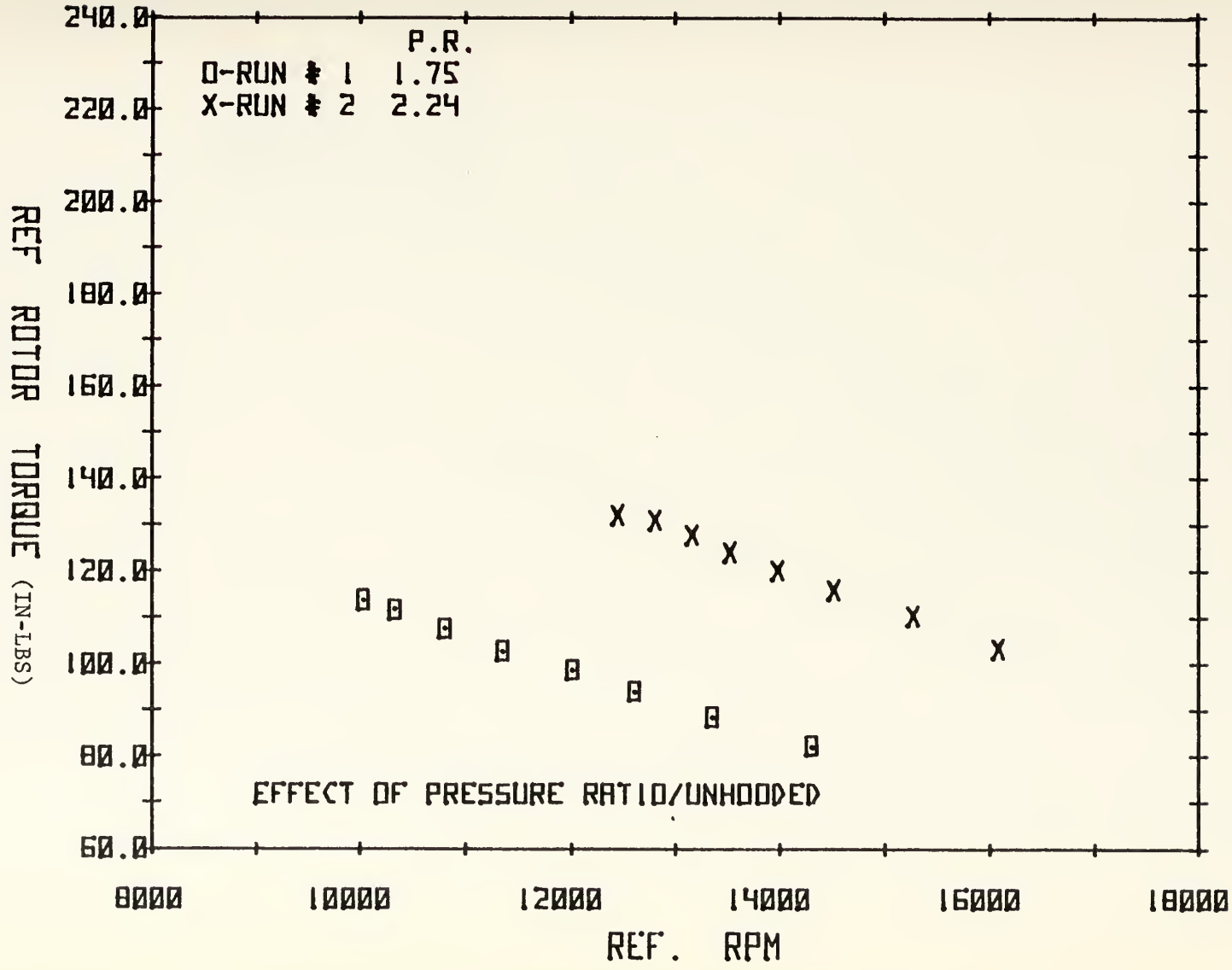

FIGURE 7a REF. ROTOR TORQUE VS REF. SPEED

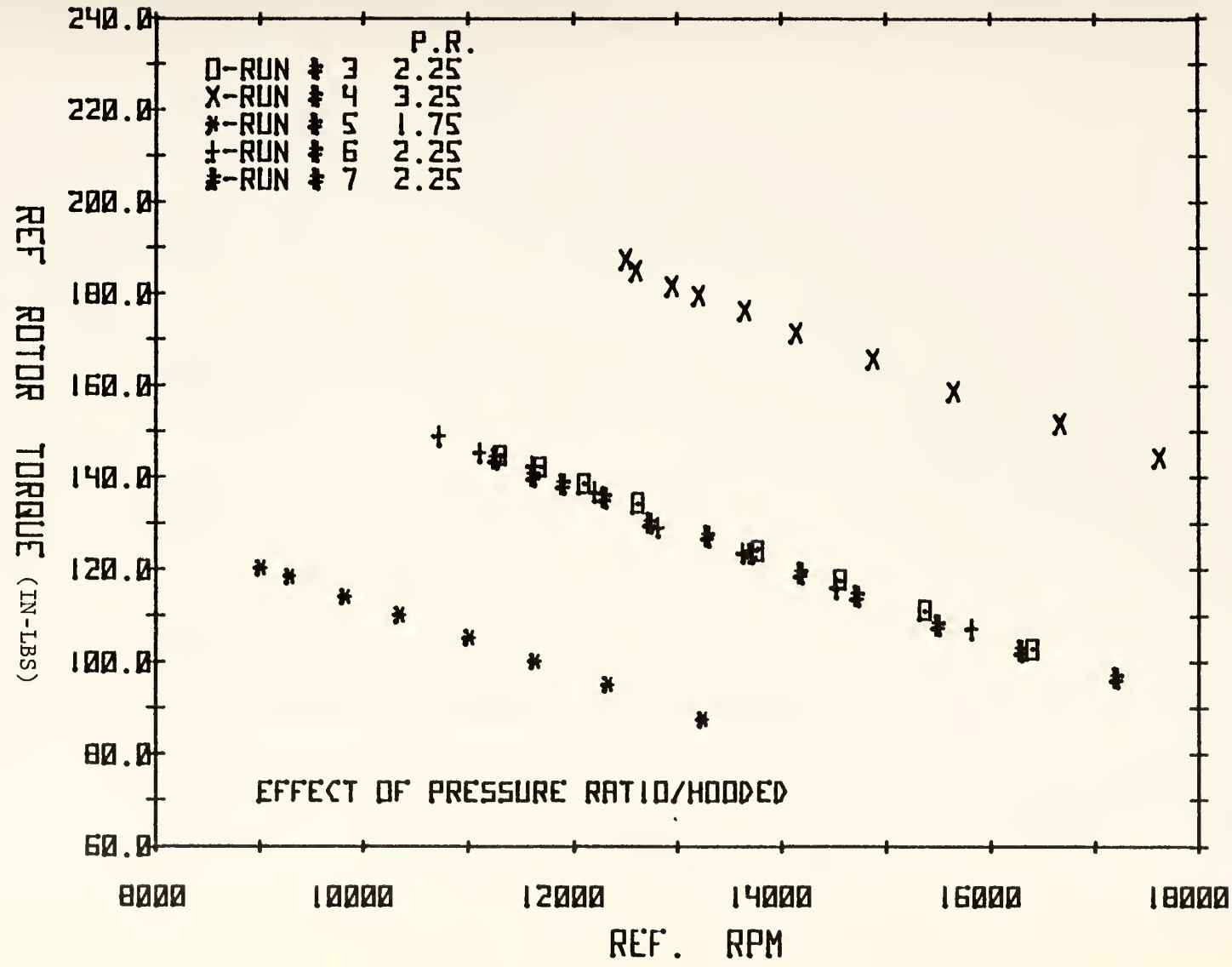

FIGURE 7b REF. ROTOR TORQUE VS REF. SPEED

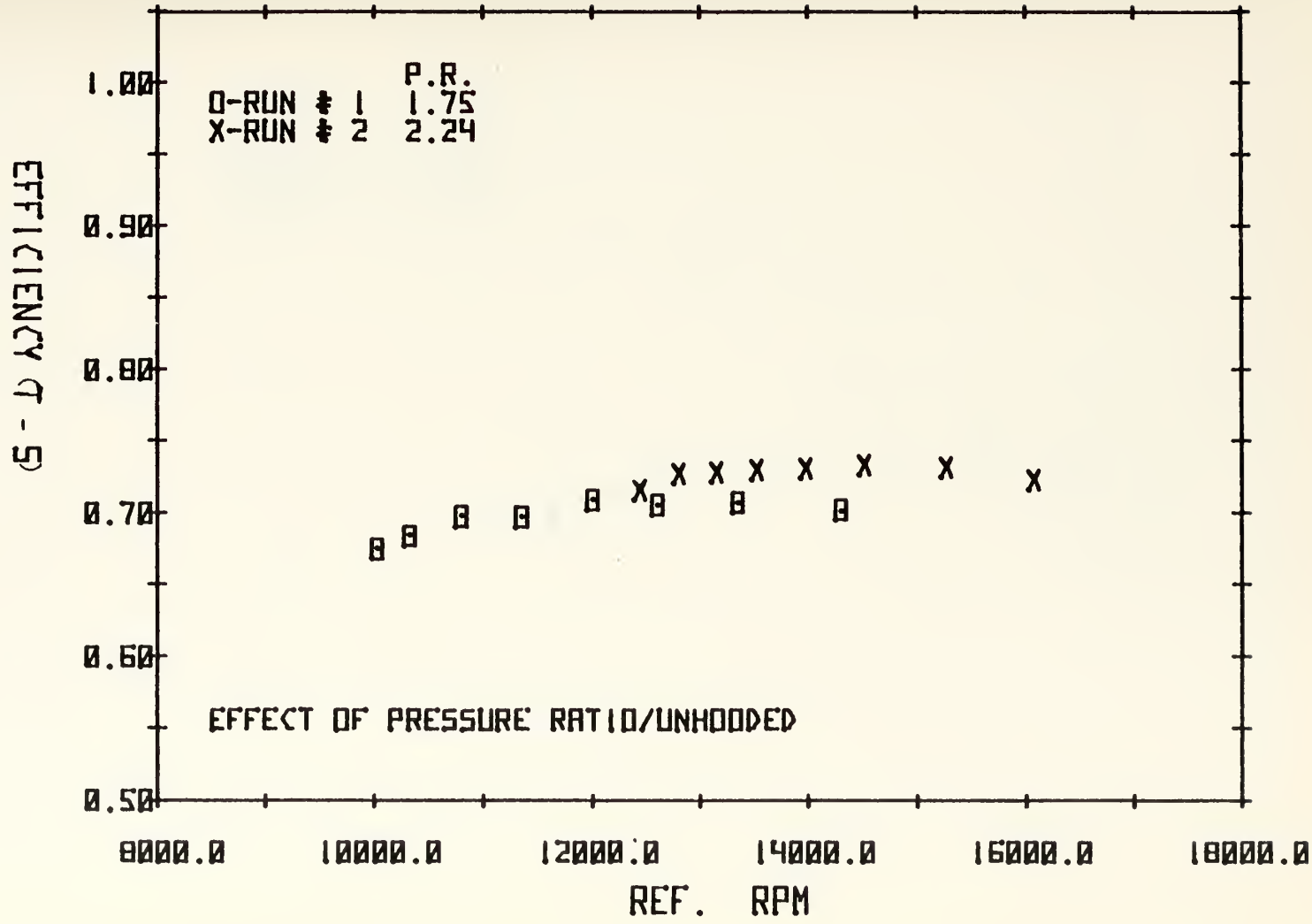

FIGURE 8a EFFICIENCY VS REF. SPEED

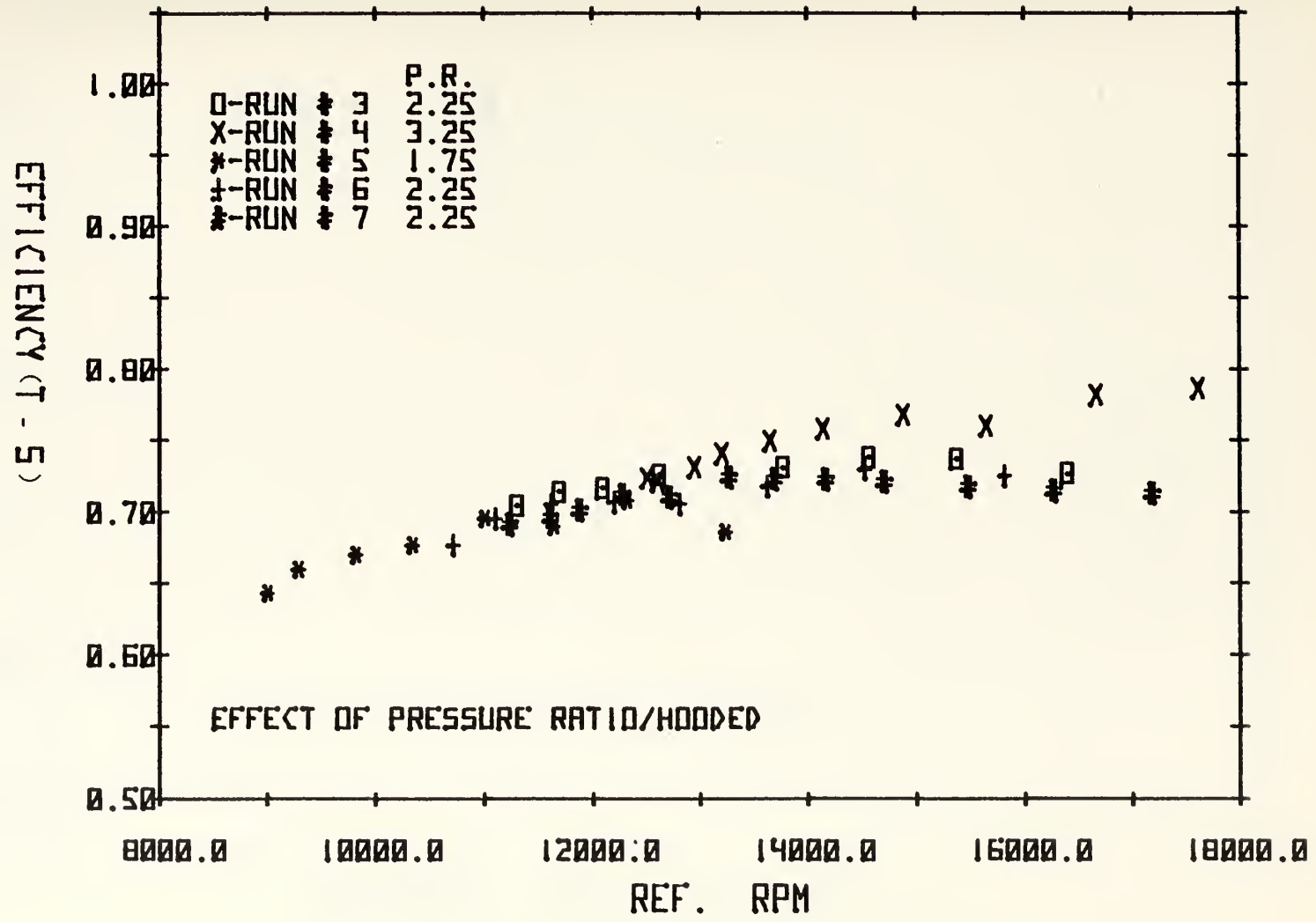

FIGURE 8b EFFICIENCY VS REF. SPEED

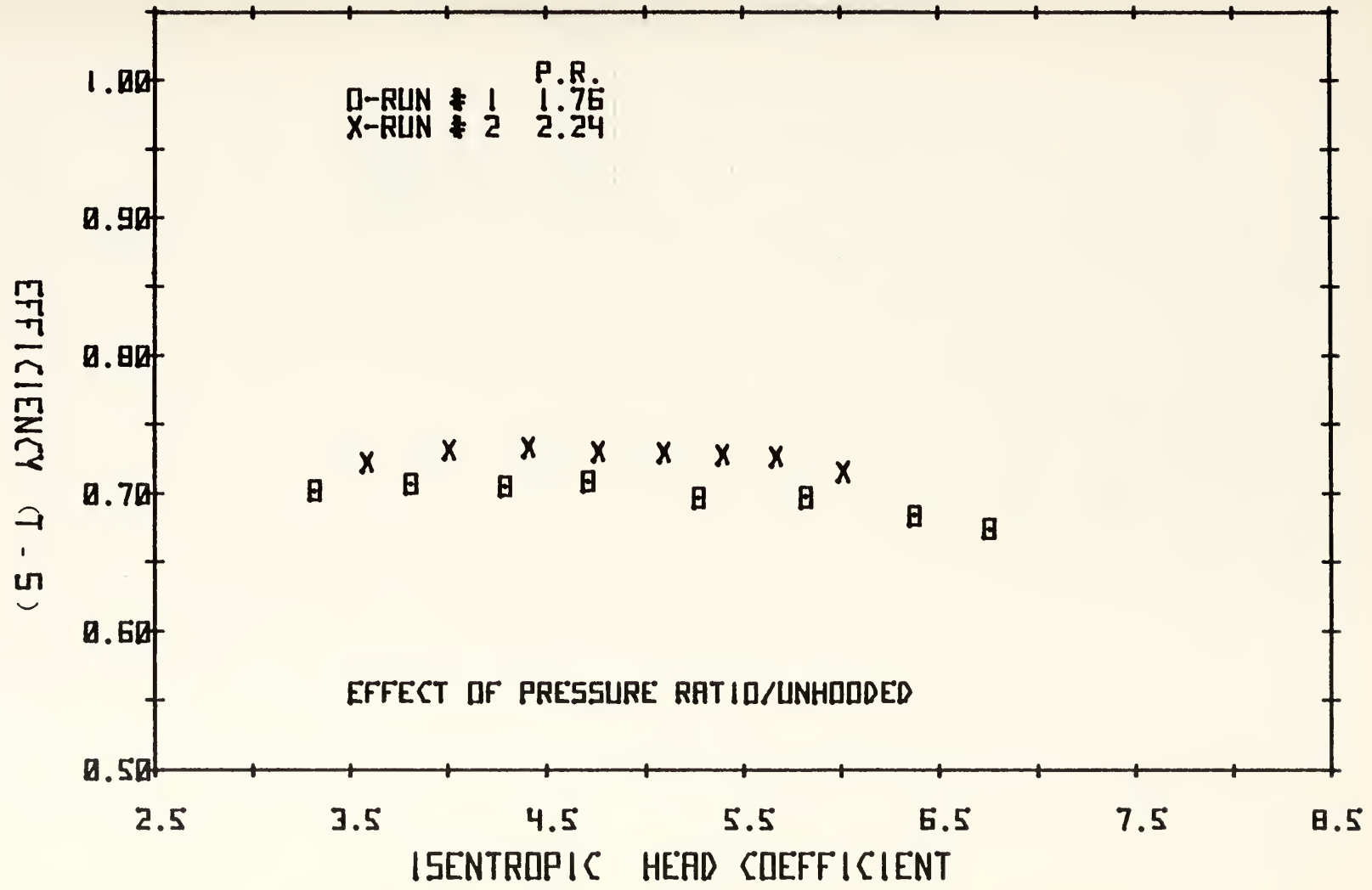

FIGURE 9a EFFICIENCY VS. ISENTROPIC HEAD COEFFICIENT

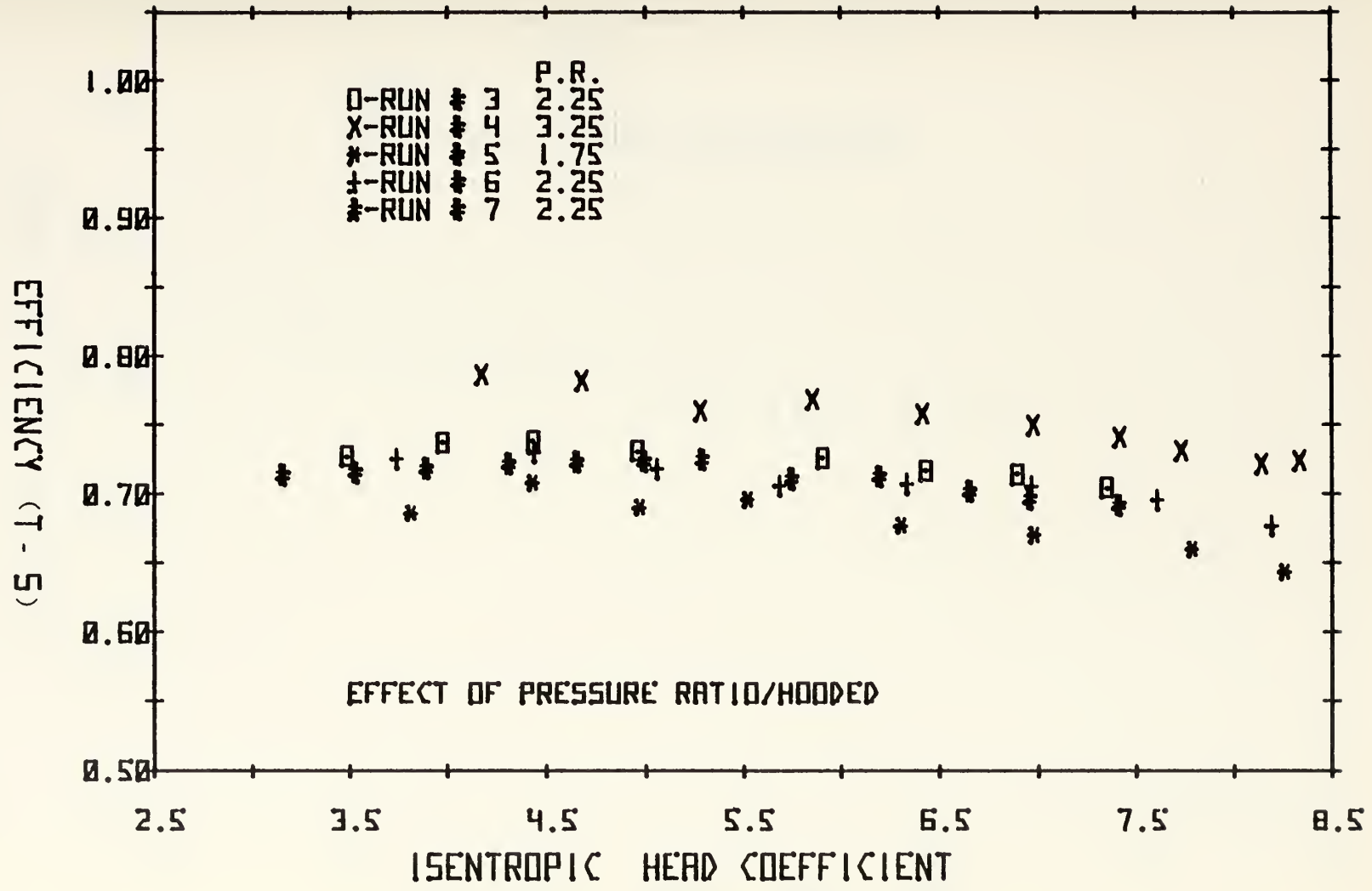

FIGURE 9b EFFICIENCY VS ISENTROPIC HEAD COEFFICIENT

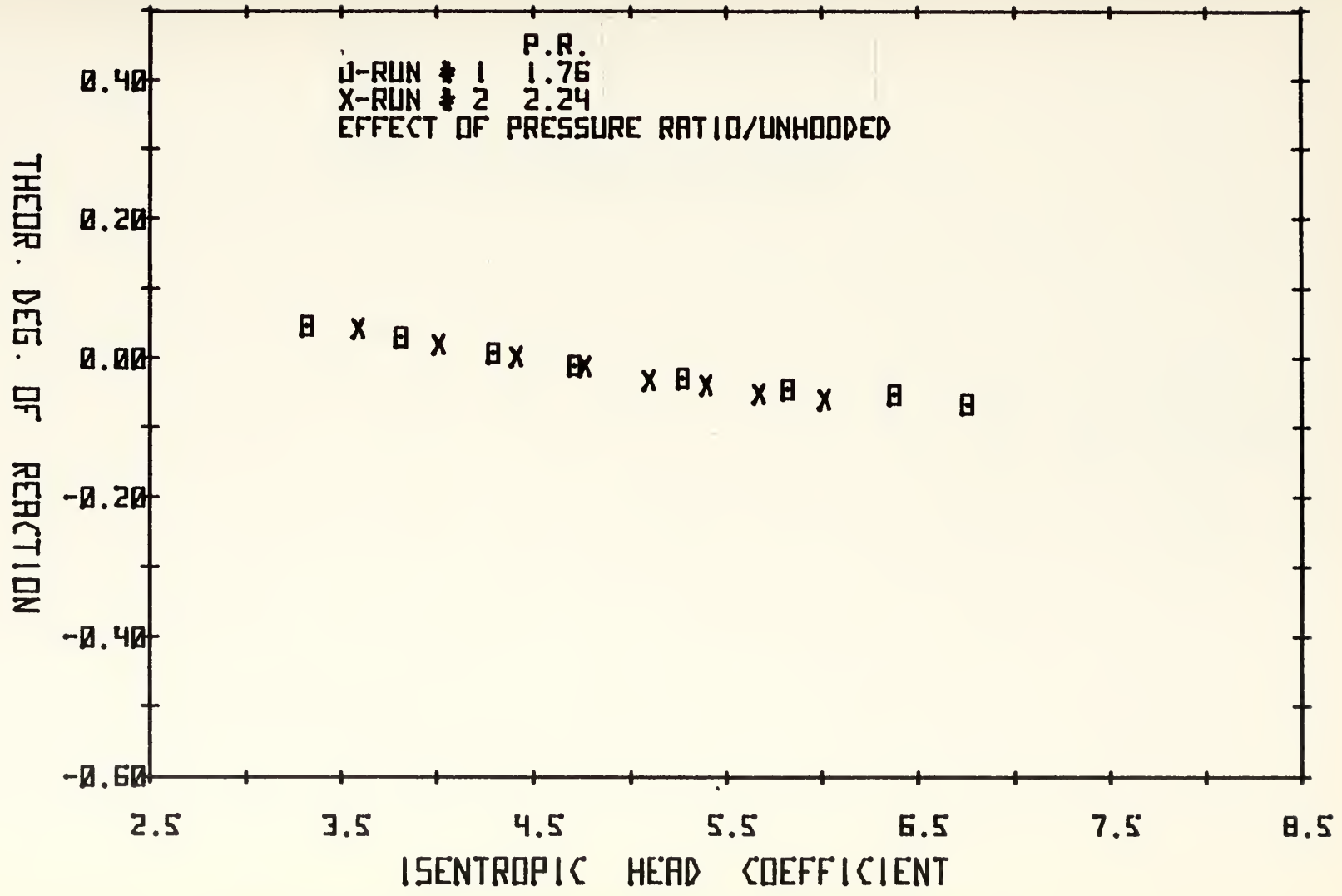

FIGURE 10a TH. DEGREE OF REACTION VS HEAD COEFFICIENT

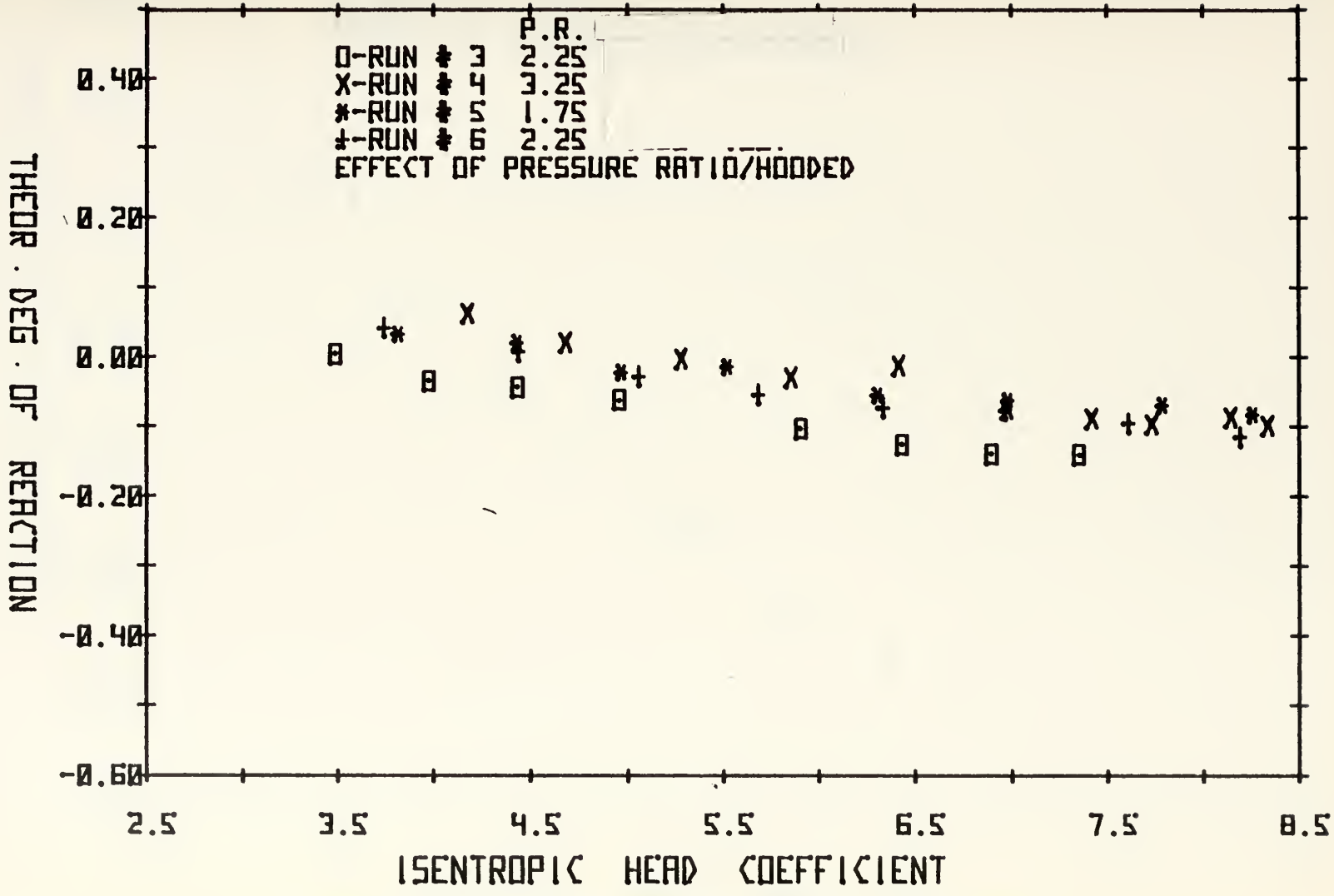

FIGURE 10b TH. DEGREE OF RACTION VS HEAD COEFFICIENT

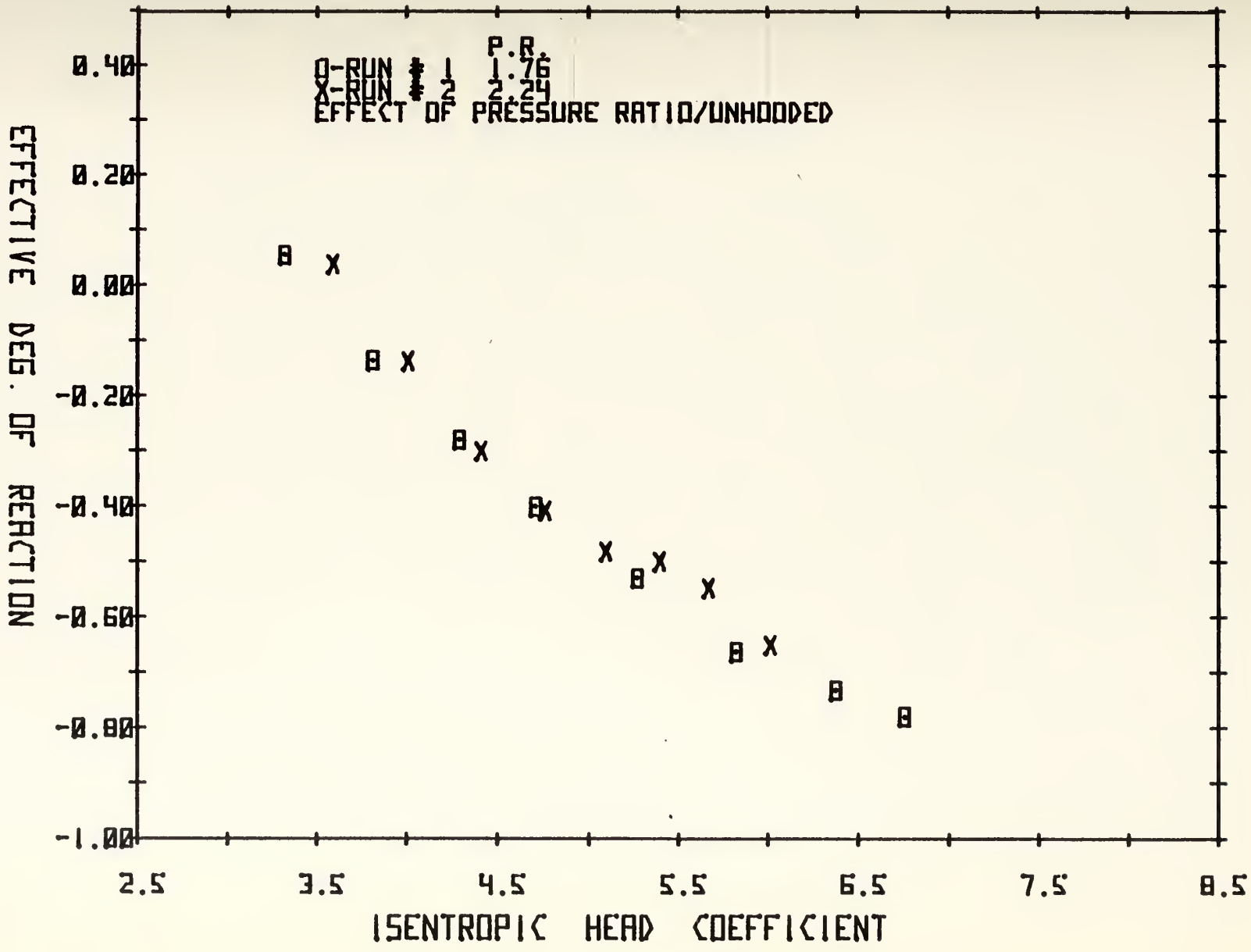

FIGURE 11a EFF. DEGREE OF REACTION VS HEAD COEFFICIENT

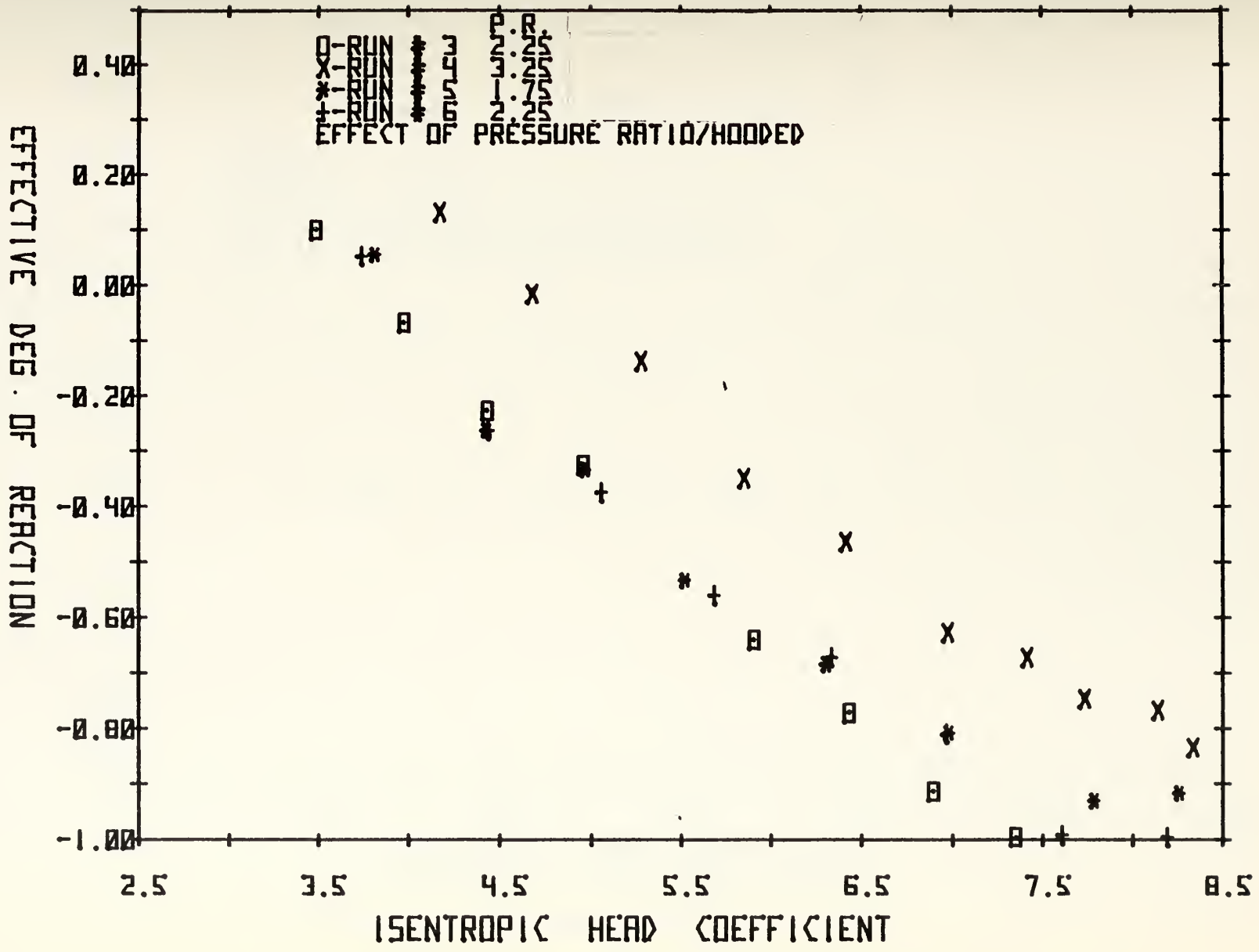

FIGURE 11b EFF. DEGREE OF REACTION VS HEAD COEFFICIENT

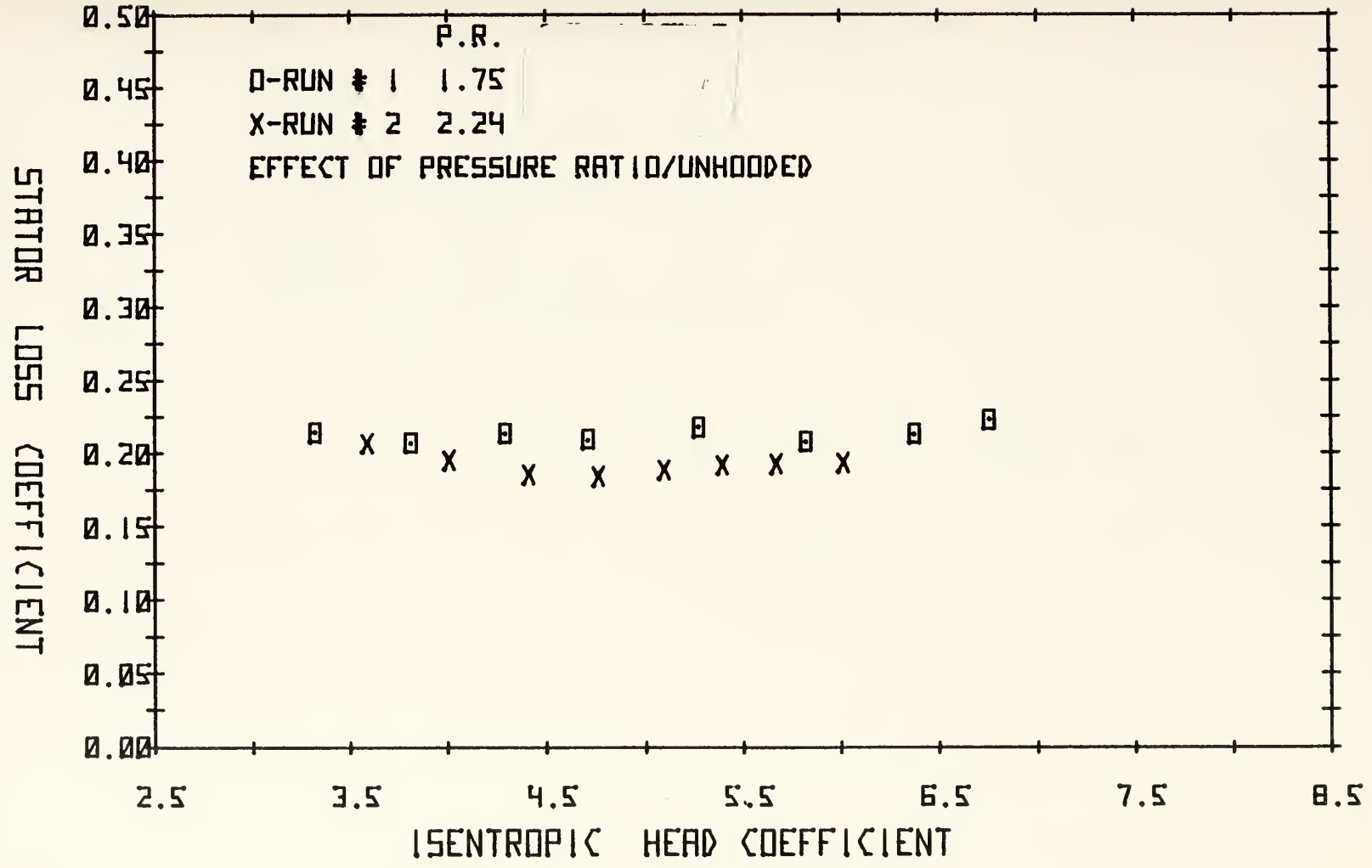

FIGURE 12a STATOR LOSS VS HEAD COEFFICIENT

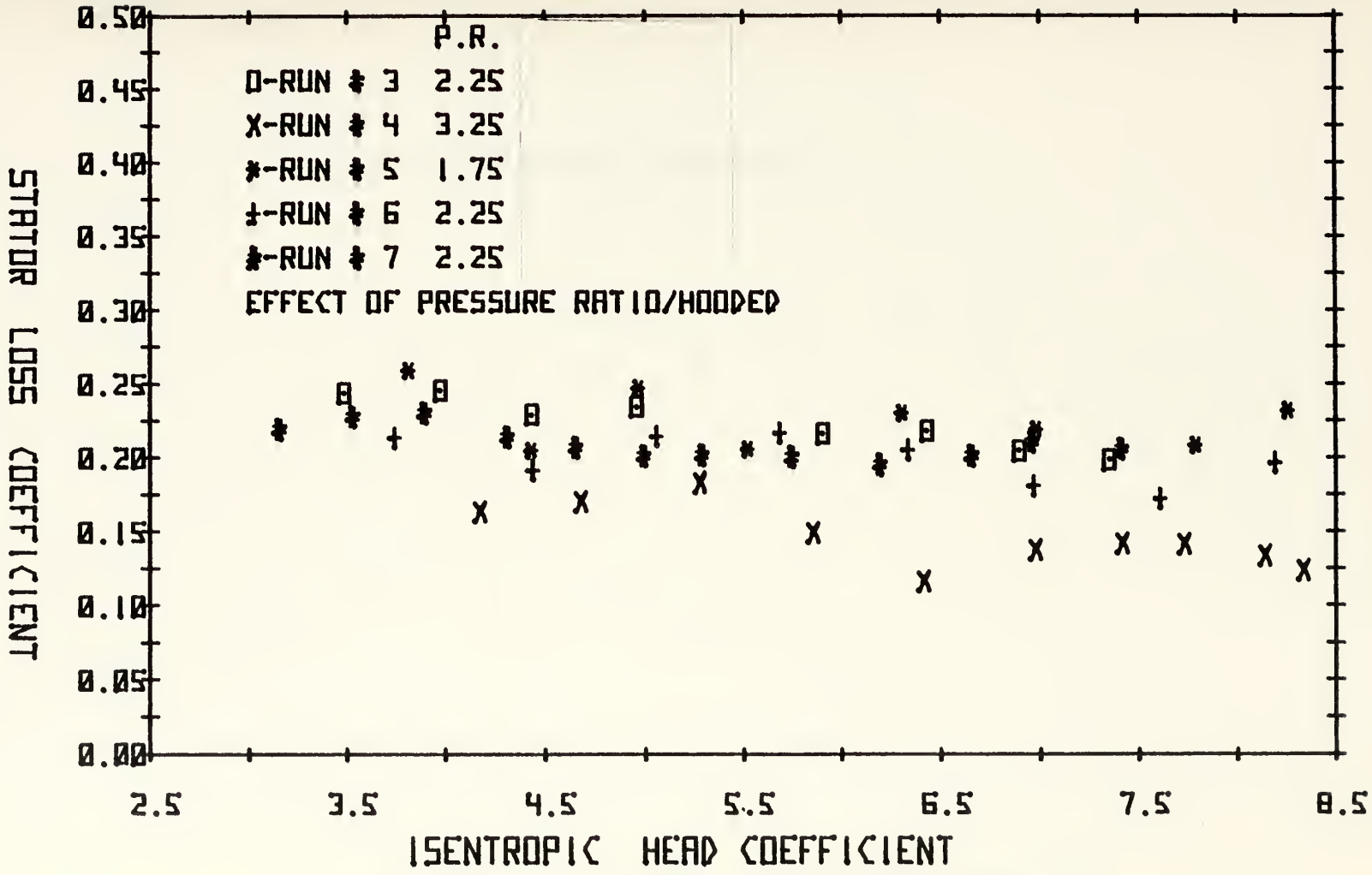

FIGURE 12b STATOR LOSS VS HEAD COEFFICIENT

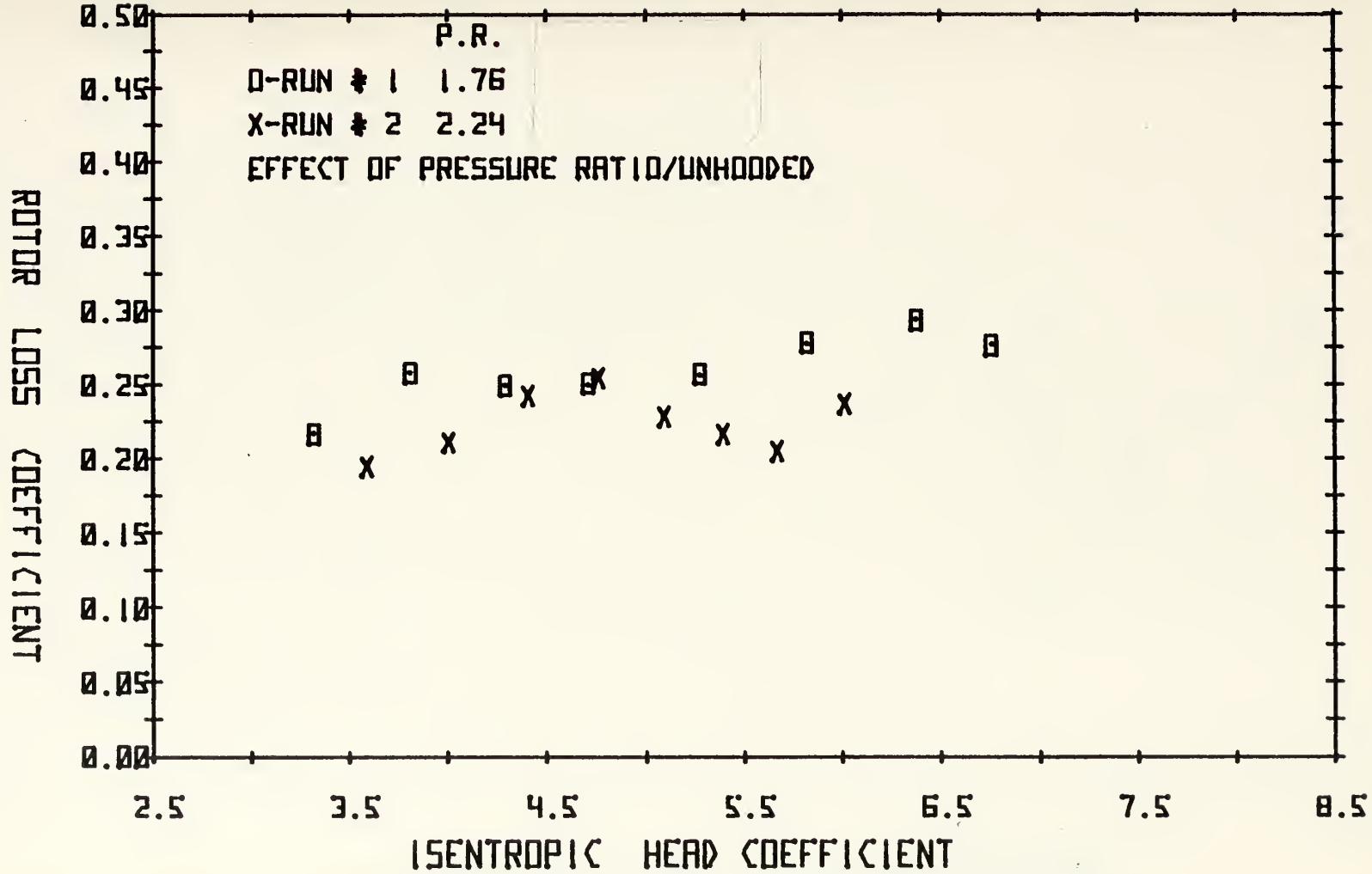

FIGURE 13a ROTOR LOSS VS. ISENTROPIC HEAD COEFFICIENT

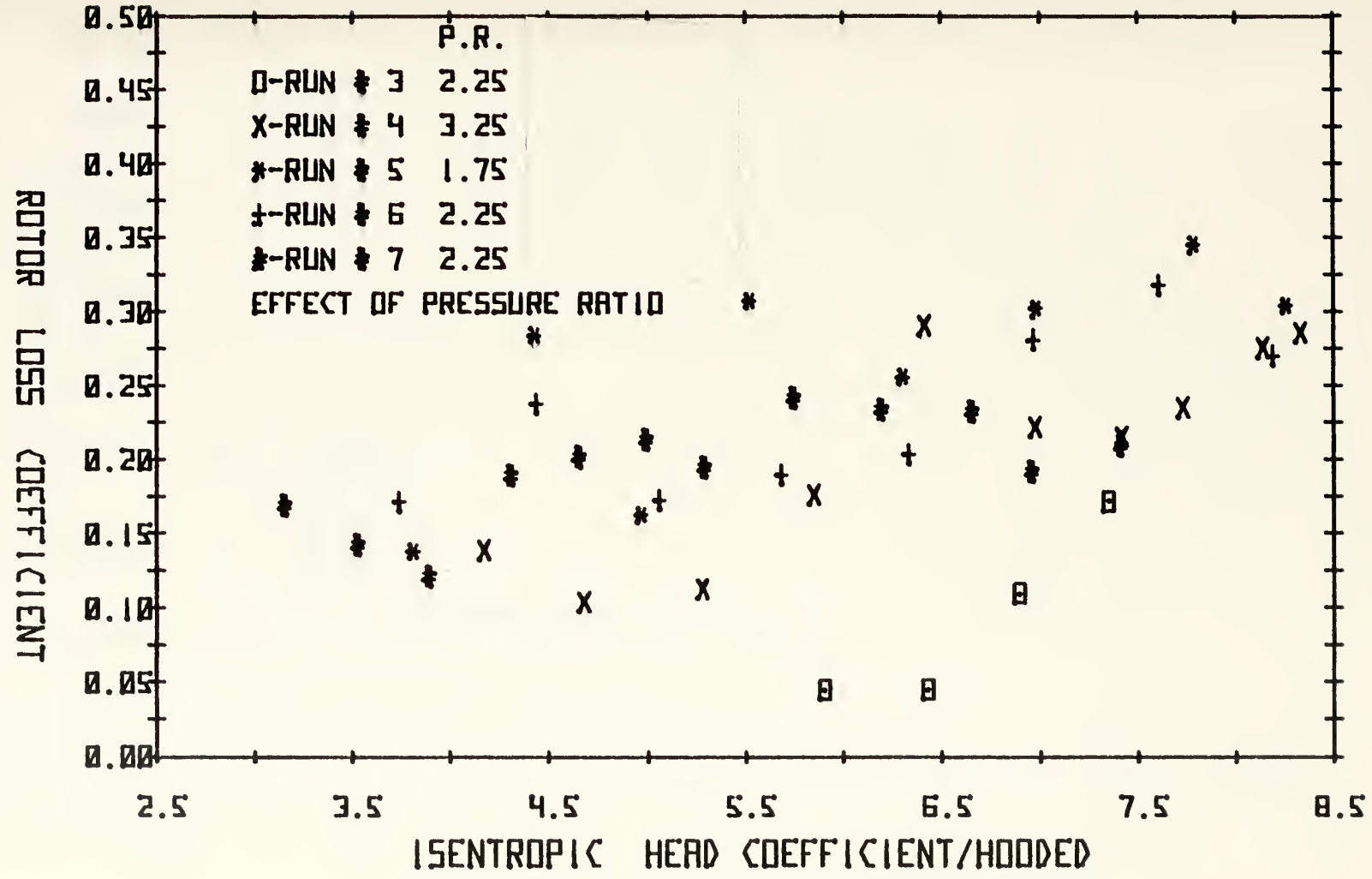

FIGURE 13b ROTOR LOSS VS. ISENTROPIC HEAD COEFFICIENT

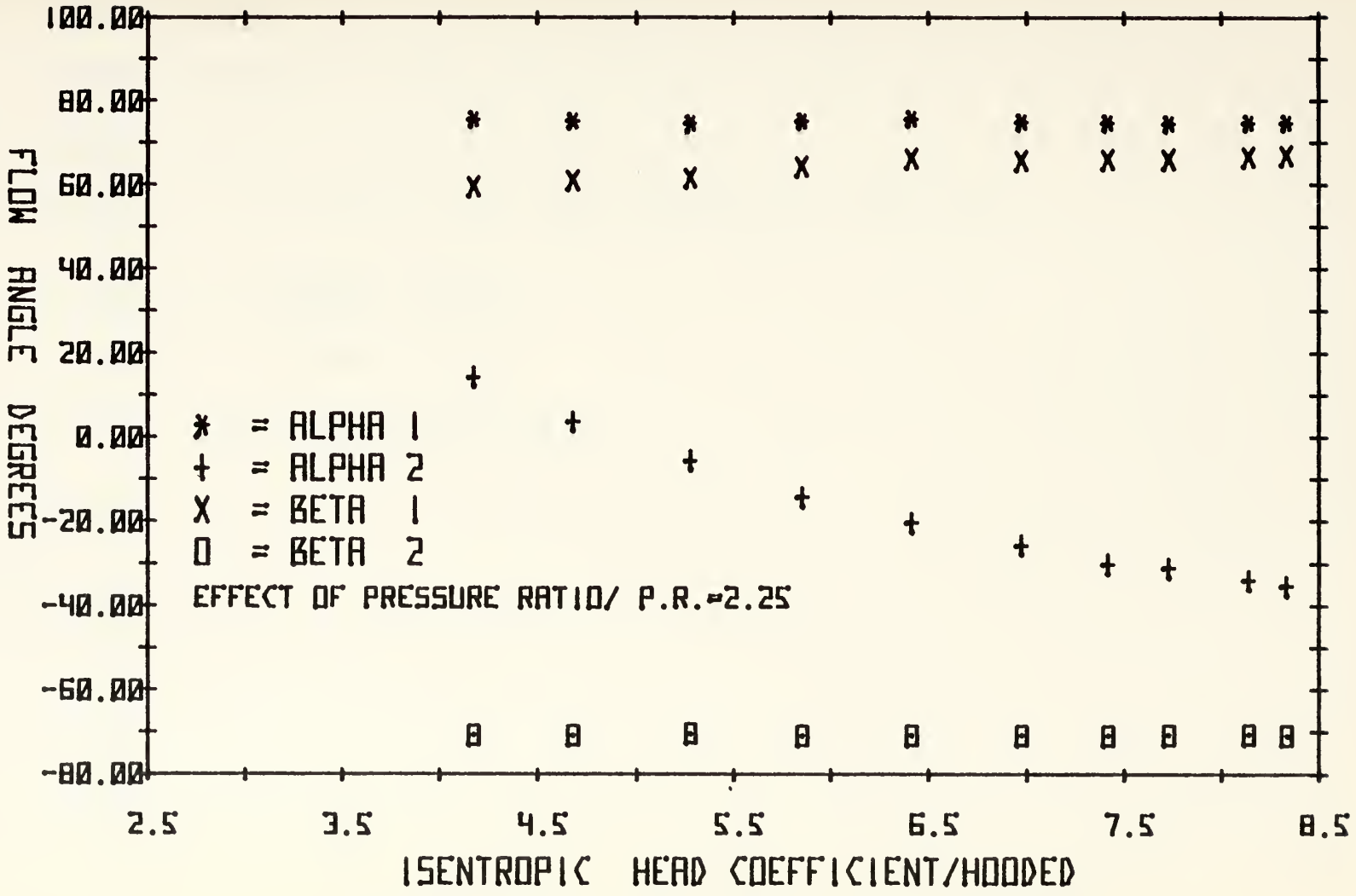

FIGURE 14 FLOW ANGLE VS. ISENTROPIC HEAD COEFFICIENT

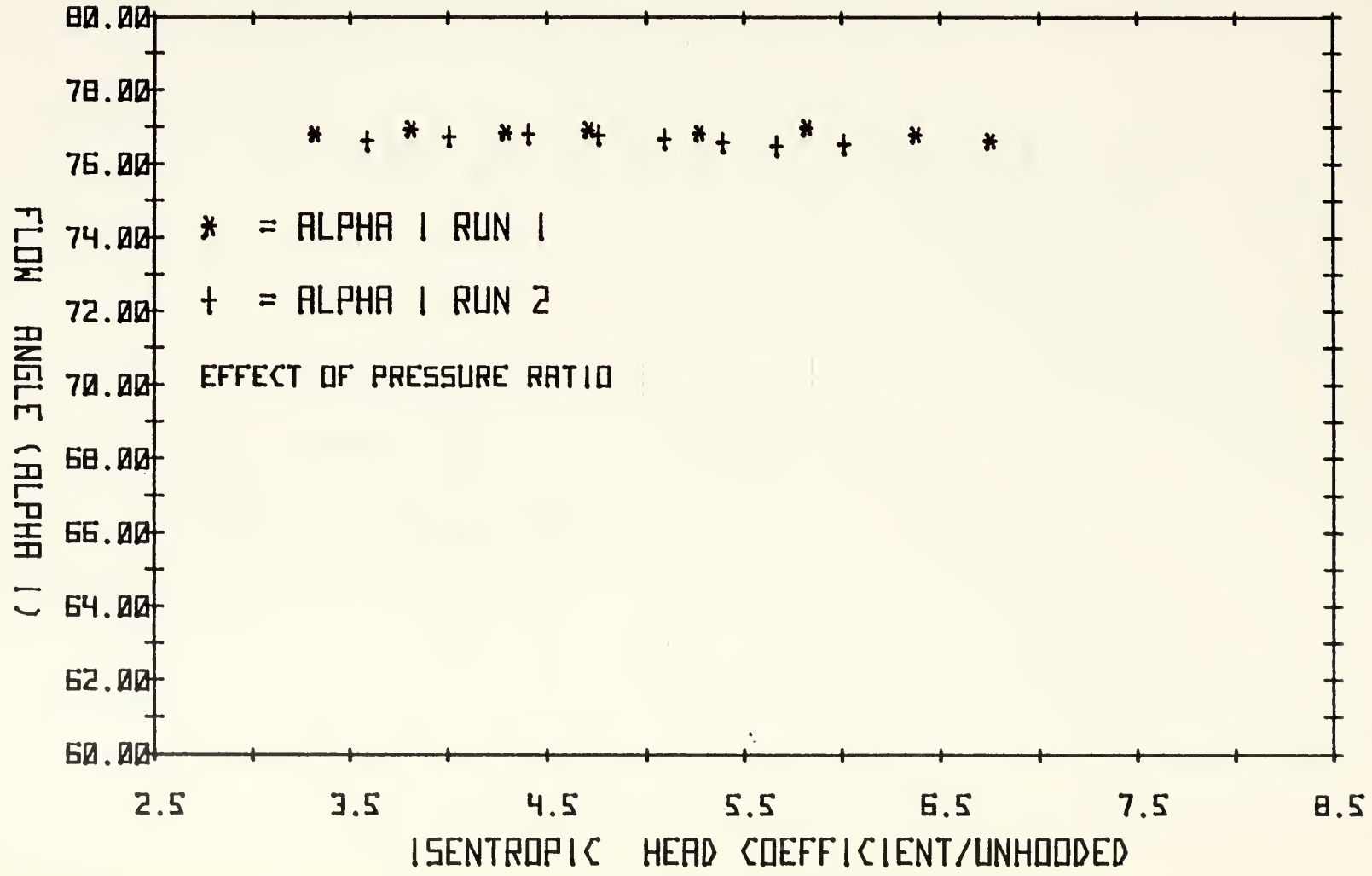

FIGURE 15a FLOW ANGLE (ALPHA 1) VS. ISENTROPIC HEAD COEFFICIENT

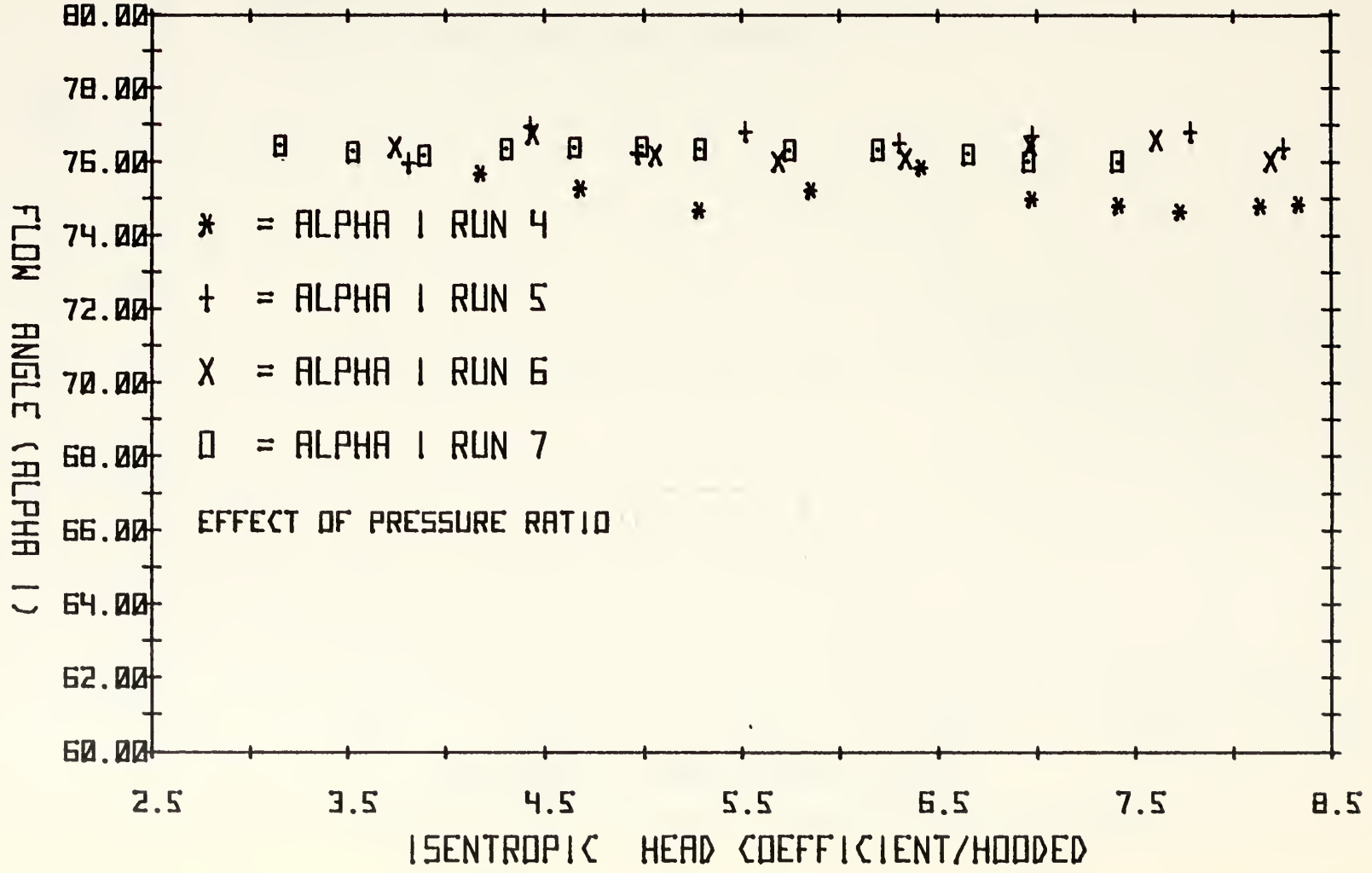

FIGURE 15b FLOW ANGLE (ALPHA 1) VS. ISENTROPIC HEAD COEFFICIENT

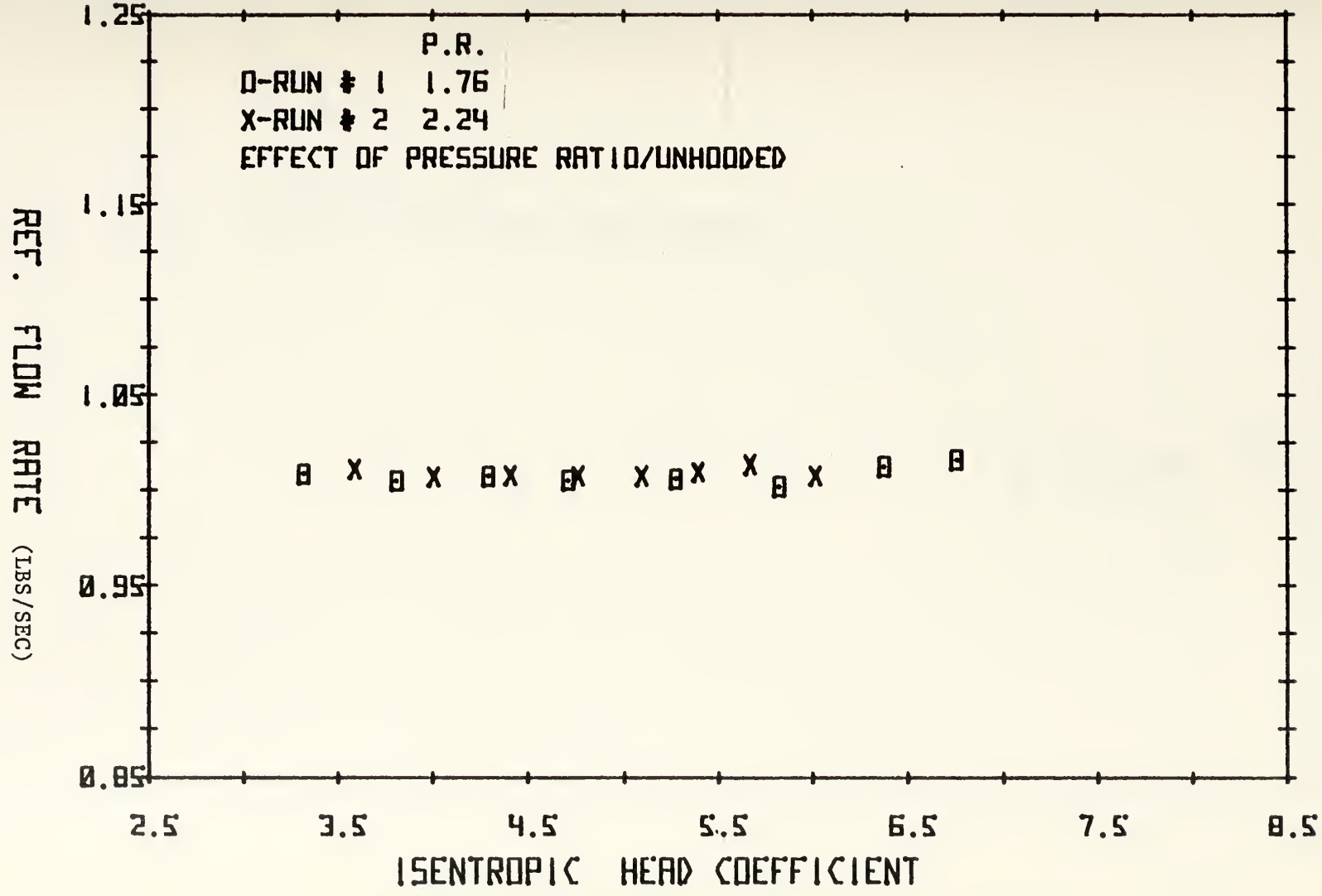

FIGURE 16a REF. FLOW RATE VS. ISENTROPIC HEAD COEFFICIENT

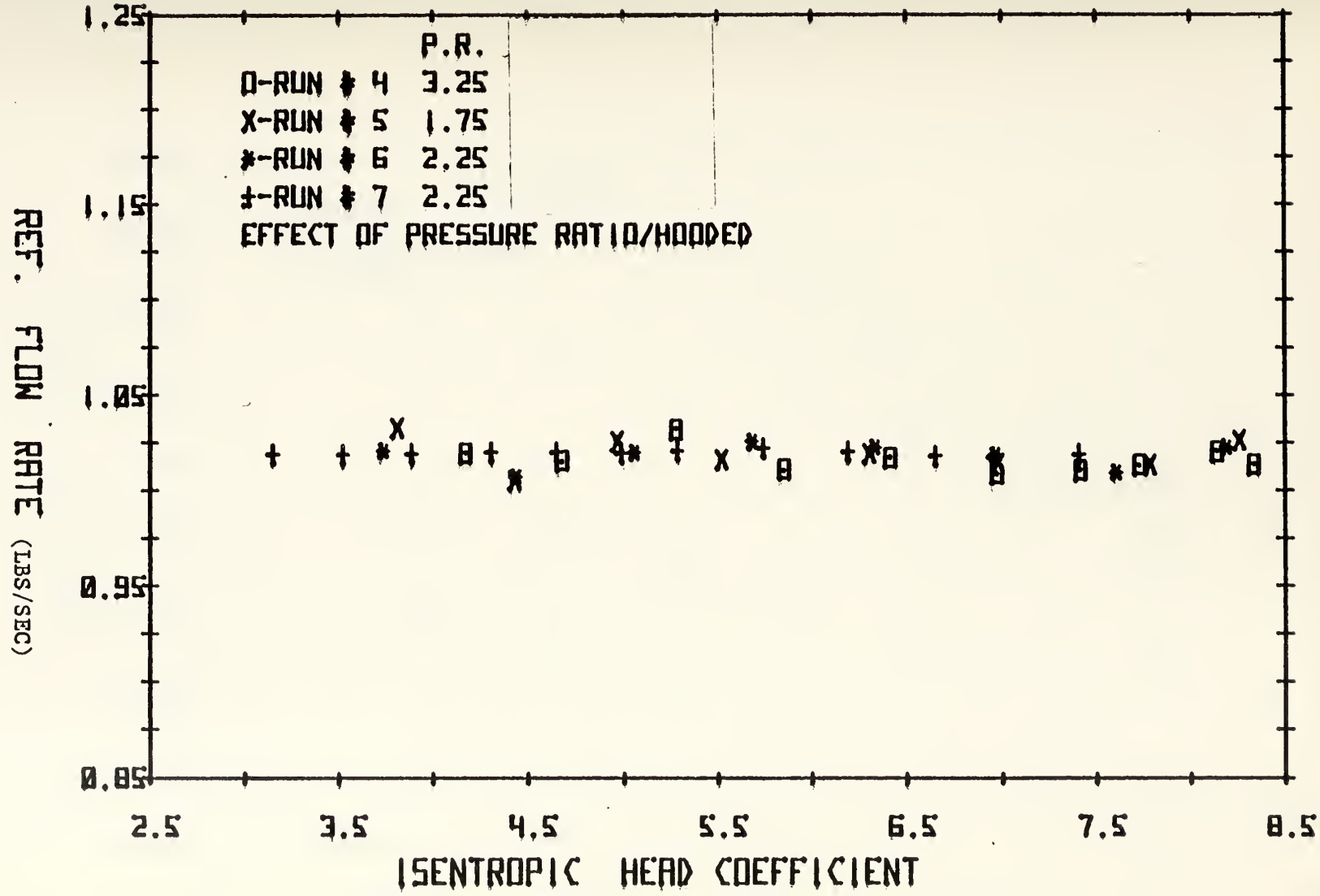

FIGURE 16b REF. FLOW RATE VS. ISENTROPIC HEAD COEFFICIENT

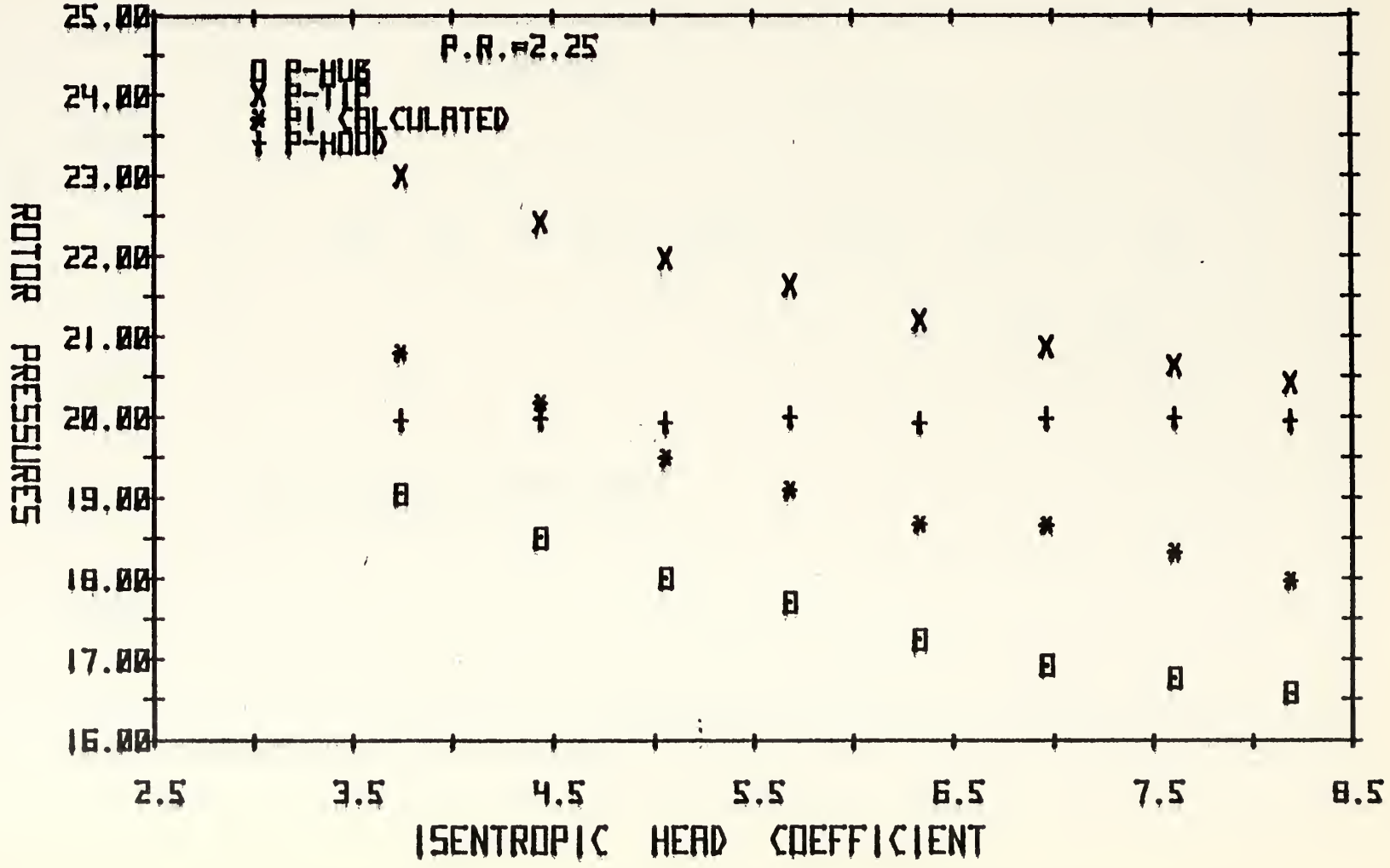

FIG. 17 CALCULATED AND MEASURED INTERSTAGE PRESSURES

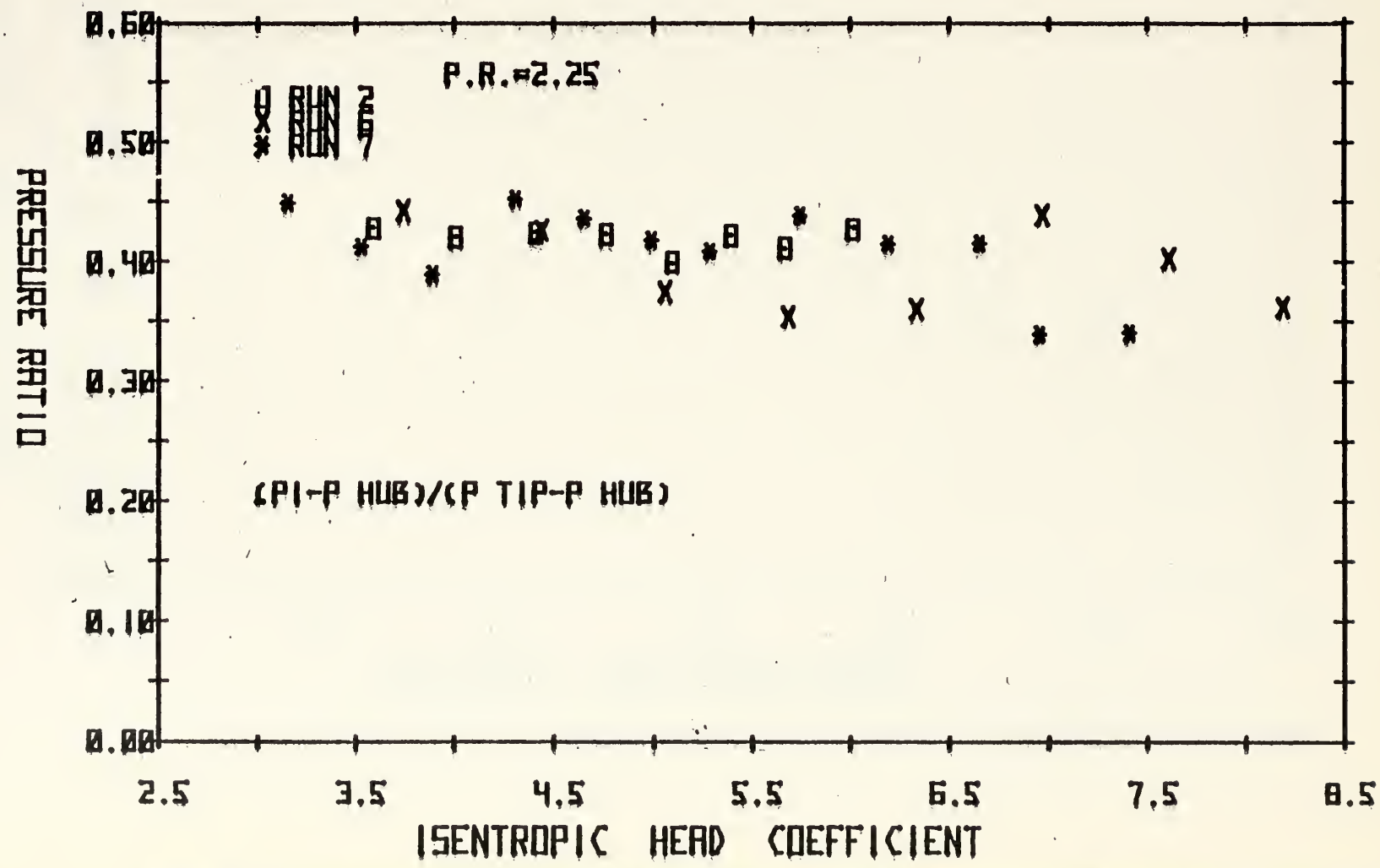

FIG. 18 CALCULATED INTERSTAGE PRESSURE AS A FRACTION OF THE HUB-TO-TIP PRESSURE DIFFERENCE

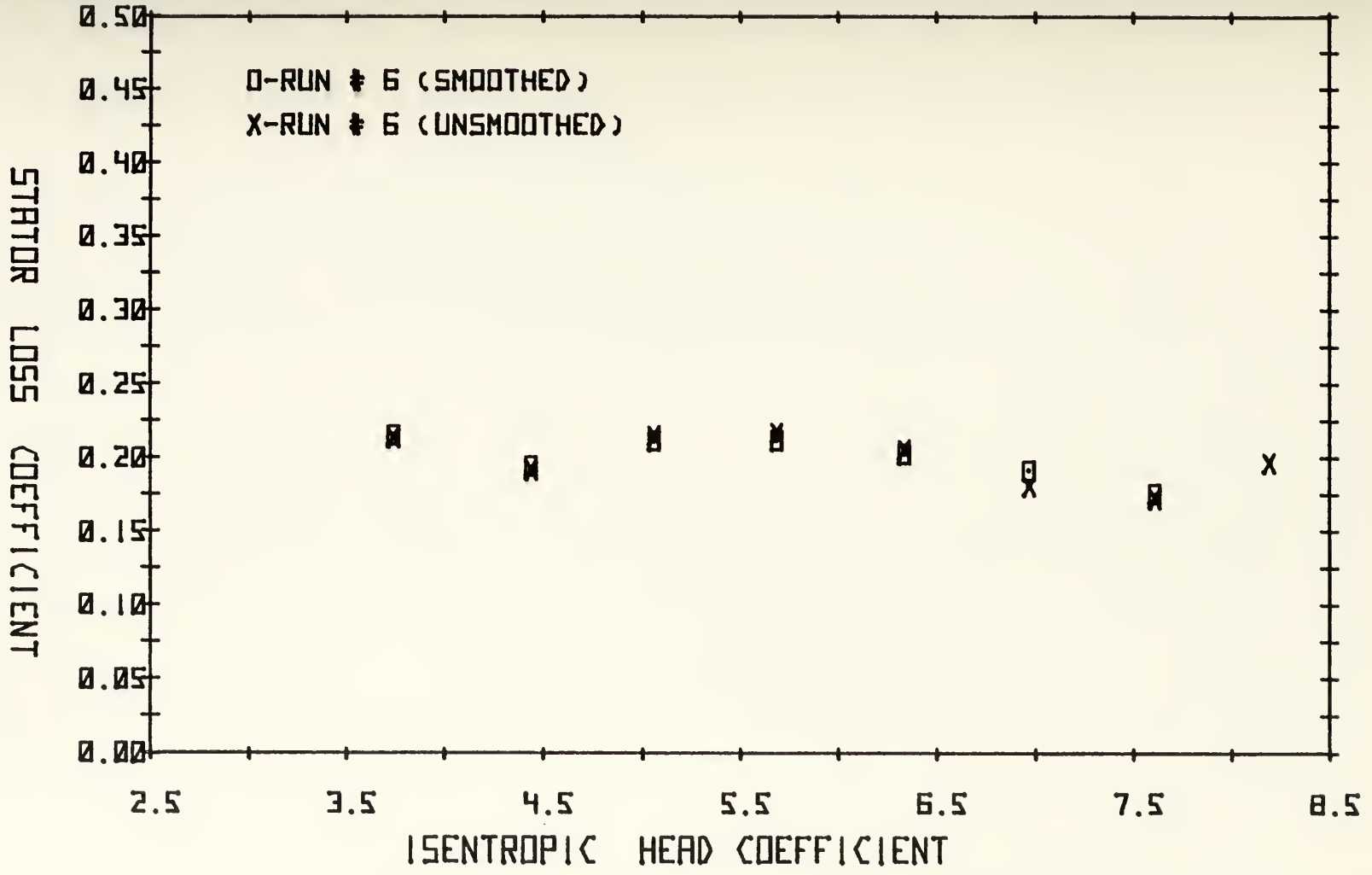

FIG. 19a EFFECT OF SMOOTHING INTERSTAGE PRESSURE ON STATOR LOSS COEFFICIENT

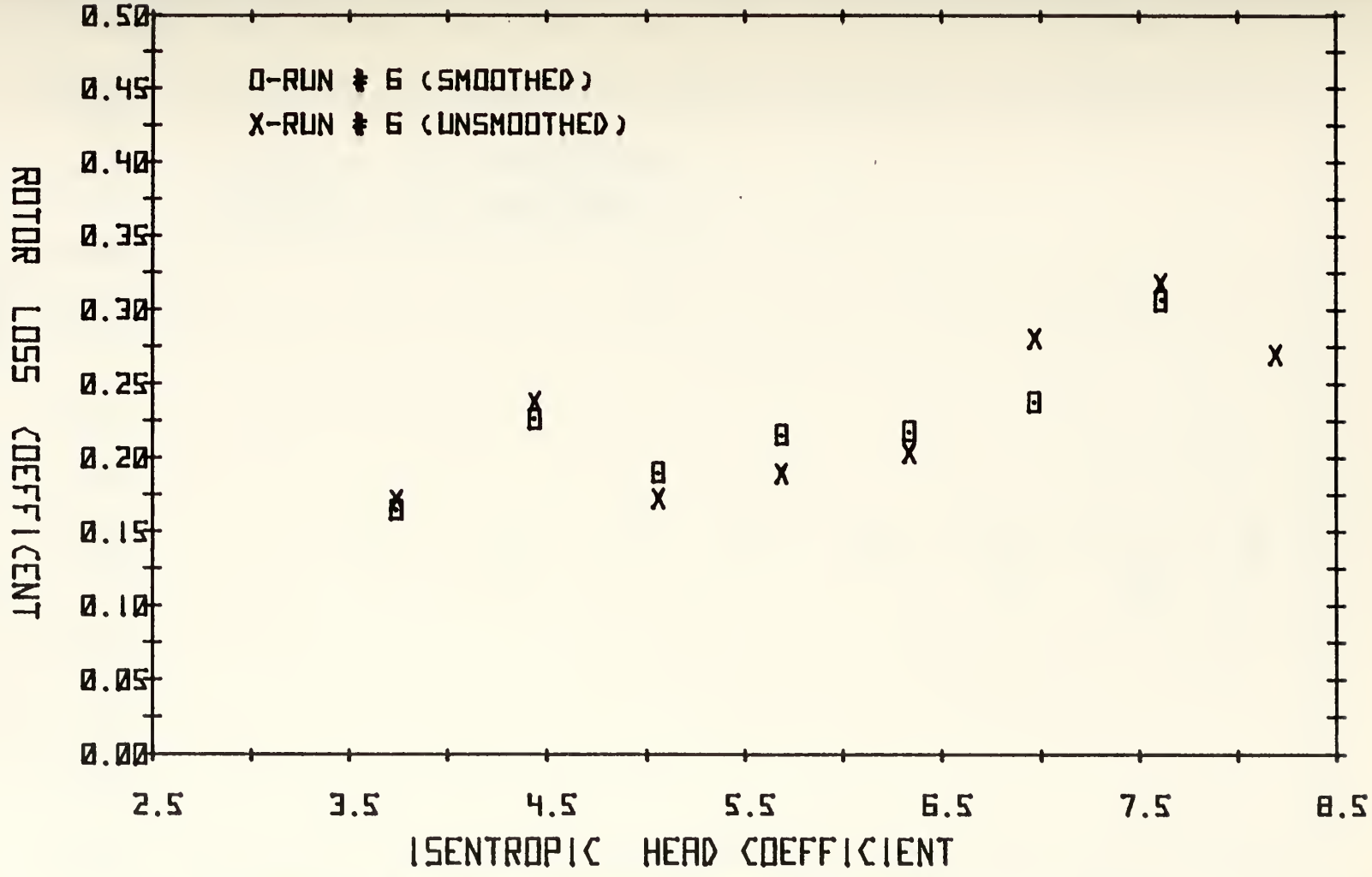

FIG. 19b EFFECT OF SMOOTHING INTERSTAGE PRESSURE ON ROTOR LOSS COEFFICIENT

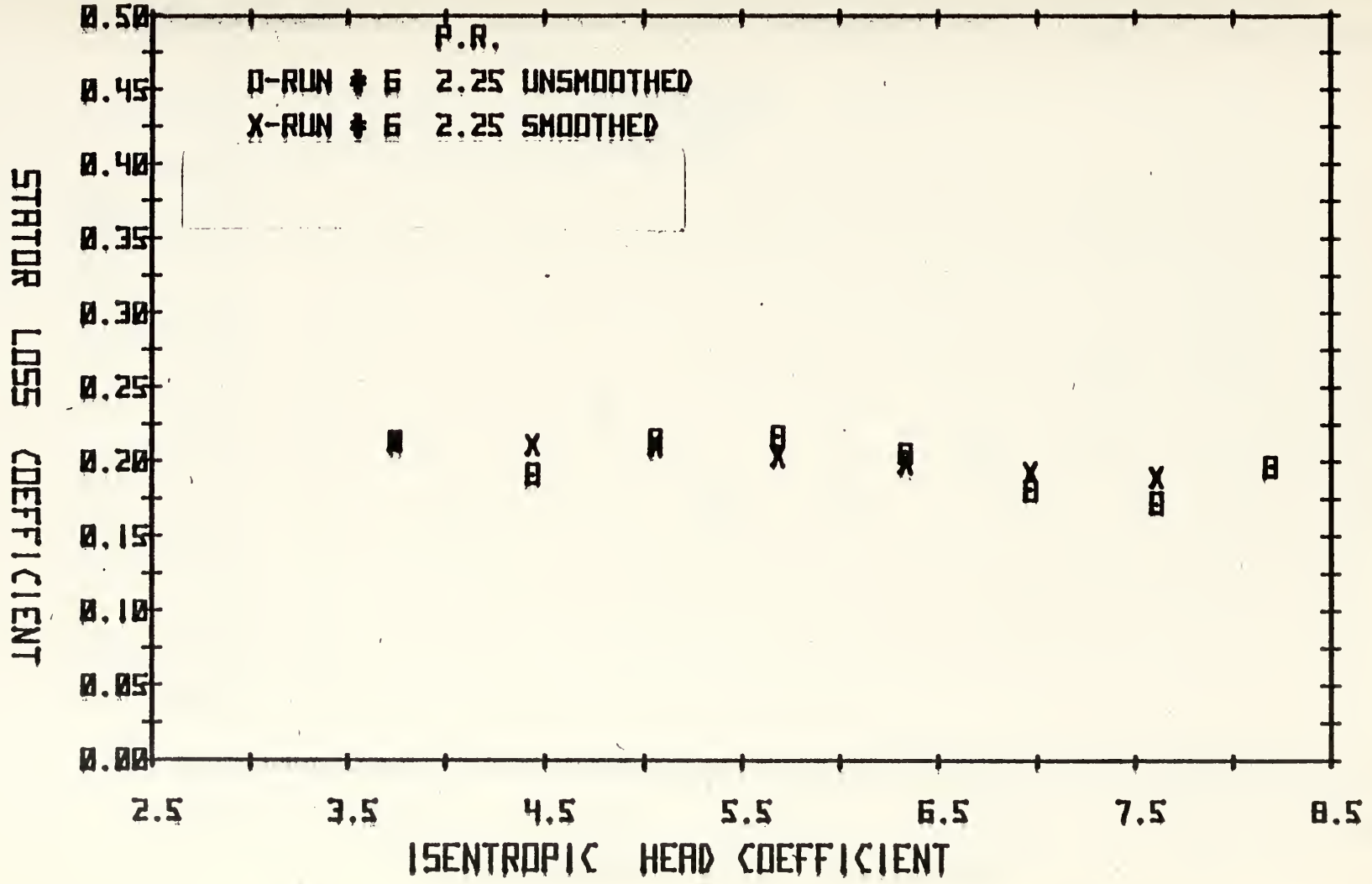

FIG. 20 EFFECT OF ASSUMING CONSTANT REFERRED FLOW RATE ON STATOR LOSS COEFFICIENT

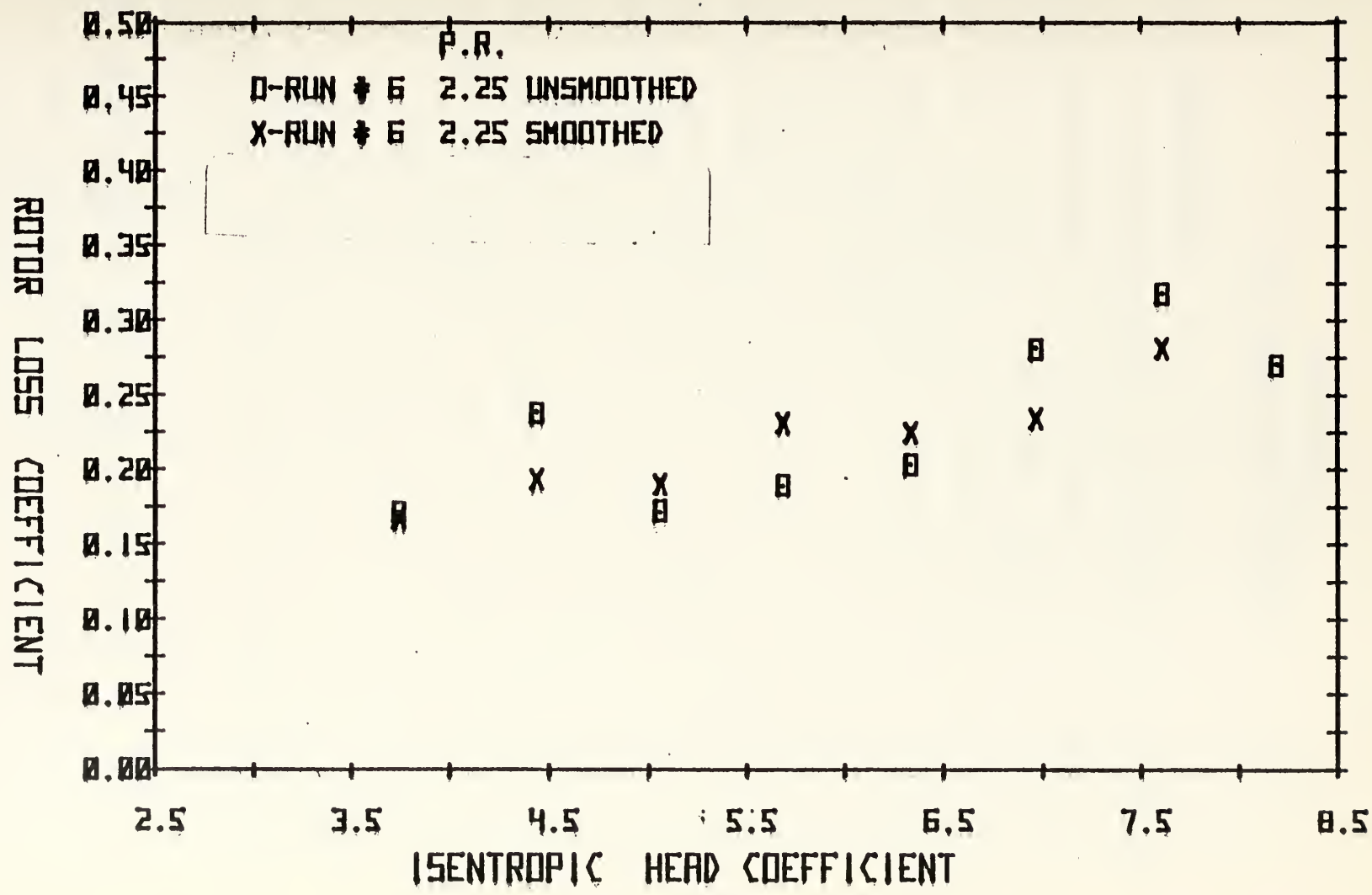

FIG. 20b EFFECT OF ASSUMING CONSTANT REFERRED FLOW RATE ON ROTOR LOSS COEFFICIENT

APPENDIX A

FLOW RATE DETERMINATION

A-1 INTRODUCTION

A precise measurement of the flow rate is necessary if the performance of an individual blade row is to be determined accurately from measurements made with the turbine test rig. Anomalies that occurred in the results from the first tests of the present supersonic turbine (Turbine C in Ref. 5) were possibly due to inaccuracies in the specified flow rates. Since the flow rate for Turbine C was smaller than for the turbines previously tested in the rig, small pressure differentials were measured with the existing nozzle. Also, the higher pressure ratios at which Turbine C was operated resulted in increased leakage through the labyrinth seals, the geometry of which might have change slightly on reassembly. Therefore, before new tests of Turbine C were begun, a new flow nozzle was provided and careful measurements were made of the labyrinth leak rate. The flow nozzle design and calibration are described in Section A-2. The labyrinth leak rate determination is given in Section A-3.

A-2 MEASUREMENTS OF THE TOTAL FLOW RATE

A-2.1 FLOW NOZZLE DESIGN

The flow nozzle is positioned in a pipe through which air is supplied to the turbine (Fig. A-1). The nozzle

generates a differential pressure to which the flow rate is related.

For a one-dimensional steady flow, the mass flow rate, $\dot{W}$, is given by

$$\dot{W} = \rho\ AV \tag{A-1}$$

where ρ is the density, V is the velocity, and A is the cross sectional area.

Using the perfect gas equation of state

$$\rho = \frac{P_t}{TR_t} \tag{A-2}$$

and Bernoulli equation

$$P_t - P = \frac{1}{2}\ \rho\ V^2 \tag{A-3}$$

Eq. (A-1) for low velocities becomes

$$\dot{W} = A\sqrt{\frac{2P_t}{RT_t}(P_t - P)} \tag{A-4}$$

The symbols P and T are pressure and temperature, respectively, and the subscript t denotes stagnation conditions. This equation, with explicit corrections for compressibility and thermal expansion, is used to calculate the flow rate through a flow nozzle from measurements of temperature and

pressures. Withe the addition of the correction factors and with conversion factors added to account for the units of measurements [Ref. 1], Eq. (A-4) becomes

$$\dot{W}_N = \frac{0.16384}{\sqrt{2.036}} D_N^2 A_N K_N Y_1 \sqrt{\frac{P_N \Delta h}{T_t}} \text{ (lbs/sec.)} \qquad \text{(A-5)}$$

where

D_N = Diameter of nozzle (inches)

A_N = Thermal expansion coefficient

Y_1 = Compressibility coefficient

P_N = Pressure at the nozzle (psia)

Δh = Water differential (in. H_2O)

T_t = Temperature (°R)

$\frac{0.16384}{\sqrt{2.036}}$ = Conversion factor

and lastly, K_N is the discharge coefficient.

The discharge coefficient accounts for the fact that the flow is not one-dimensional, and that the pressures measured are not P_t and $(P_t - P)$. Generally, the discharge coefficient has a value above 0.95 for a standard ASME nozzle at high Reynolds numbers. Establishing the relationship between Reynolds number and the discharge coefficient is what constitutes the calibration.

The flow rates expected in the supersonic turbines were 1.3 to 3.5 lbm/sec. A flow nozzle with a diameter of 3.25 inches was chosen (by applying Eq. (A-5) with unity for the coefficients) to give sutiable water column measurements of approximately 9.8 to 58.1 inches. The nozzle design followed the criteria given in Ref. 1 for "Low Beta series" designs. The geometry of the flow nozzle is shown in Fig. A-2 and views are given in Fig. A-3. The locations of the pressure taps are shown in Fig. A-2. Four throat taps are located 1.5 nozzle diameters from the nozzle face and are manifolded together. The upstream pressure is measured using taps in the upstream flange.

A-2.2 FLOW NOZZLE CALIBRATION

The discharge coefficient is given in terms of measurements, if the flow rate is determined by independent means. One of the most accurate methods of determining the flow rate of a gas is by choking the flow at a known area. This is because the mass flux is nearly uniform where choking occurs, and because the boundary layer can be kept thin in a rapid smooth contraction from a relatively large pipe. Hence, in order to determine the discharge coefficient of the new flow nozzle as a function of Reynolds number, the arrangement shown in Fig. A-4 was used.

A-2.2.1 Method

Flow nozzle calibration runs were made at controlled supply pressures from 15 psia to 45 psia. Three

different orifice plates with diameters of 1.6, 2.065, and 2.24 inches were mounted in turn to provide choked flows over the desired range of Reynolds numbers. The differential pressure at the flow nozzle was varied in increments of 2 to 4 inches of water. The range of flow rates over which the orifice plates were choked at the supply pressure was from 1.33 to 3.55 lbm/sec. The maximum pressure ratio obtained was 2.92.

A-2.2.2 Analysis

The discharge coefficient was given by Eq. (A-5), and the Reynolds number was determined by

$$Re_N = \frac{48\ \dot{W}_N\ \beta}{\pi\ D_p\ \mu} \qquad (A-6)$$

where μ is the viscosity and β is the ratio of the diameter of the nozzle to the diameter of the pipe. The flow rate, which was the same for the nozzle as for the choked plate, was determined by the following equation

$$\dot{W}_N = \Gamma \frac{P_t\ A\ K_B}{\sqrt{RT_t/g}} \qquad (A-7)$$

where

P_t = pressure at choked nozzle (psia)

A = area of choked nozzle (in^2)

K_B = blockage factor

R = gas constant (ft-lb_f/lbm - °R)

T_t = Temperature at choked nozzle (°R)

The function Γ is a known function of the specific heats and is given by

$$\Gamma = \sqrt{\gamma \left(\frac{2}{\gamma+1}\right)^{\frac{\gamma+1}{\gamma-1}}} \qquad \text{(A-8)}$$

The blockage factor K_B accounts for the boundary layer and for the axisymmetric surface; K_B is given by [Ref. 3]

$$K_B = 1 - \frac{4\delta^*}{D^*_N} \qquad \text{(A-9)}$$

where the star on D_N signifies sonic conditions, and δ^* is the boundary layer displacement thickness.

The boundary layer growth was estimated using the method of Falkner and Garner given in Ref. 6. The displacement thickness, δ^*, is given by

$$\frac{\delta^*}{s_1} = \frac{Ha^{\frac{n}{n+1}}}{Re_1^{\frac{1}{n+1}}} \psi^{\frac{n}{n+1}} \qquad \text{(A-10)}$$

where s_1 is the distance from the stagnation point to the choking station. H is the form factor, and a and n are empirical constants. ψ is a factor which depends on the pressure gradient along the surface. Re_1 is the Reynolds number based on conditions at the throat and s_1.

It is shown in Ref. 6 that the value of ψ for a similar contraction was 0.38. With $\psi = 0.38$, and with $H = 1.4$, $a = 0.0076$ and $n = 6$ for air, Eq. (A-10) becomes

$$\delta^* = \frac{0.0932174}{Re_1^{0.1429}} s_1 \qquad \text{(A-11)}$$

The Reynolds number is given by

$$Re_1 = 12 \frac{\dot{W}_n}{A_1} \frac{s_1}{\mu_1} \qquad \text{(A-12)}$$

where μ_1 is the viscosity at the throat where the temperature is 5/6 times the stagnation temperature.

For each operating condition for each orifice plate, Re_1 was calculated from Eq. (A-12) using $\dot{W}$ calculated from Eq. (A-7) with $K_B = 1.0$. δ^* was then calculated using Eq. (A-11) and K_B obtained from Eq. (A-9). $\dot{W}_N$ was recalculated from Eq. (A-7). It was found that the blockage factor could be taken to be constant with pressure for each choked plate at the following values:

PLATE #	THROAT DIAMETER	s_1 (ins.)	K_B
1.	1.6	3.51	0.9928
2.	2.065	3.10	0.9935
3.	2.24	3.22	0.9901

The flow chart for the analysis of the calibration test results is given in Fig. A-5 and the equations used are summarized in Table A-1.

A-2.2.3 Results

The nozzle calibration extended over a range of Reynolds numbers from 0.081×10^5 to 0.213×10^5. The results are given in Fig. A-6, where the data for three different orifices are shown for the range of pressures for which the flow was choked. A second order polynomial was found to represent the flow nozzle coefficient as a function of the Reynolds number.

$$K_N = 1.0272 - 0.1598 \left(\frac{Re_N}{10^6}\right) + 0.3805 \left(\frac{Re_N}{10^6}\right)^2 \quad \text{(A-13)}$$

where Re_N is given by Eq. (A-6), was used to reduce data from tests of the turbine test rig.

A-2.3 APPLICATION

The discharge coefficient is a function of Reynolds number. However, in application the flow rate is to be determined and therefore the Reynolds number is unknown. The determination of the flow rate from measurements requires the solution of three equations which have the general forms:

$$\dot{W}_N = \alpha_1 K_N \tag{A-14}$$

$$K_N = K_N (Re_N) \tag{A-15}$$

$$Re_N = \alpha_2 \dot{W}_N \tag{A-16}$$

These equations represent Eq. (A-5), Eq. (A-13), and Eq. (A-6), respectively, where α_1 and α_2 are known in terms of the geometry and measurements for any operating point. Clearly, by substituting for Re_N and K_N using Eq. (A-15), and Eq. (A-16) in Eq. (A-14), a single function for the unknown $\dot{W}$ is obtained.

An iterative procedure is used to solve the three equations for the unknown flow rate. The procedure is given in Appendix B.

A-3 MEASUREMENT OF THE LABYRINTH LEAK RATE

A-3.1 Labyrinth Leak Rate Calibration Test

Since the leak rate of the plenum labyrinth cannot be measured during turbine operations, the relationship of the leakage flow rate to supply and hood pressures and supply temperature was determined in a separate calibration test. For this test, the main flow through the turbine was blocked by a plate and the labyrinth was allowed to leak into the hood as in normal operation. The flow was passed through a two-inch pipe (Fig. A-4b & Fig. A-1), containing an ASME standard sharp-edged orifice. The usual supply pipe was

blocked. The flow was discharged through the labyrinth seal into the hood in which the pressure was controlled by the ejector.

In determining the leakage rate using the ASME orifice, vena contracta taps were used. The differential pressure was measured in inches of water on a manometer which had 0.1-inch graduations. The upstream pressures in the labyrinth and in the nozzle were measured in inches of mercury on U-tube manometers with atmospheric pressure as a reference. The supply pressure was varied from 14 to 83 psia, while the differential pressure across the vena contracta taps varied from 2.75 to 37.3 inches of water. The maximum pressure ratio across the labyrinth was 5.6.

A-3.2 Calculation of the Leakage Flow Rate

Since the flow orifice was in a standard installation according to the criteria given in Ref. 1, Table 5 of Ref. 1 was used to obtain the discharge coefficient as a function of Reynolds number. In order to program the data reduction, the data of Table 5, for the appropriate values of Beta, were first approximated in the range of Reynolds numbers from 8,000 to 1,000,000 by a polynomial as shown in Fig. A-7. The discharge coefficient at each operating point was then given by

$$K_N = 0.603698259 + 0.004688755 \left(\frac{10^5}{Re_N}\right) \qquad \text{(A-17)}$$

$$- 1.250025 \times 10^{-3} \left(\frac{10^5}{Re_N}\right)^2 + 2.0320771882 \times 10^{-4} \left(\frac{10^5}{Re_N}\right)^3$$

$$- 1.56980769 \times 10^{-5} \left(\frac{10^5}{Re_N}\right)^4 + 4.5277098 \times 10^{-7} \left(\frac{10^5}{Re_N}\right)^5$$

The flow rate was calculated at each point using Eq. (A-5), using the expressions for the compressibility and thermal expansion coefficients given in Table A-2, and the discharge coefficient given by Eq. (A-17).

A-3.3 Analysis of the Results

A-3.3.1 Simple Method

A non-dimensional flow rate, or flow function, for the flow through the labyrinth can be defined as

$$\Phi = \frac{\dot{W}_L \sqrt{(R/g)\ T_L}}{P_L\ A_L} \qquad \text{(A-18)}$$

During the calibration tests, the stagnation pressure (P_L) was varied in steps for constant values of the hood pressure (P_h). The stagnation temperature was approximately constant. The flow function was calculated for each operating point using Eq. (A-18) and the values plotted as a function of the pressure ratio (P_h/P_L). The results are given in Fig. A-8.

A second order polynomial was found to fit the data to an accuracy of ± 4% as shown in Fig. A-8:

$$\Phi = 0.2721 + 0.0365\ (P_h/P_L) - 0.2357\ (P_h/P_L)^2 \qquad \text{(A-19)}$$

While Eq. (A-19) represents the calibration tests results quite well, it is an empirical result for a limited variation in test parameters. Operation at different temperatures, for example, could give a different behavior.

A-3.3.2 Use of the Kinetic Energy Factor

It is shown in Ref. 7 that, under reasonable assumptions, the flow through a labyrinth with many teeth (N) can be represented by

$$\Phi = \beta\ Ke \qquad \text{(A-20)}$$

where

$$\beta = \sqrt{\frac{1-(P_h/P_L)^2}{N-Ln\,(P_h/P_L)}} \qquad \text{(A-21)}$$

and Ke is the "Kinetic Energy Factor". Here, the dependence of the leak rate on the upstream and downstream pressures (β) has been obtained analytically. The Kinetic Energy Factor is a measure of how much kinetic energy is recovered as stagnation pressure as the flow passes successive teeth. It is expected to be a function of Reynolds number, and hence would include the correct behavior with stagnation temperature.

The geometry of the labyrinth is given in Fig. A-9. Using the notation in Fig. A-9, the Reynolds number for the leakage flow is given by

$$Re_L = \frac{12\ \dot{W}_L\ C}{A_L\ \mu_L} \qquad \text{(A-22)}$$

where

$$A_L = 2\ \pi\ D\ C \qquad \text{(A-23)}$$

and μ_L is the viscosity based on the labyrinth supply temperature, T_L.

For the flow rates obtained in the calibration tests, Φ was obtained from Eq. (A-18). β was calculated using Eq. (A-21) and Ke determined using Eq. (A-20). The Reynolds number was obtained using Eq. (A-22) with Eq. (A-23). The Kinetic Energy Factor was plotted as a function of the Reynolds number and the result is shown in Fig. A-10. A fourth order polynomial was found to fit the data to an accuracy of ± 2%:

$$Ke = 0.601373889 + 4.36695141 \times 10^{-4} \left(\frac{Re}{10^3}\right) - 2.4530860 \times 10^{-7} \left(\frac{Re}{10^3}\right)^2 + 6.5672233 \times 10^{-11} \left(\frac{Re}{10^3}\right)^3 - 6.086573 \times 10^{-15} \left(\frac{Re}{10^3}\right)^4 \qquad \text{(A-24)}$$

It is noted that the use of Eq. (A-24) and Eq. (A-21) gives a factor of two improvement in accuracy over the use of the purely empirical result given as Eq. (A-19). Also, the dependence of the Kinetic Energy Factor on the supply temperature is at least partially included in the representation as a function of Reynolds number.

The flow chart for the calibration data reduction is given in Fig. A-11 and a summary of the equations is given in Table A-2.

A-3.2 APPLICATION

In order to use Eq. (A-24) to calculate the leak rate at a given operating point, an iterative procedure is necessary since the Reynolds number is again a function of the flow rate. The procedure is similar to that followed in calculating the total flow rate (Section A-2.3) and is described in Appendix B.

TABLE A-1

SUMMARY OF FORMULAS FOR NOZZLE CALIBRATION DATA REDUCTION PROGRAM

FLOW RATE	$\dot{W}_N = \frac{0.16384}{\sqrt{2.036}} D_N^2 A_N K_N Y_1 \sqrt{\frac{P_N \Delta h}{T_N}}$
THEMAL EXPANSION COEFFICIENT	$A_N = 1+0.00193 \left[\frac{T_N - 528}{100} \right]$
COMPRESSIBILITY COEFFICIENT	$Y_1 = 1 - 0.05246 \left[0.41 + 0.35\beta^4 \right] \frac{\Delta h}{P_N}$
BETA	$\beta = \frac{D_N}{D_p}$, $D_N = 3.25$ ins., $D_p = 7.975$ ins
VISCOSITY	$\mu = \frac{1.153 \times 10^{-5} \times 0.06333 \; T_N}{198.72 / T_N + 1}$
REYNOLDS NUMBER:	$R_{e_N} = \frac{48 \dot{W} \beta}{\Pi D_p \mu}$
FLOW FUNCTION:	$\Gamma = \sqrt{\gamma \left[\frac{2}{\gamma + 1} \right]^{\frac{\gamma+1}{\gamma-1}}}$
BLOCKAGE FACTOR:	$K_B = 1 - \frac{4\delta^*}{D_N^*}$
BOUNDARY LAYER THICKNESS	$\delta^* = \frac{0.21364}{Re_1^{0.129}} (0.38)^{6/7} s_1$
REYNOLDS NUMBER:*	$Re_1 = 12 \frac{\dot{W} s_1}{A_1 \mu_1}$
FLOW RATE CHOKED NOZZLE	$\dot{W} = \frac{P_t A K_B}{\sqrt{RT_t/g}} \Gamma$

TABLE A-2

SUMMARY OF FORMULAS FOR LABYRINTH CALIBRATION REDUCTION PROGRAM

FLOW FUNCTION:	$\Phi = \dfrac{2.036\ \dot{W}_L \sqrt{\dfrac{RT_t}{g}}}{P_L\ A_L}$
FLOW RATE:	$\dot{W}_L = \dfrac{0.16384}{\sqrt{2.036}}\ D_N^{\,2}\ A_N\ K_N\ Y_1 \sqrt{\dfrac{P_t \Delta h}{T_t}}$
BETA:	$\beta = \sqrt{\dfrac{1 - \left(\frac{P_h}{P_L}\right)^2}{N - \text{Log}\ (P_h / P_L)}}$ $\qquad N = 10$
REYNOLDS NUMBERS:	$Re_L = \dfrac{12\ \dot{W}_L\ C}{A_L\ \mu}$
AREA LAB:	$A_L = 2\pi\ D\ c$
KINETIC ENERGY FACTOR:	$Ke = \dfrac{\Phi}{\beta}$
THERMAL EXPANSION COEFFICIENT:	$A_N = 1 + 0.00193 \left[\dfrac{T_N - 528}{100}\right]$
COMPRESSIBILITY COEFFICIENT:	$Y_1 = 1 - 0.05246\ (0.41 + 0.35\beta^4)\ \dfrac{\Delta h}{P_N}$
BETA:	$\beta = \dfrac{D_N}{D_P}$, $D_N = 3.25$ ins., $D_p = 7.975$ ins.
VISCOSITY:	$\mu = \dfrac{1.153 \times 10^{-5} \times 0.06333\sqrt{T_N}}{198.72 / T_N + 1}$

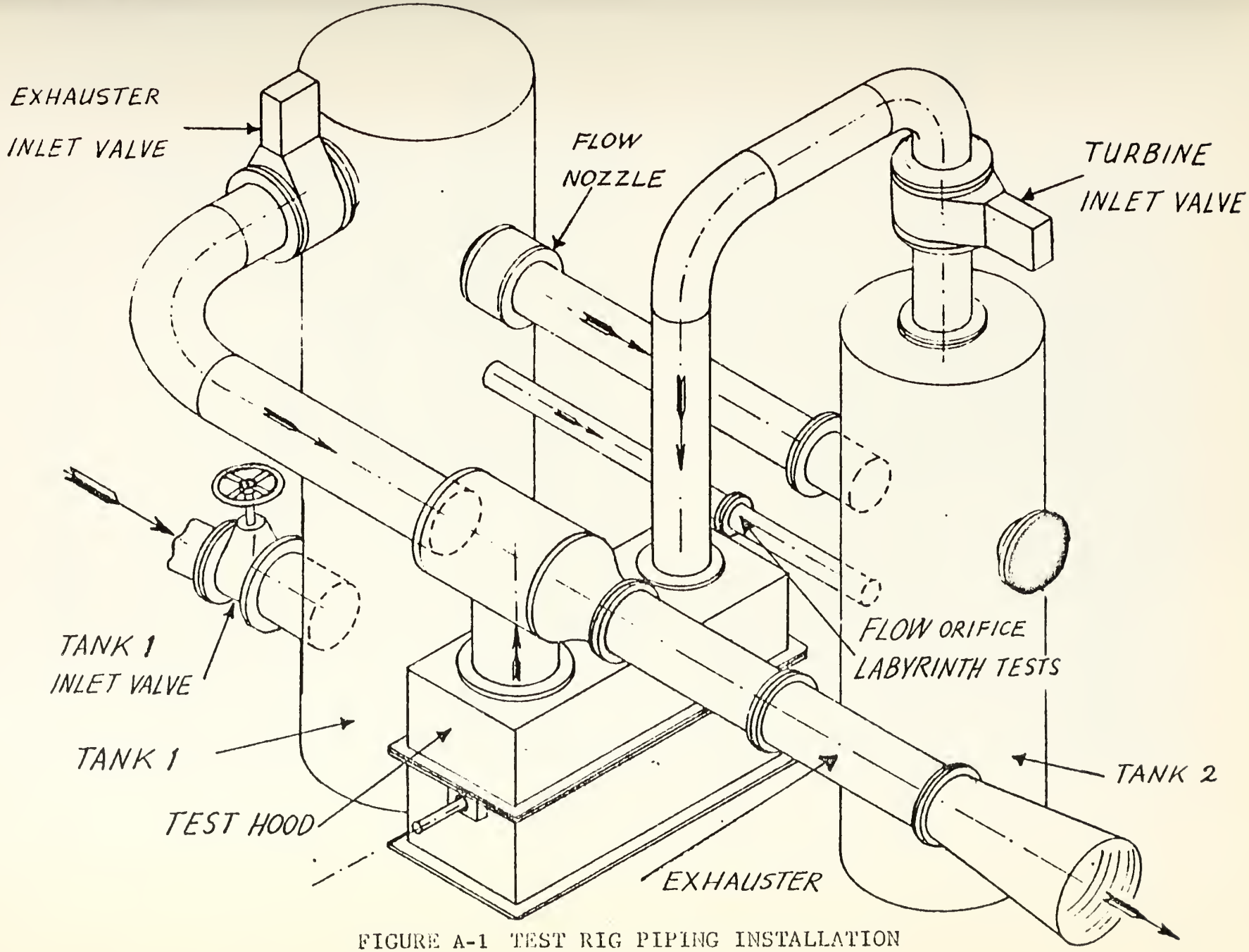

FIGURE A-1 TEST RIG PIPING INSTALLATION

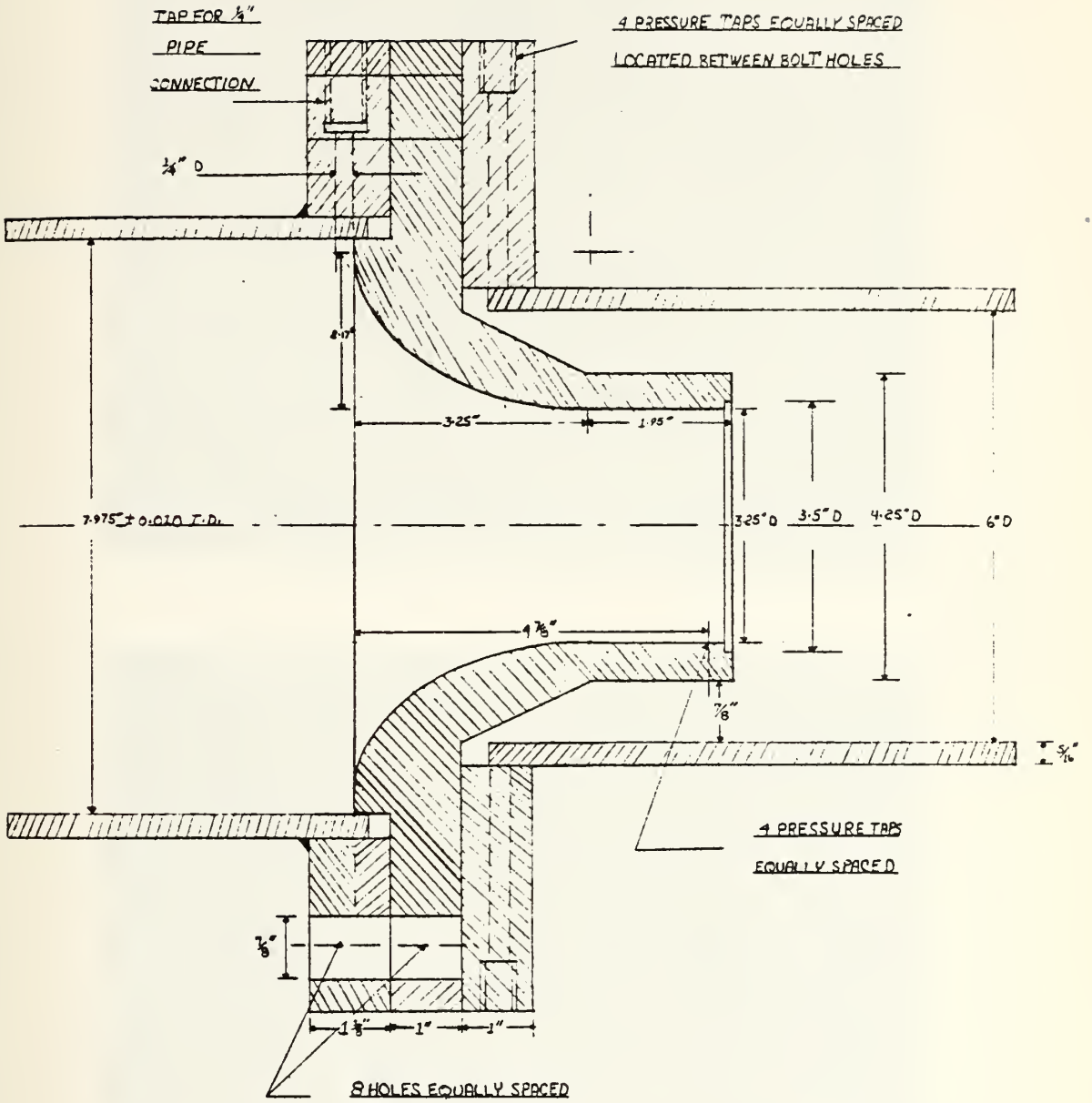

FIG. A-2 FLOW NOZZLE GEOMETRY

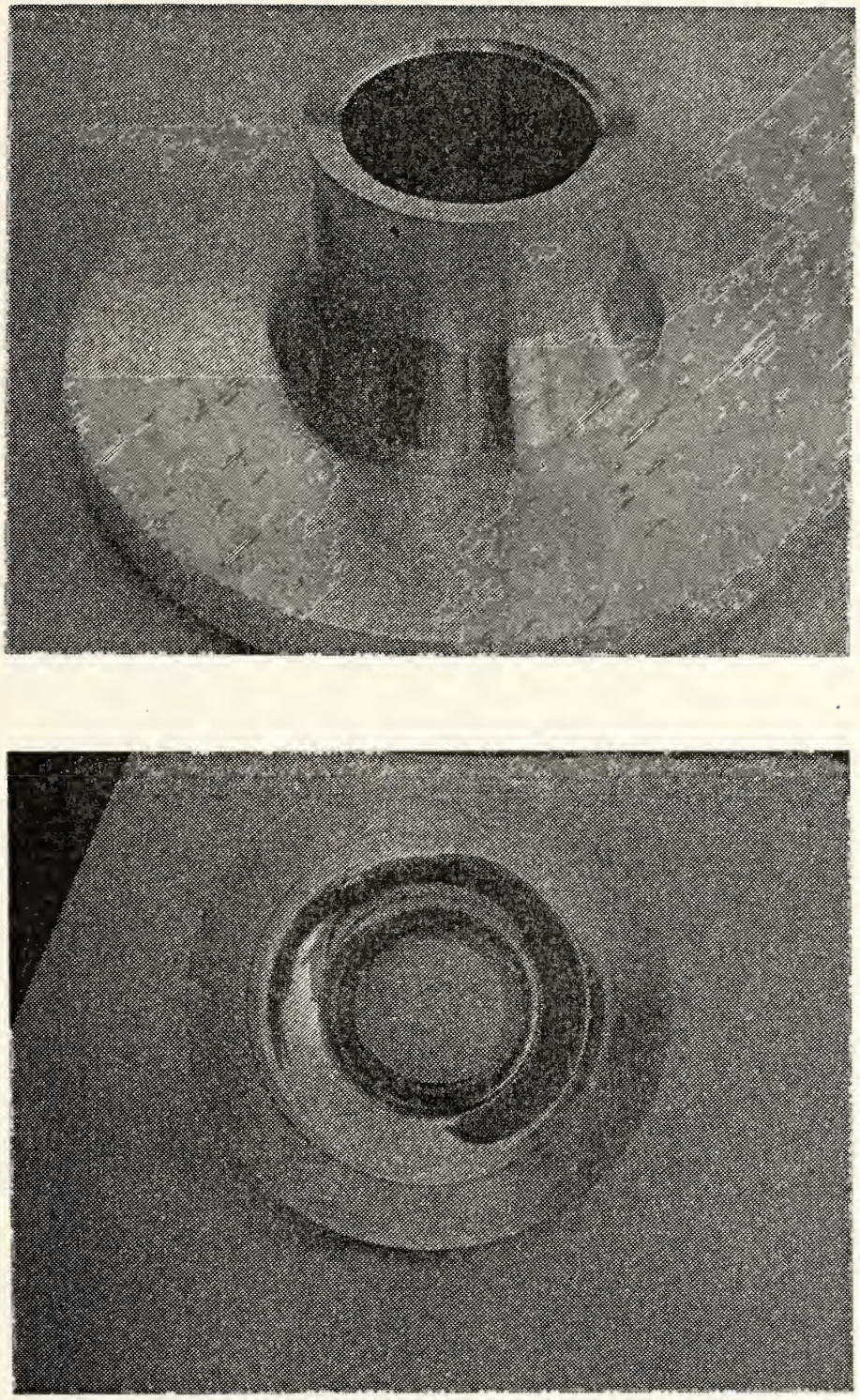

FIG. A-3 VIEWS OF THE FLOW NOZZLE

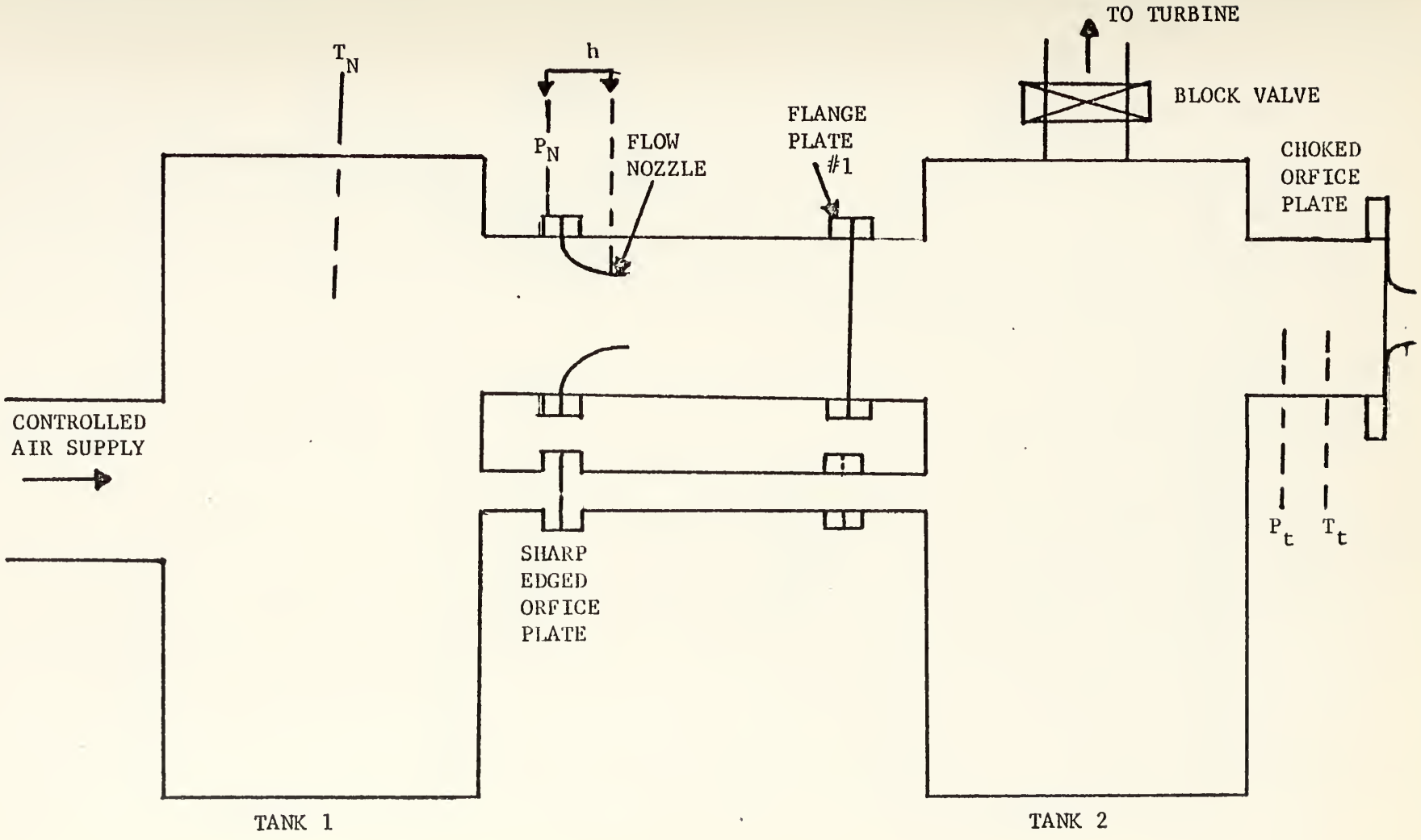

FIG. A-4a PIPING ARRANGEMENT FOR LABYRINTH LEAKAGE CALIBRATION TESTS

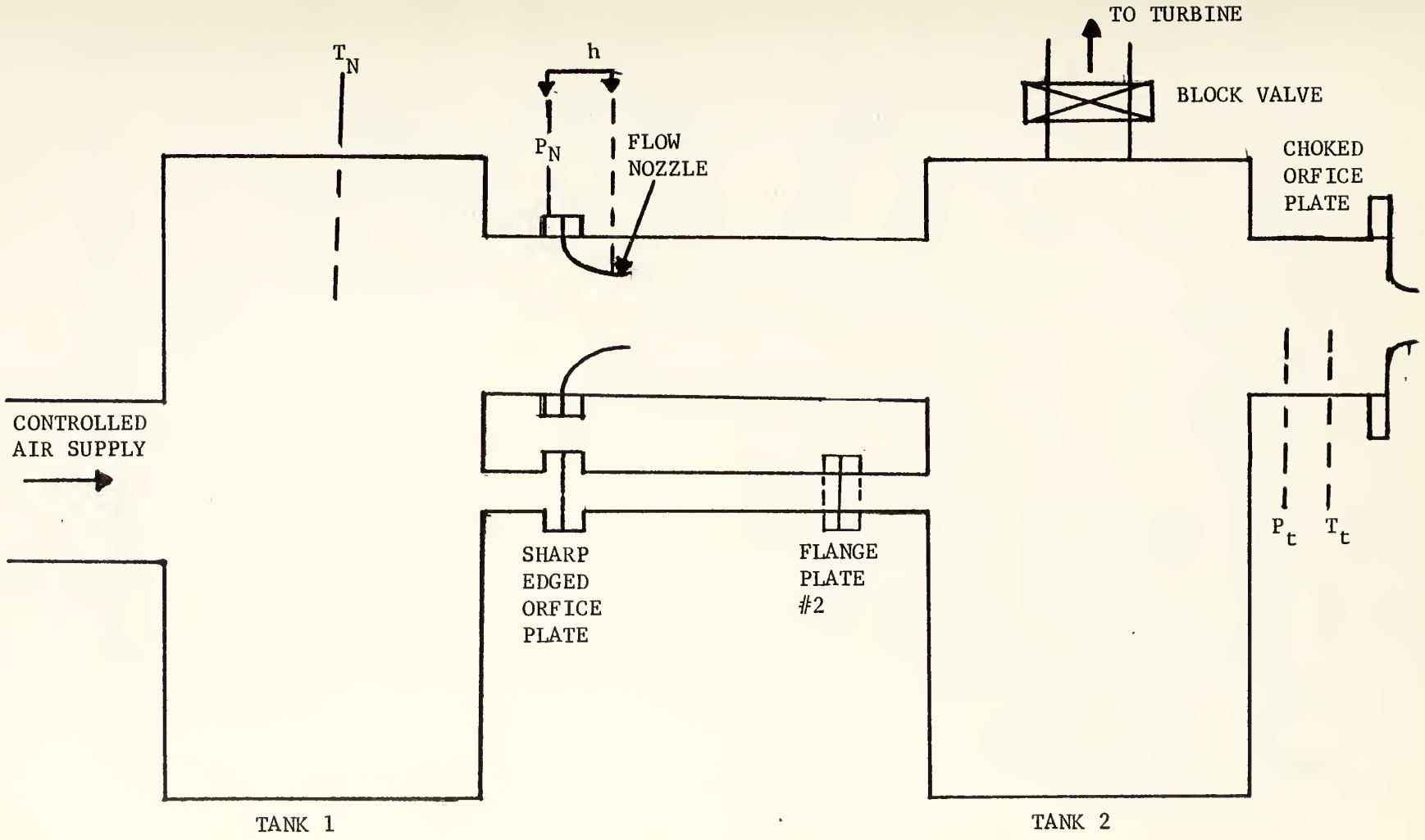

FIG. A-4b PIPING ARRANGEMENT FOR FLOW NOZZLE CALIBRATION TESTS

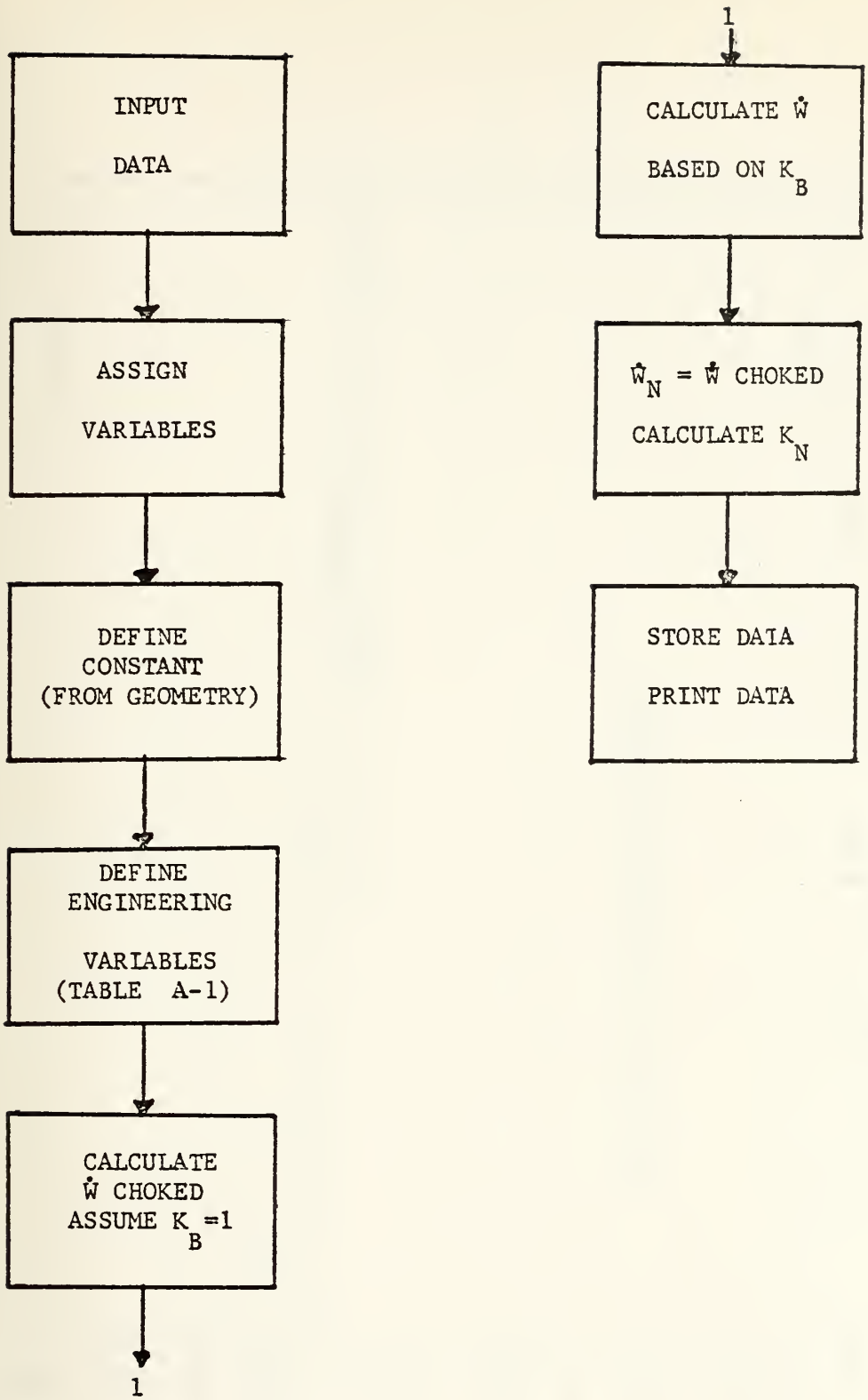

FIG. A-5 FLOW NOZZLE CALIBRATION DATA REDUCTION FLOW CHART

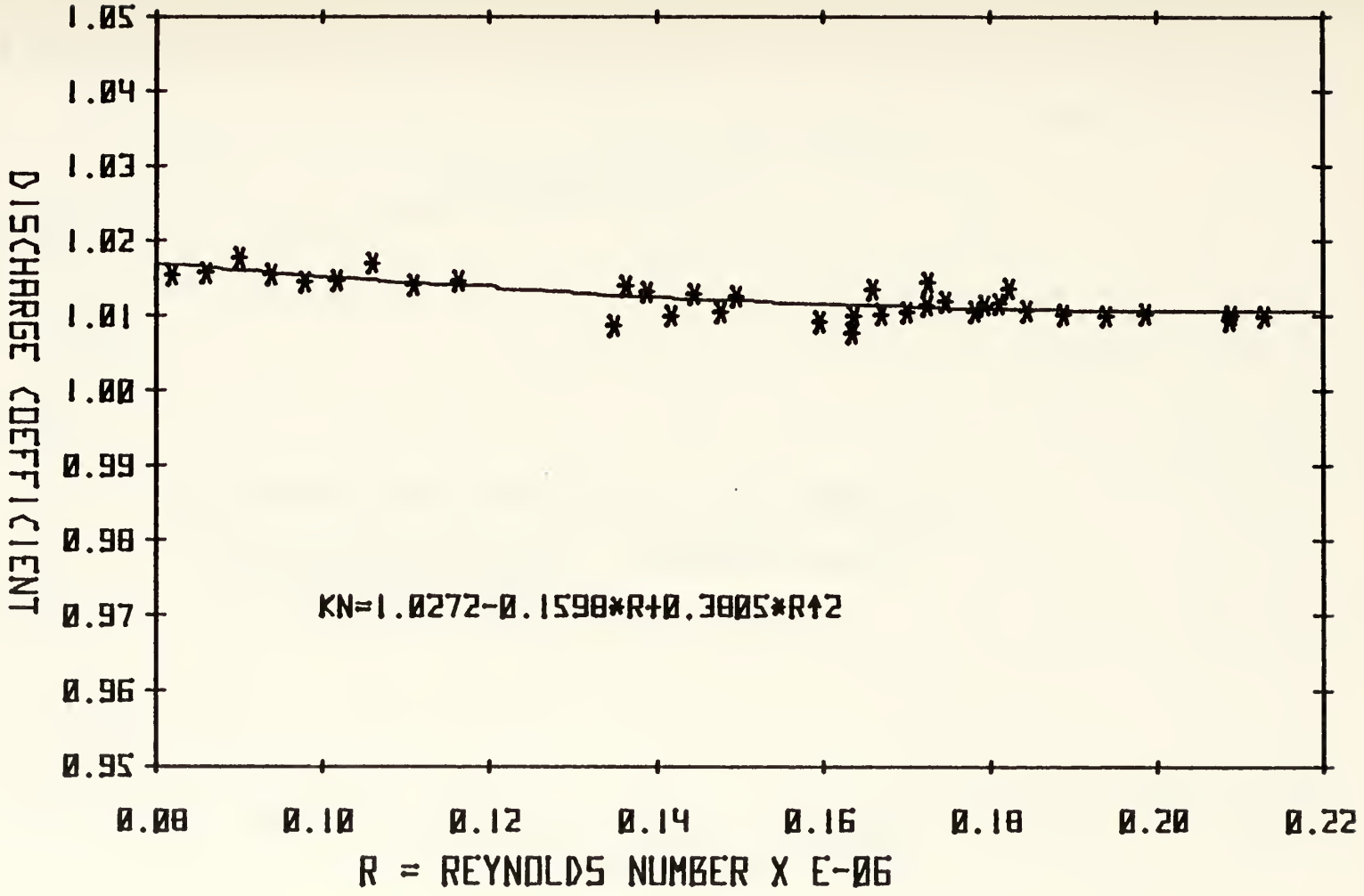

FIG. A-6 FLOW NOZZLE CALIBRATION

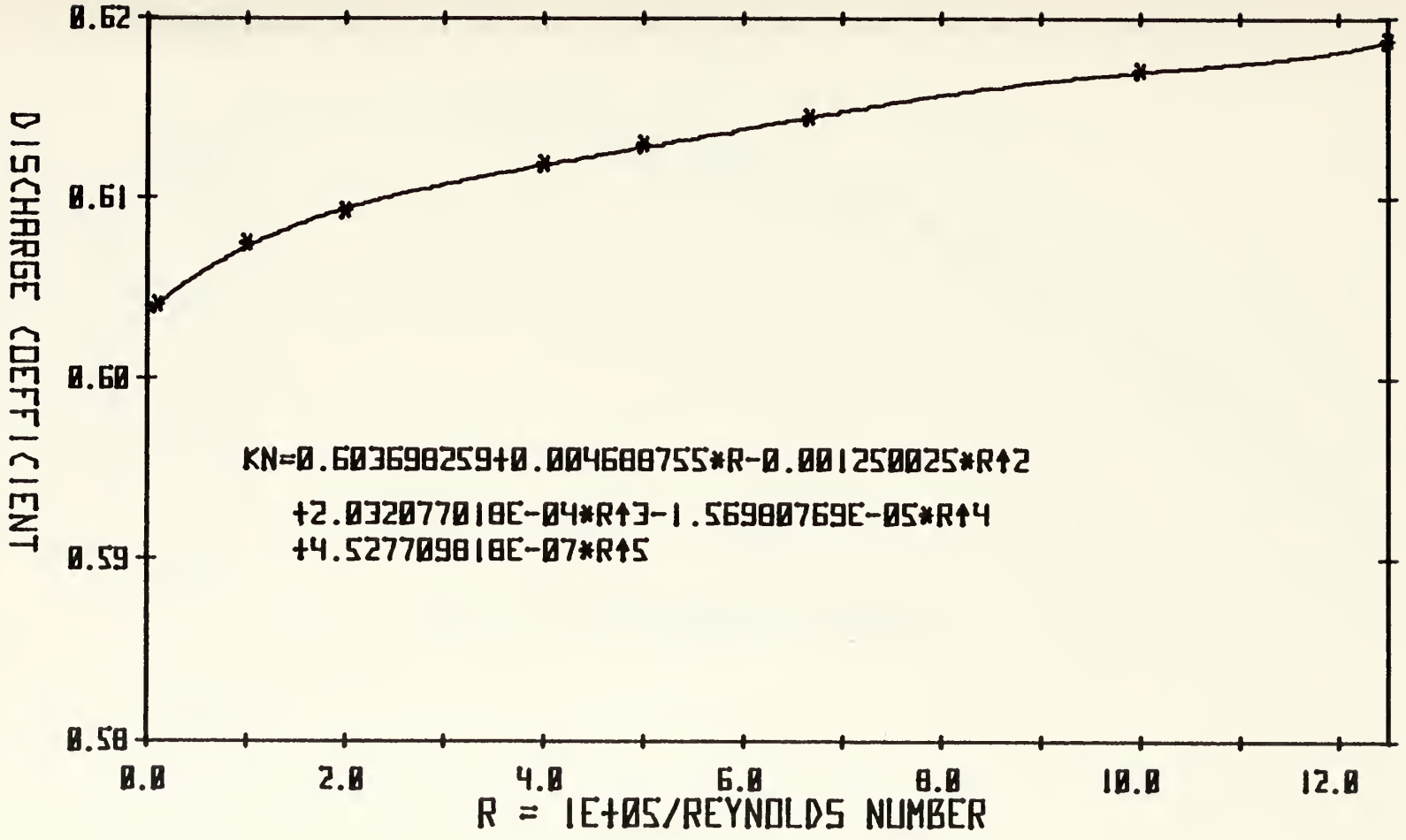

FIG. A-7 ASME DISCHARGE COEFFICIENT

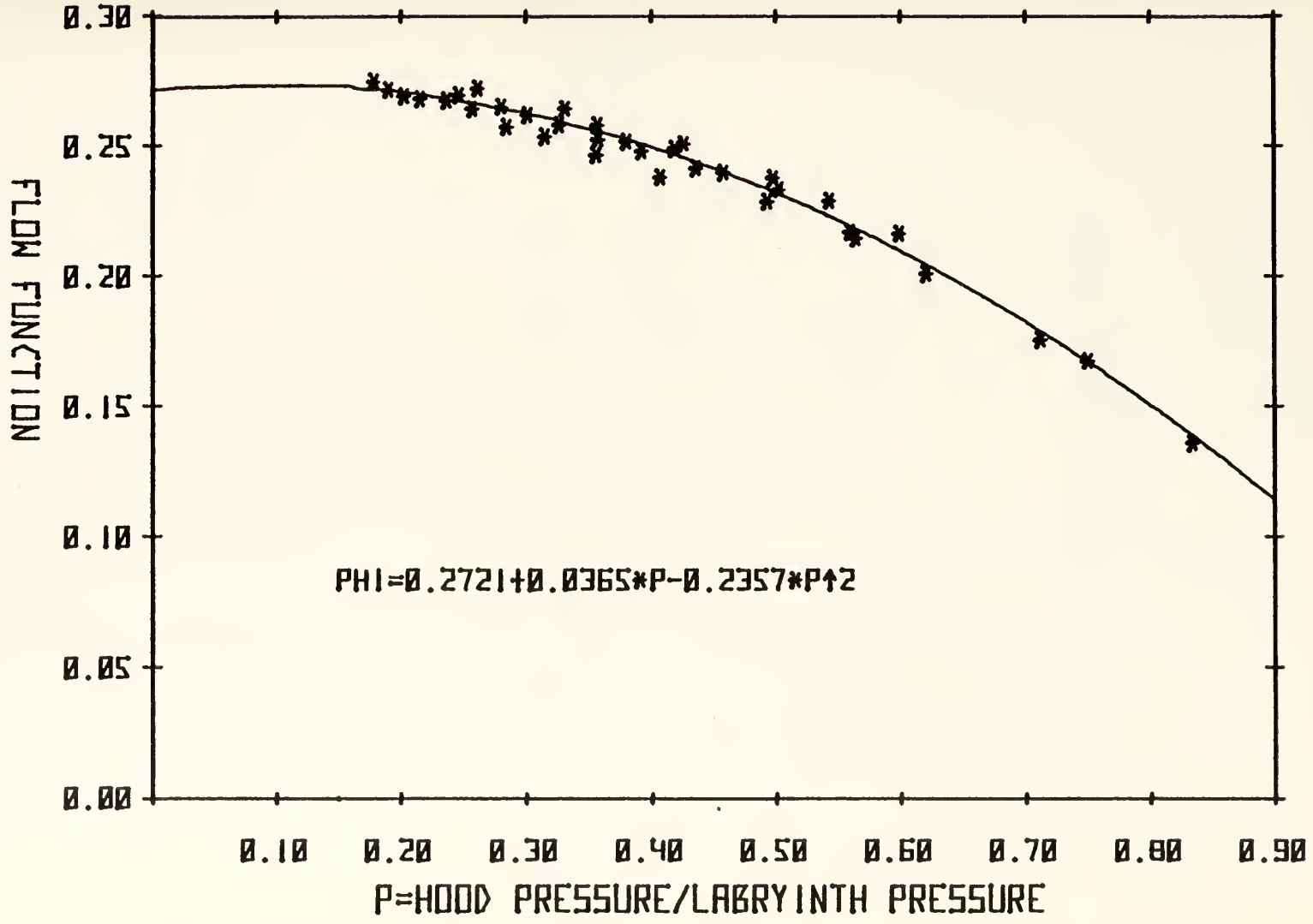

FIG. A-8 PLENUM LABYRINTH SEAL LEAK RATE

LABYRINTH SEAL
TRANSONIC TURBINE TEST RIG

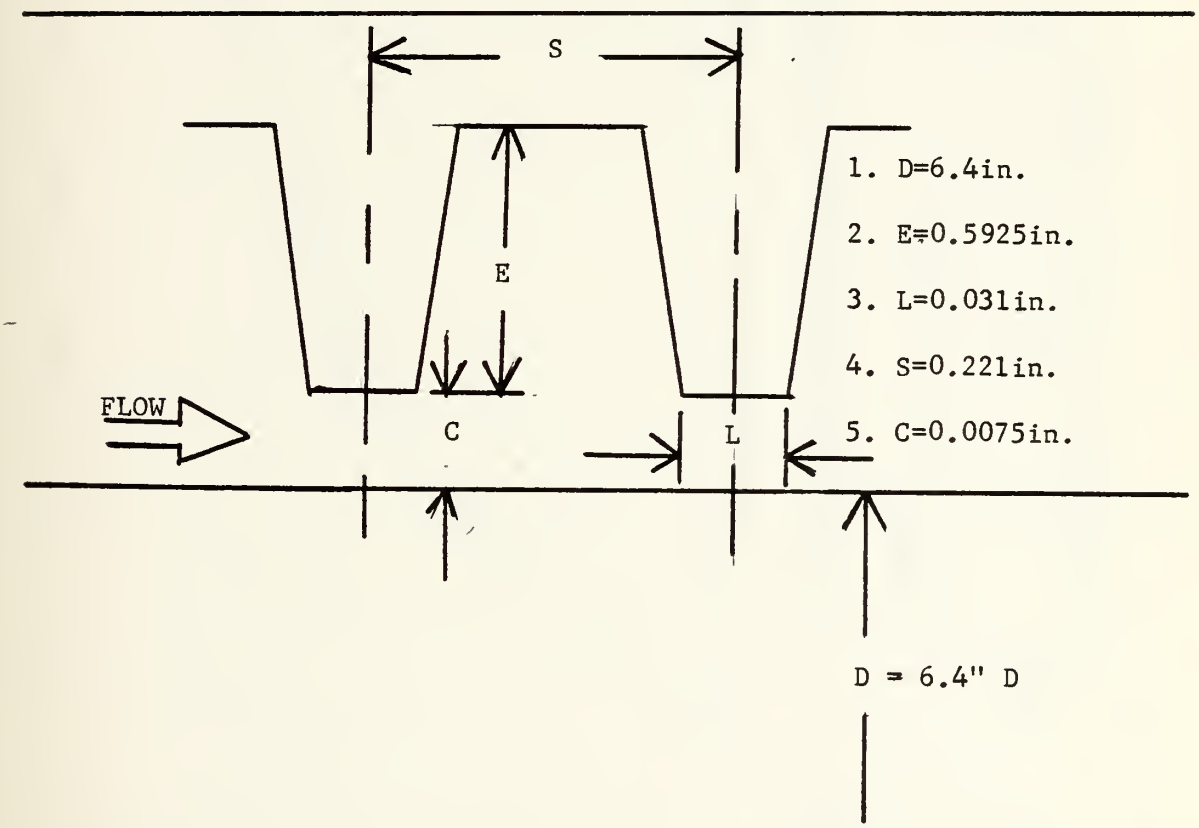

FIG. A-9 PLENUM LABYRINTH

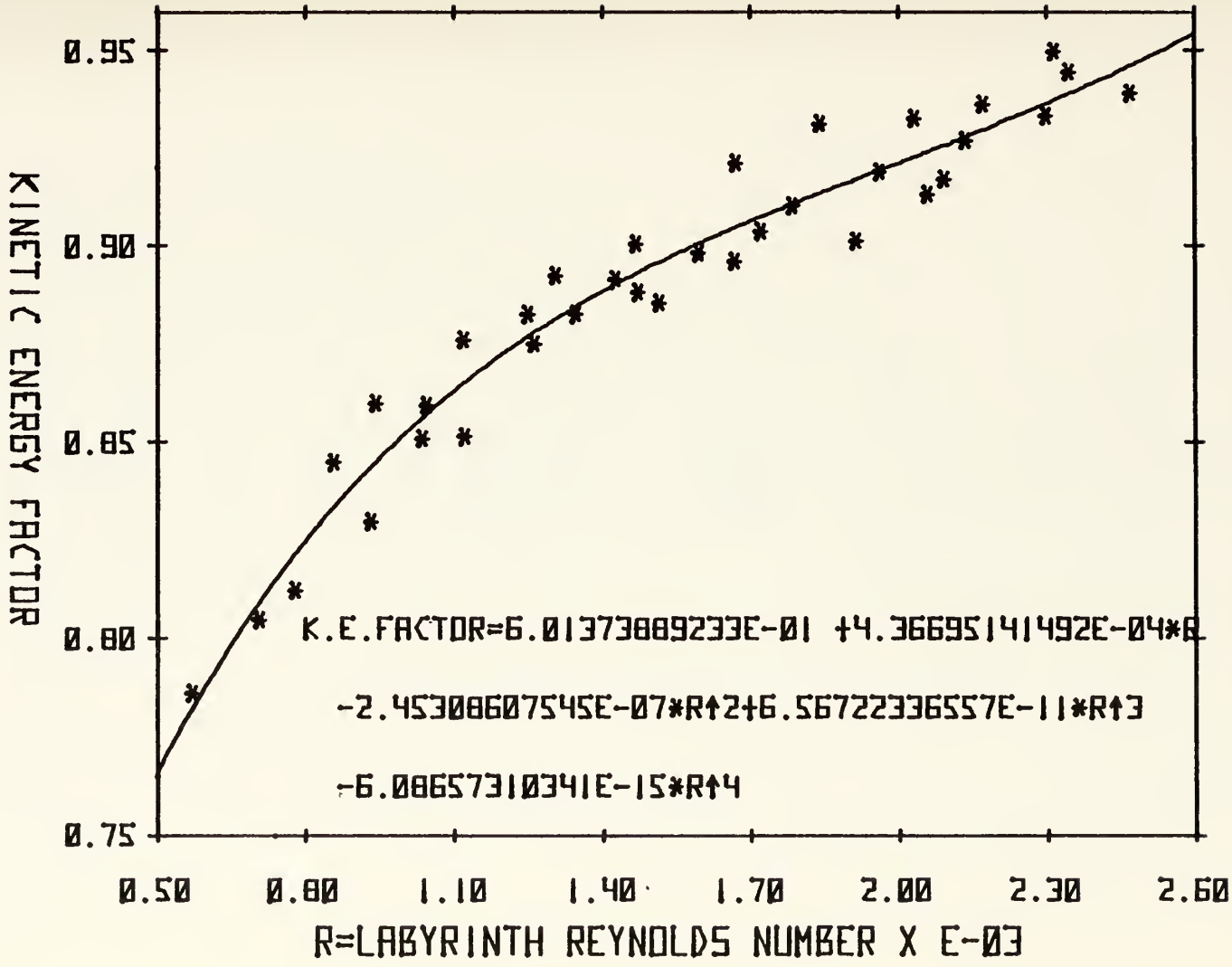

FIG. A-10 LABYRINTH SEAL KINETIC ENERGY FACTOR

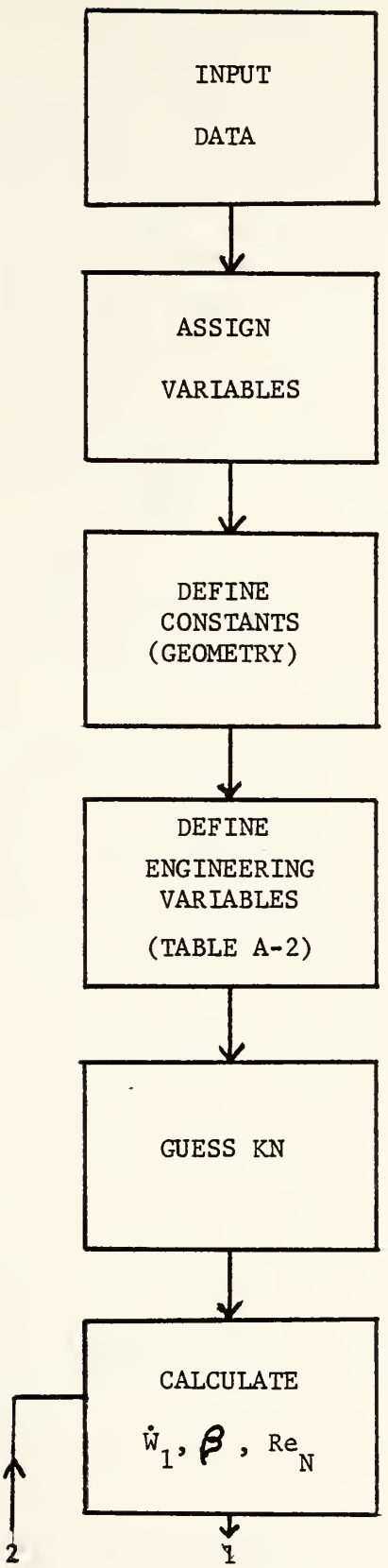

FIG. A-11 LABYRINTH CALIBRATION DATA REDUCTION FLOW CHART

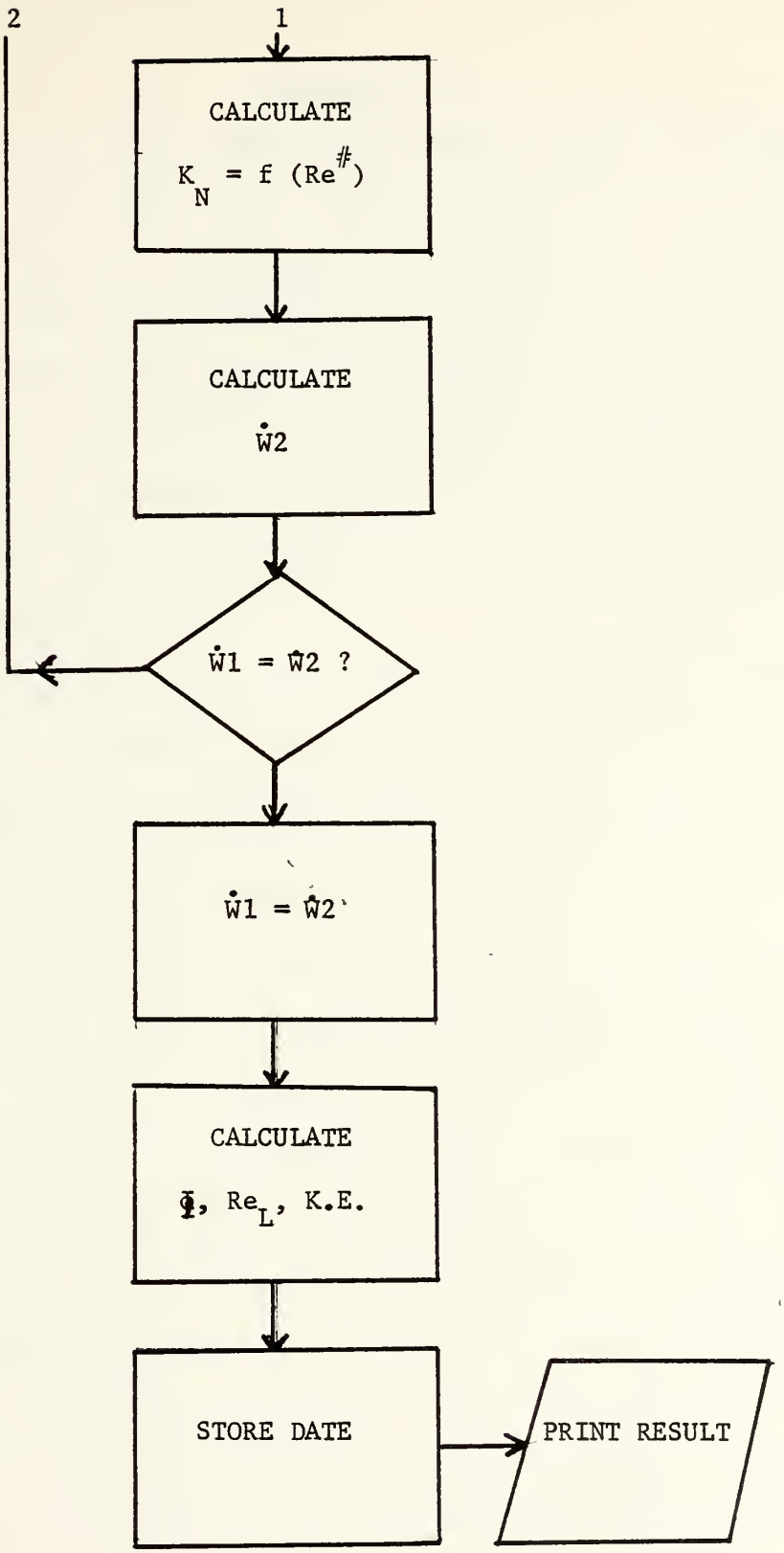

FIG. A-11 LABYRINTH CALIBRATION DATA REDUCTION FLOW CHART

APPENDIX B

TURBINE TEST RIG (TTR) DATA REDUCTION AND PROCESSING

B-1 INTRODUCTION:

This appendix documents the current data reduction program which was revised and updated from the program used in Ref. 5. The present program uses the "Mass Memory" disc storage unit attached to the Hewlett-Packard Model 9830A Calculator. The equations developed in Ref. 5 apply to the present program.

A description of the programs is given in Section B-2 and the variables are listed and defined. Procedures for running the program are given in Section B-3.

B-2 DESCRIPTION OF PROGRAMS:

The reduction program is divided into eight separate sub-programs. Fig. B-1 shows the contents of each sub-program. Table B-1 gives the channel and port numbers for each of the test measurements and the respective matrix elements assigned in the data reduction program. Table B-2 defines the variables and equations (Ref. 5 & 16) used in the program. Table B-3 is a record or score sheet of the variables used in the program.

B-3 PROCEDURE FOR DATA REDUCTION PROGRAM USING MASS MEMORY:

1. CHECK:

    a.) Mass Memory to UNLOAD Position
    b.) ROM installed
    c.) NO cassettes in transport

2. Turn on HP 9830A Calculator
3. Turn on HP9866A Printer
4. Turn on HP 9868A I/O Expander
5. Turn on HP9863A Tape Reader
6. Turn on HP 9867B Mass Memory
7. Turn on HP 11305A Controller
8. Load platter number TTR when the DOOR UNLOCKED light is lit.
9. Switch to LOAD position; wait 30 seconds until DRIVE READY light is lit.
10. Key in: GET "TTR 1:" Wait for completion
11. Press "RUN EXECUTE."
12. The display will read "ENTER NEXT RECORD # ON DATA FILE." Input your next record number for raw data storage and press "EXECUTE."
13. The display will read "TAPE: 1ST HOLE?-ON START?:-CONT." By pressing "CONTINUE, EXECUTE" the paper tape will be read.
14. After the paper tape is read, the display will read "CORRECTIONS TO DATA? YES=1, NO=0;" This option permits you to correct any erroneous corrections. PRESS "1 EXECUTE" if you have corrections. Press "0 EXECUTE" if no corrections; go to step 19.
15. With Corrections to be made, the display will read "PRESS PRT ALL KEY FOR RECORD." This enables you to have a record of your data points.

16. The display will read "ENTER CORRECTION AS MATRIX ELEMENTS." When a scanivalve is detected to have given an erroneous value, the manometer board can be read and correct value recorded. See Table B-2 for the appropriate matrix identification.
17. The display will read "ENTER CORRECT VALUE = ?;" Input the correct value and press "EXECUTE."
18. The display will read "ANY MORE CORRECTIONS? YES=1, NO=0." Press "1 EXECUTE" if more corrections; go to step 17.
19. 1.5 inches of paper will emerge from the printer and the raw data will be printed. Afterwards the display will read "STORE DATE? ENTER YES=1, NO=0." If raw data is to be stored in Mass Memory press "1 Execute." The raw data is stored. Below the tables will be printed the words "THE RAW DATA IS STORED IN RAW DAT FILE #? Along with the file number that was input in step 12. If data is not to be stored press "0 EXECUTE" and the words "THIS DATA WAS NOT STORED" will be printed.
20. The calculator will automatically CHAIN with "TTR 2."
21. Temperatures of the nozzle, labyrinth and T_{to} will be printed in degrees Rankine. The labyrinth seal flow rate, its Reynolds number and kinetic energy factor will be printed. Also, the nozzle discharge coefficient, nozzle flow rate, its Reynolds number, and flow rate will be printed.

22. The display will read "CALC NEW W-DOT? YES=1, NO=0." If you elect to calculate a new theoretical flow rate, based on a stator blockage factor of 0.965, and employ this value in the remainder of the program, press "1 EXECUTE." However, if you use the original flow rate, press "0 EXECUTE." Go to step 24.

23. The election for a new calculation of flow rate was chosen; a new flow rate, the stator flow function and blockage factor will be printed out. Note that the flow function and blockage factor were employed to calculate the new flow rate. Go to step 25.

24. The original flow rate is used. The stator flow function and blockage factor based on the flow rate and measurement are printed.

25. The display will read "INPUT ALPHA 1 (DEG), OR 0." Inputing any number other than 0 will fix the stator exit flow angle in degrees. This method assumes VU_1 is calculated from the stator torque and adjusts the value of VA_1 to agree with the elected stator exit angle. By pressing "0 EXECUTE" the stator exit angle is not chosen. Go to step 27.

26. By choosing to fix the stator exit flow angle, the value you selected will be printed. The value of K, which is the ratio of VA_1 determined by the momentum equation to VA_1 determined by continuity, will be printed. VAlues from 1.0 to 1.2 are within acceptable limits. Go to step 29.

27. The value of the stator exit as calculated from measurements will be used. The display will read "ENTER K." Values between 1.0 and 1.2 are within acceptable limits. Press "(K) EXECUTE." This value will be printed and the program will CHAIN with "TTR 3."

28. TTR 3 will evaluate Control Volume B and will CHAIN with "TTR 4."

29. The display will read "CALC THEOR. LOSSES ? YES = 1, NO = 0." This program option permits you to calculate both the theoretical rotor and stator loss coefficients. Copies of REF. 16 and 18 will be needed. By pressing "1 EXECUTE," you have elected to calculate the losses. Press "0 EXECUTE" if you do not desire to calculate the losses. Go to step 37.

30. The display will read "DEL ALPHA = (SOME NUMBER)." Note the number and press "CONTINUE EXECUTE."

31. The display will read "BETA 1 = (SOME NUMBER)." Note the number and press "CONTINUE EXECUTE."

32. The display will read "INPUT ZETA PO, FIG. 15, 1174 VA_1?" Turn to Fig. 15 in Ref. 16. Select the value of ZETA PO which corresponds to the values of DEL ALPHA, BETA 1; and ALPHA EXIT. press ("ZETA PO) EXECUTE."

33. The display will read "RE ROTOR = (SOME NUMBER)." Note this number and press "CONTINUE EXECUTE."

34. The display will read "INPUT K-RE, FIG. 23, GA1074VA2." Turn to Fig. 23 in Ref. 18 and select the value of K_{RE} that corresponds to the rotor blade Reynolds number given in step 33. Press "(K-RE) EXECUTE."

35. The display will read "M2 (IS) = (SOME NUMBER)." Note this number and press "CONTINUE EXECUTE."

36. The display will read "INPUT KM, FIG. 18, 1174VA$_1$." Turn to Fig. 18 in Ref. 16, and select the value of KM that corresponds to the blade exit Mach Number as calculated from isentropic conditions. Press "(KM) EXECUTE."

38. The program will CHAIN with "TTR 6." The display will read "ENTER NEXT RED REC. #." Input the same record number from step 12 and press "EXECUTE."

39. The display will read "STORE RED. DATA ? YES = 1, NO = 0." Press "1 EXECUTE" if you desire reduced data to be stored and used for plotting and tabulation. Press "0 EXECUTE" if you do not desire to store reduced data. Go to step 41.

40. You have elected to store the reduced data in the Mass Memory, and the words "REDUCED DATA IS STORED IN FILE/ REDDAT/RECORD (NUMBER FROM STEP 12)." will be printed.

41. Electing not to store the reduced data the words "THIS DATA WAS NOT STORED" will be printed.

42. The display will read "(CONT)(EXEC) MORE DATA - OR (END)."

43. If more data points are to be reduced, press "CONTINUE EXECUTE." The display will read "TAB RAW DATA ? YES = 1 NO = 0." If you desire not to tabulate raw data, press "0 EXECUTE." Then the display will read "TAB REDUCED

DATA ? YES = 1, NO = 0." If you desire not to tabulate reduced data, press "0 EXECUTE." By inputting zeros for both of these tabulation questions the program will display "REDUCE NEXT POINT," and will CHAIN with "TTR 1." Go to step 12. Note: Tabulation is usually elected after all points are reduced for a run.

44. To tabulate the raw data press "1 EXECUTE." The program will GET "TTR 7." The display will read "EXECUTE RECORD #'S: LOWEST, HIGHEST." Input your first and last record numbers and press "EXECUTE." The display will read "OMIT 4 RECORDS. ENTER #'S OR 0'S." This option permits you to omit any points. Input the record numbers and press "EXECUTE."

45. The display will read, read "REQUEST DATA CH #: 0, 1 OR 10." Press "1 EXECUTE" will cause the 48 measurements to be tabulated under the heading: TTR INPUT DATA. Afterwards, the calculator will request the next channel number. Press "10 EXECUTE" will cause all other channels to be tabulated and printed with the same heading. Next, press "0 EXECUTE." The display will read "TAB REDUCED DATA ? YES = 1, NO = 0." Press "1 EXECUTE" and the program will GET "TTR 8." Go to step 46. Press "0 EXECUTE" and the program will GET "TTR 1." Go to step 12.

46. By electing to tabulate the reduced data, the program will GET "TTR 8." The display will read "ENTER LOWEST,

HIGHEST REC. #." Input the first and last record numbers, and press "EXECUTE."

47. The display will read "ENTER 1ST AND LAST PT. #." Input the two points, and press "EXECUTE.'

48. The display will read "ENTER RUN #." Input the run number, and press "EXECUTE."

49. The velocities, Mach Number, and losses will be tabulated and printed. The tabulation will stop to allow the page to be removed from the printer. Then press "CONTINUE EXECUTE."

50. Tabulation and printing will resume until "DATA TABULATION COMPLETE" is printed. The display will read "CHAIN WITH TAPE READER." There is a 3 second pause, and the program will GET "TTR 1." Go to step 12.

TABLE B-1

CHAN-PORT	MEASUREMENT	X SCALE =	UNIT	ASSIGNMENT	
001- 01	Atmospheric Pressure	x 0 . 01	in. Hg Abs	A (1) = J_2	
001- 02	Transducer Cal. Ref. Pressure	x 0 . 01	in. Hg Abs	A (2)	
001- 03	P_1 Nozzle (Upstream)	x 0 . 01	in. Hg Abs	A (3) = P_7	
001- 04	P_2 Nozzle (Downstream)	x 0 . 01	in. Hg Abs	A (4)	
001- 05	Ps P1 - Plenum	x 0 . 01	in. Hg Abs	A (5) = QØ	
001- 06	P_{to} #1	x 0 . 01	in. Hg Abs	A (6)	
001- 07	P_{to} #2	x 0 . 01	in. Hg Abs	A (7)	
001- 08	P_{to} #3	x 0 . 01	in. Hg Abs	A (8)	Avg = Q1
001- 09	P_{to} #4	x 0 . 01	in. Hg Abs	A (9)	
001- 10	P_{to} #5	x 0 . 01	in. Hg Abs	A (10)	
001- 11	PHd - Hood Pressure	x 0 . 01	in. Hg Abs	A (11) = Q3	
001- 12	Stator Nozzle - Suction Side # 1	x 0 . 01	in. Hg Abs	A (12) = D1	
001- 13	Stator Nozzle - Suction T Side # 2	x 0 . 01	in. Hg Abs	A (13) = D3	
001- 14	Stator Nozzle - Suction Side # 3	x 0 . 01	in. Hg Abs	A (14) = D6	
001- 15	Stator Nozzle - Suction Side # 4	x 0 . 01	in. Hg Abs	A (15) = D7	

TABLE B-1

CHAN-PORT	MEASUREMENT	X SCALE =	UNIT	ASSIGNMENT
001- 16	Stator Nozzle - Suction Side # 5	x 0 . 01	in. Hg Abs	A (16) = E3
001- 17	Stator Nozzle - Pressure Side # 1	x 0 . 01	in. Hg Abs	A (17) = DØ
001- 18	Stator Nozzle - Pressure Side #2	x 0 . 01	in. Hg Abs	A (18) = D2
001- 19	Stator Nozzle - Pressure Hub #1	x 0 . 01	in. Hg Abs	A (19) = D4
001- 20	Stator Nozzle - Hub # 2	x 0 . 01	in. Hg Abs	A (20) = D8
001- 21	Stator Nozzle - Hub # 3	x 0 . 01	in. Hg Abs	A (21) = R8
001- 22	Stator Nozzle - Tip # 1	x 0 . 01	in. Hg Abs	A (22) = D5
001- 23	Stator Nozzle - Tip # 2	x 0 . 01	in. Hg Abs	A (23) = D9
001- 24	Stator Nozzle - Tip # 3	x 0 . 01	in. Hg Abs	A (24) = Q4
001- 25	Barometric	x 0 . 01	in. Hg Abs	A (25)
001- 26	Reference	x 0 . 01	in. Hg Abs	A (26)
001- 27	Labyrinth Pressure	x 0 . 01	in. Hg Abs	A (27)
001- 28	PSO - Inlet Static	x 0 . 01	in. Hg Abs	A (28)
001- 29	Rotor Shroud # 1	x 0 . 01	in. Hg Abs	A (29) = N8
001- 30	Rotor Shroud # 2	x 0 . 01	in. Hg Abs	A (30) = N9

TABLE B-1

CHAN-PORT	MEASUREMENT	X SCALE =	UNIT	ASSIGNMENT
001- 31	Rotor Shroud # 3	x 0 . 01	in. Hg Abs	A (31) = O1
001- 32	Rotor Shroud # 4	x 0 . 01	in. Hg Abs	A (32) = S3
001- 33	Rotor Shroud # 5	x 0 . 01	in. Hg Abs	A (33) = S4
001- 34	Rotor Shroud # 6	x 0 . 01	in. Hg Abs	A (34) = S5
001- 35	Rotor Shroud # 7	x 0 . 01	in. Hg Abs	A (35) = S6
001- 36	Rotor Shroud # 8	x 0 . 01	in. Hg Abs	A (36) = S7
001- 37	Rotor Shroud # 9	x 0 . 01	in. Hg Abs	A (37) = S8
001- 38	Rotor Shroud # 10	x 0 . 01	in. Hg Abs	A (38) = S9
001- 39	Rotor Shroud # 11	x 0 . 01	in. Hg Abs	A (39) = NØ
001- 40	Rotor Shroud # 12	x 0 . 01	in. Hg Abs	A (40) = N1
001- 41	Rotor Shroud # 13	x 0 . 01	in. Hg Abs	A (41) = N2
001- 42	Rotor Shroud # 14	x 0 . 01	in. Hg Abs	A (42) = N3
001- 43	Rotor Shroud # 15	x 0 . 01	in. Hg Abs	A (43) = N4
001- 44	Rotor Shroud # 16	x 0 . 01	in. Hg Abs	A (44) = N5
001- 45	Rotor Shroud # 17	x 0 . 01	in. Hg Abs	A (45) = N6

TABLE B-1

CHAN-PORT	MEASUREMENT	X SCALE =	UNIT	ASSIGNMENT
001- 46	Rotor Shroud # 18	x 0 . 01	in. Hg Abs	A (46) = N7
15- 00	Flow Nozzle h	x 0 . 1	in. H_2O	C (12) = HØ
16- 00	Stator Axial Force	x 0 . 1	lbs Force	C (16) = F4
17- 00	Closure Plate Force	x 0 . 01	lbs Force	C (17) = F5
18- 00	Stator Torque	x 0 . 1	in. - lbs.	C (18) = M6
19- 00	Rotor Torque	x 0 . 1	in. - lbs.	C (19) = M5
20- 00				
21- 00	T_1 Flow Nozzle	x 0 . 001	MV "J"	C (21) = T5=T_{noz}
22- 00	T_{p1}	x 0 . 001	MV "J"	
23- 00	T Closure	x 0 . 001	MV "J"	
24- 00	T_{to} Inlet Temp.	x 0 . 001	MV "J"	C (24) = T2=T_{to}
25- 00	T Rotor Exit	x 0 . 001	MV "J"	
26- 00	T Lab	x 0 . 001	MV "J"	C (23) = T6=T_{hd}
27- 00	T Ref	x 0 . 001	MV "J"	TØ = 518 . 7^0R

TABLE B-2

DEFINITION OF VARIABLES AND EQUATIONS

A	Array
A0	Area of Control Volume (Fig. B-2, B-3)
A1	Area of Control Volume
A3	Alpha 1
A4	Alpha 2
A5	Decision Variables
A8	Rotor Shroud Pressure Integrated Over Area
A9	Rotor Shroud Pressures Integrated Over Area
B0	EQ A (8) Ref. 5
B1	B2 Eq. A (16) Ref. 5
B2	Beta 1
B3	Beta 2
B4	Units (2*CP*g)
B5	Rotor Shroud Pressures Integrated Over Area
B6	Rotor Shroud Pressures Integrated Over Area
B7	Rotor Shroud Pressures Integrated Over Area
B8	Del Alpha
B9	Mixing Loss Coefficient, Referred to Average Kinetic Energy, Eq. 71, Ref. 16
C	Array
C0	Gas constant (ft-lbf/lbm-R)
C1	Specific Heat (BTU/lbm-R)
C2	Nozzle Diameter (in.)

C3 Gravitational Constant (32.174 lbm-ft/lbf-sec^2)

C4 Pipe Diameter (upstream)

C5 Ratio (D_{noz}/D_p)

C6 Conversion factor: $\frac{0.16384}{\sqrt{2.036}}$

C7 Discharge Coefficient

C8 Thermal Expansion Coefficient

C9 Compressibility Coefficient

D Array

D0 See Table B-1

D1 See Table B-1

D2 See Table B-1

D3 See Table B-1

D4 See Table B-1

D5 See Table B-1

D6 See Table B-1

D7 See Table B-1

D8 See Table B-1

D9 See Table B-1

E0 Effective Total-to-Static Efficiency Eq. A (18) Ref. 5

E1 Next record Number

E2 Input Variables

E3 See TRble B-1

E4 Profile Loss Coefficient of Turbine At Design Point

E5 Profile Loss Coefficient (ζ_p) Eq. 46, Ref. 16

E6 Secondary Flow Loss (ζ_s) Eq. 63, Ref. 16

E7 Mixing Loss Coefficient (ζ_m) Eq. 74, Ref. 16

E8	Stator Loss Theoretical (Total Blading Losses) Eq. 77, Ref. 16
E9	Rotor Loss Theoretical (Total Blading Losses) Eq. 77, Ref. 16
F0	Overall Axial Force
F1	Partial Sum of Overall Axial Force
F2	$P_{cl}A_{cl}$
F3	$P_{a}A_{tot}$
F4	Stator Axial Force
F5	Closure Plate Force
F6	Ratio: (Thickness to Spacing) Eq. 73, Ref. 16
F7	Mixing Loss Coefficient, Referred to Average Kinetic Energy, Eq. 71, Ref. 16
F9	Correction Factor for Blade Thickness, Eq. 47, Ref. 16
G	Array
G0	$\frac{\gamma - 1}{\gamma}$
G1	Input Variable
G2	$\frac{\gamma}{\gamma - 1}$
G6	Decision Variable
G7	Decision Variable
G8	Secondary Flow Loss, Eq. 63, Ref. 16
G9	Thickness to Spacing, Eq. 73, Ref. 16
H	Pressure at Hub
H0	See Table B-1
H1	Horsepower
H2	Referred Horsepower
H5	Correction Factor For Effects of Reynolds Number (K_{Re})

H6	Correction Factor For Blade Thickness (K_t) Eq. 47, Ref. 16
H8	Density Appendix B, Ref. 5
H9	Reynolds Number of Rotor, Table B-2, Ref. 5
I	First Point (Used in Tabulation Program)
I0	Ratio: Non-Dimensional Pressures At Various Tap Locations In Stator (Fig. 5) - DO in Table B-1
I1	Ratio: Non-Dimensional Pressures at Various Tap Locations In Stator (Fig. 5) - D1 in Table B-1
I2	Ratio: Non-Dimensional Pressures At Various Tap Locations In Stator (Fig. 5) - D2 in Table B-1
I3	Ratio: Non-Dimensional Pressures At Various Tap Locations In Stator (Fig. 5) - D3 in Table B-1
I4	Ratio: Non-Dimensional Pressures At Various Tap Locations In Stator (Fig. 5) - D4 in Table B-1
I5	Ratio: Non-Dimensional Pressures At Various Tap Locations In Stator (Fig. 5) - D5 in Table B-1
I6	Ratio: Non-Dimensional Pressures At Various Tap Locations In Stator (Fig. 5) - D6 in Table B-1
I7	Ratio: Non-Dimensional Pressures At Various Tap Locations In Stator (Fig. 5) - D7 in Table B-1
I8	Ratio: Non-Dimensional Pressures At Various Tap Locations In Stator (Fig. 5) - D8 in Table B-1
I9	Ratio: Non-Dimensional Pressures At Various Tap Locations In Stator (Fig. 5) - D9 in Table B-1
J	Mach # At Station 9 In Stator
J0	Joules Constant (778.16 Ft-lbf/BTU)
J2	See Table B-1
J4	Input Variable
J5	Profile Loss Coefficient Eq. 46, Ref. 16
J6	Velocity at Station 9 in Stator
J7	Non-Dimensional Stator Pressure

J8	Velocity at EX-TIP
J9	Velocity at Station 5 in Stator
K	Fourth Degree Polynomial For K.E Factor (Fig. 4)
K0	Viscosity (Sutherland Formula)
K1	Kinetic Energy Factor (G. E. Report)
K2	Beta (G. E. Report)
K3	K x B x A_L x P_L (KxK2xk6xQ0)
K4	Isentropic Head Coefficient Eq. a (22), Ref. 5
K5	Slope of K. E. Curve (Newtonian Method)
K6	Area of Labyrinth
K7	K. E. Factor (Convergence)
K8	Second Degree Polynomial $K_n(R_e)$ For Nozzle (Fig. 5)
K9	See Table B-1
L	Counter
L0	$X^2 a^2 + (Xu2 - U2)^2$ Eq. A (21), Ref. 5
L1	Rotor Loss Coefficient Eq. A (21), Ref. 5
L2	Mach # At Various Pressure Tap Locations in Stator (Fig. 5)
L3	Mach # At Various Pressure Tap Locations in Stator (Fig. 5)
L4	Mach # At Various Pressure Tap Locations in Stator (Fig. 5)
L5	Mach # At Various Pressure Tap Locations in Stator (Fig. 5)
L6	Mach # At Various Pressure Tap Locations in Stator (Fig. 5)
L7	Mach # At Various Pressure Tap Locations in Stator (Fig. 5)
L8	Mach # At Various Pressure Tap Locations in Stator (Fig. 5)

L9	Mach # At Various Pressure Tap Locations in Stator (Fig. 5)
M0	Referred Moment
M1	Mach # At Station 1
M2	Axial Mach # At Station 1
M3	Mach # At Station 2
M4	Axial Mach # At Station 2
M5	See Table B-1
M6	See Table B-1
M7	Referred Stator Moment
M8	Mach # At Exit - Tip
M9	Mach # At SS - Aft
N0	See Table B-1
N1	See Table B-1
N2	See Table B-1
N3	See Table B-1
N4	See Table B-1
N5	See Table B-1
N6	See Table B-1
N7	See Table B-1
N8	See Table B-1
N9	See Table B-1
O0	Incidence Loss Coefficient
O1	See Table B-1
O2	Velocities at Various Pressure Tap Locations In Stator (Fig. 5)
O3	Velocities at Various Pressure Tap Locations In Stator (Fig. 5)

O4	Velocities at Various Pressure Tap Locations In Stator (Fig. 5)
O5	Velocities at Various Pressure Tap Locations In Stator (Fig. 5)
O6	Velocities at Various Pressure Tap Locations In Stator (Fig. 5)
O7	Velocities at Various Pressure Tap Locations In Stator (Fig. 5)
O8	Velocities at Various Pressure Tap Locations In Stator (Fig. 5)
O9	Velocities at Various Pressure Tap Locations In Stator (Fig. 5)
P0	Reference Pressure (29.92 in. Hg)
P1	P-HOOD/P-LAB(RATIO)
P2	$\frac{\dot{w}}{g} V_{to}/AP_{t_o} \frac{\gamma-1}{2} [1 - \frac{X_{ul}^2}{(\sin \alpha_1)^2}]/X_{al}$ (Alpha Input)
P3	P_1/P_{t_o} Eq. A (10) Ref. 5 (K Input)
P4	P_2
P5	P_1/Pt_1
P6	Pressure Ratio (P_{to}/P_2)
P7	See Table B-1
P9	Average Pressure At Rotor Exit
Q0	See Table B-1
Q1	See Table B-1
Q2	P_{to}/P_{atm}
Q3	See Table B-1
Q4	See Table B-1
Q5	Decision Variable
R	Array
Re	Reynolds Number (Nozzle)

R0	Referred RPM ($N/\sqrt{\theta}$)
R1	Reynolds Number (Labyrinth)
R2	$\overline{R}$ Eq. A (4), Ref. 5
R3	Theoretical Degree of Reaction Eq. A (23), Ref. 5
R4	Actual Degree of Reaction Eq. A (24), Ref. 5
R8	See Table B-1
R9	Ratio ($14.696/P_{atm}$)
S	Array
S	Temperature Subroutine Variable
S0	P_1
S1	Temperature Value
S2	Temperature Value
S3	See Table B-1
S4	See Table B-1
S5	See Table B-1
S6	See Table B-1
S7	See Table B-1
S8	See Table B-1
S9	See Table B-1
T	Pressure at Tip
T0	Reference Temperature (518.7 °R)
T2	T_{to} (Upstream Temperature °R)
T3	$\sqrt{\theta}$ Temperature Ratio
T5	T_{tn} (Nozzle Temperature °R)
T6	T_{tp} (Plenum Temperature °R)
T7	T_e (Fig. B-4)
T8	T_1 (Fig. B-4)

T9	T_{2is} (Fig. B-4)
U	Array
U0	Mixing Loss Coefficient, Eq. 74, Ref. 16
U1	$(D_0 + D_i)/48$
U2	$(D_0 + D_i)/48$
U3	Dimensionless Velocity
U4	Dimensionless Velocity
U5	Factor ξ, P. 37, Ref. 16
U6	Loss Due to Tip Clearance Flow, Eq. 75, Ref. 16
U7	Tip Clearance Loss Coefficient, Referred To Isentropic Conditions Eq. 76, Ref. 16
U8	P_{to}/P_1
U9	Stator Flow Function
V	Array
V0	Tangential Rotor Velocity (V_{ul})
V1	Limiting Velocity (V_{to})
V2	$\overline{V}_{u2}$ Average Tangential Velocity Eq. A (11), Ref. 5
V3	V_{a1}
V4	V_{a2}
V5	V_2
V6	V_1
V7	Eq. A (10), Ref. 5
V8	Stator Blockage Factor
W	Array
W0	Total Flow Rate ($\dot{W} = W_{noz} - W_{lab}$)
W1	Labyrinth Flow Rate Based on K. E. Factor (G. E. Report)

W2 Labyrinth Convergence Flow Rate

W3 Flow Rate (ASME Equation)

W4 Ratio (WO/g)

W5 Referred Flow Rate

W6 W_1 (See Fig. B-5)

W7 W_2 (See Fig. B-5)

W8 $W^*_1 = W_1 \text{ Cos } (B_1 - 62)$

W9 W_{u2} (See Fig. B-5)

X Array

X0 Dimensionless Velocity X_{u1}

X1 X_{a1} - Eq. A (7), Ref. 5 (K Input)

X1 X_{a1} (Alpha Input)

X2 $X = X_{u2} + X_a^2$

X3 1/A PdA

X4 X_{u2} Eq. A (7), Ref. 5

X5 X_{a2} Eq. A (15), Ref. 5

X6 X_2

X7 $\bar{R}/P_{to}A$ (Alpha Input)

X8 $\gamma(2K-1) + 1$

X9 Denominator of Eq. 63, Ref. 16

Y Array

Y0 $\sqrt{1 - (\frac{P}{P_{to}})^{\frac{\gamma-1}{\gamma}}}$ For I0

Y1 $\sqrt{1 - (\frac{P}{P_{to}})^{\frac{\gamma-1}{\gamma}}}$ For I1

Y2 $\sqrt{1 - (\frac{P}{P_{to}})^{\frac{\gamma-1}{\gamma}}}$ For I2

Y3 $\sqrt{1 - (\frac{P}{P_{to}})^{\frac{\gamma-1}{\gamma}}}$ For I3

Y4 $\sqrt{1 - (\frac{P}{P_{to}})^{\frac{\gamma-1}{\gamma}}}$ For I4

Y5 $\sqrt{1 - (\frac{P}{P_{to}})^{\frac{\gamma-1}{\gamma}}}$ For I5

Y6 $\sqrt{1 - (\frac{P}{P_{to}})^{\frac{\gamma-1}{\gamma}}}$ For I6

Y7 $\sqrt{1 - (\frac{P}{P_{to}})^{\frac{\gamma-1}{\gamma}}}$ For I7

Y8 $\sqrt{1 - (\frac{P}{P_{to}})^{\frac{\gamma-1}{\gamma}}}$ For I8

Y9 $\sqrt{1 - (\frac{P}{P_{to}})^{\frac{\gamma-1}{\gamma}}}$ For I9

Z Array

Z0 C1 Eq. A (8a), Ref. 5

Z1 Stator Loss Coefficient

Z2 C2 Eq. A (16), Ref. 5

Z3 Rotor Loss Coefficient Eq. A (21), Ref. 5

Z6 Non-Dimensional Pressure At Exit - Hub

Z7 Loss Due Tip Clearance, Eq. 75, Ref. 16

Z8 Rotor Loss Coefficient (Other Factors)

PROGRAM:

TABLE B-3

ARRAY	SIMPLE VARIABLE SUBSCRIPT									
		0	1	2	3	4	5	6	7	8	9
A	X		X	X		X	X	X			X	X
B			X	X	X	X	X	X	X	X	X	X
C	X		X	X	X	X	X	X	X	X	X	X
D	X		X	X	X	X	X	X	X	X	X	X
E			X	X	X	X	X	X	X	X	X	X
F			X	X	X	X	X	X	X	X		X
G	X		X	X	X	X			X	X	X	X
H		X	X	X	X			X	X		X	X
I		X	X	X	X	X	X	X	X	X	X	X
J		X	X		X		X	X	X	X	X	X
K		X	X	X	X	X	X	X	X	X	X	X
L		X	X	X	X	X	X	X	X	X	X	X
M			X	X	X	X	X	X	X	X	X	X
N			X	X	X	X	X	X	X	X	X	X
O			X	X	X	X	X	X	X	X	X	X
P	X		X	X	X		X	X	X	X		X
Q			X	X	X	X	X	X				
R	X	X	X	X	X	X	X				X	X
S		X	X	X	X	X	X	X	X	X	X	X
T		X	X		X	X	X	X	X	X	X	X
U	X		X	X	X	X	X	X	X	X	X	X
V	X		X	X	X	X	X	X	X	X	X	
W	X	X	X	X	X	X	X	X	X	X	X	X
X	X		X	X	X	X	X	X	X	X	X	X
Y	X		X	X	X	X	X	X	X	X	X	X
Z	X		X	X	X	X			X	X	X	

SCORE SHEET: RECORD OF VARIABLES USED.

FIG. B-1 DATA REDUCTION SCHEMATIC

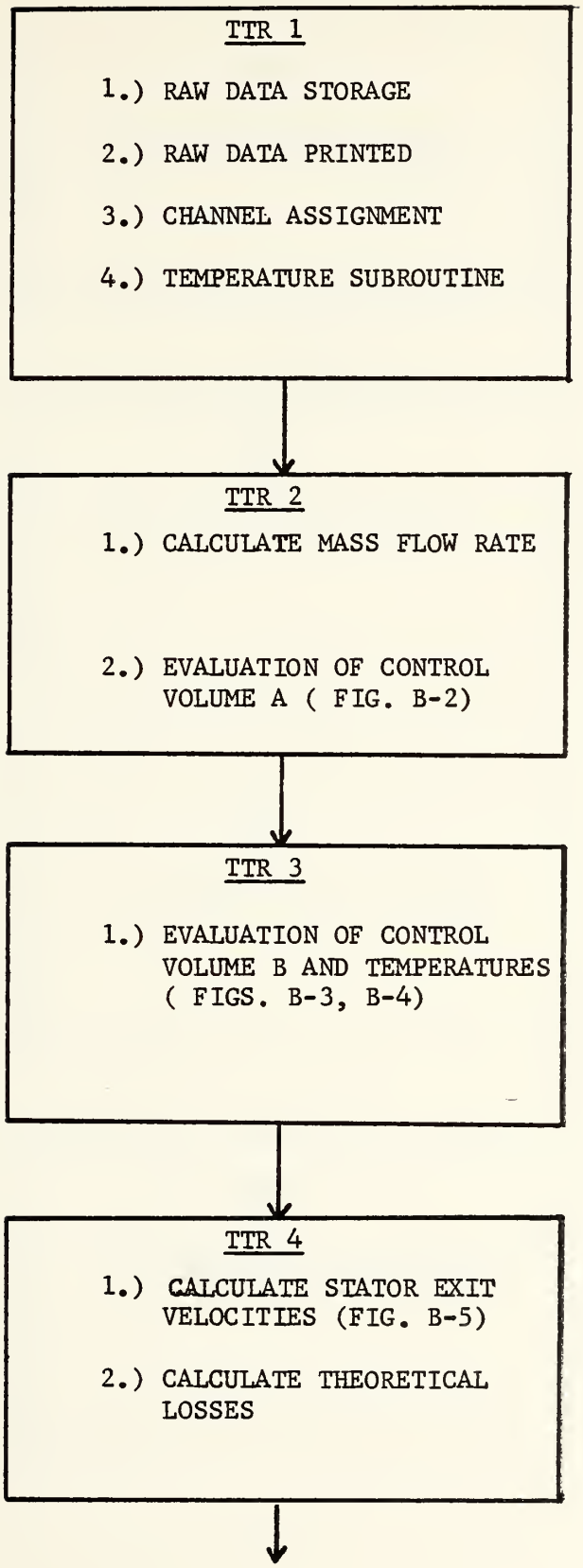

FIG. B-1 DATA REDUCTION SCHEMATIC

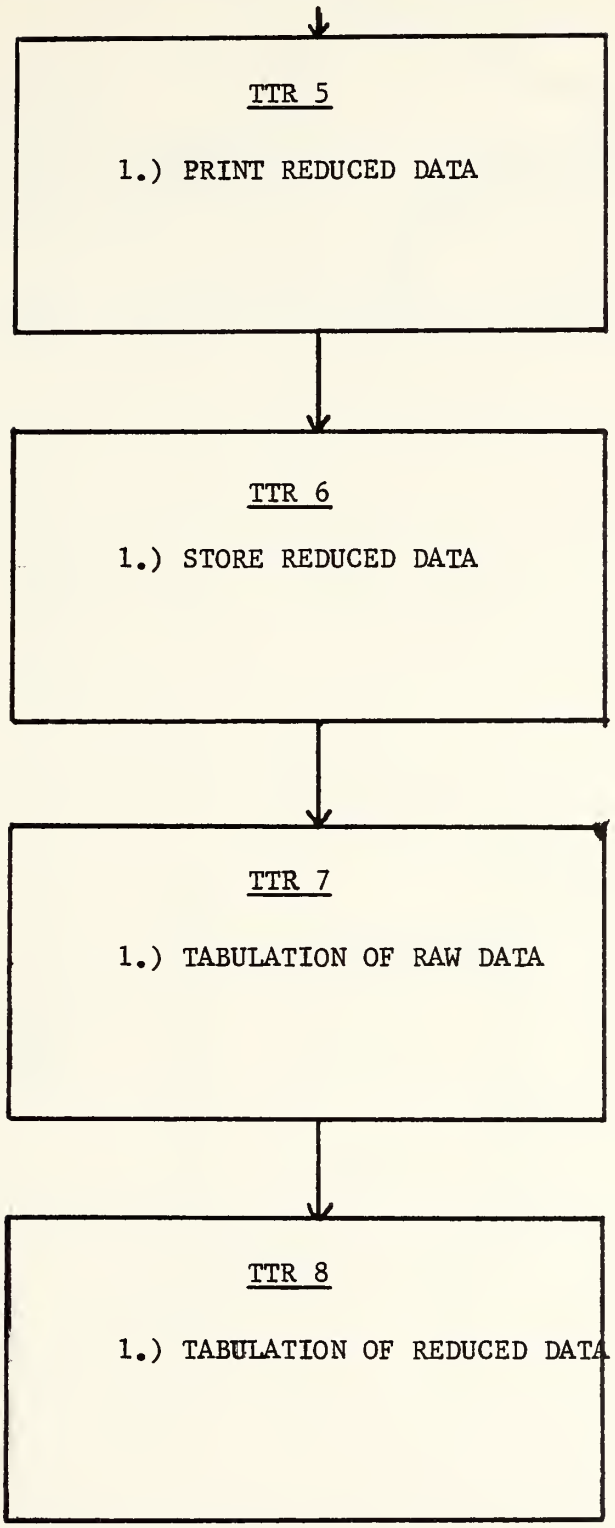

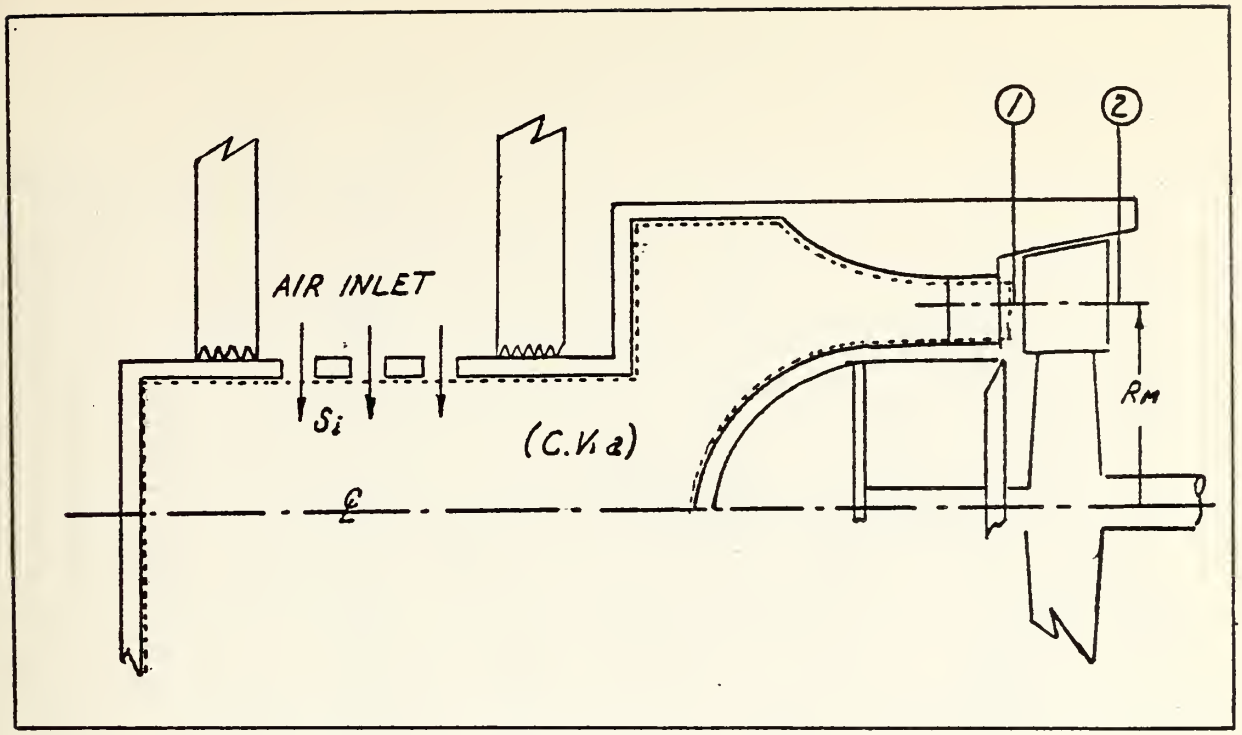

FIGURE B-2 CONTROL VOLUME a

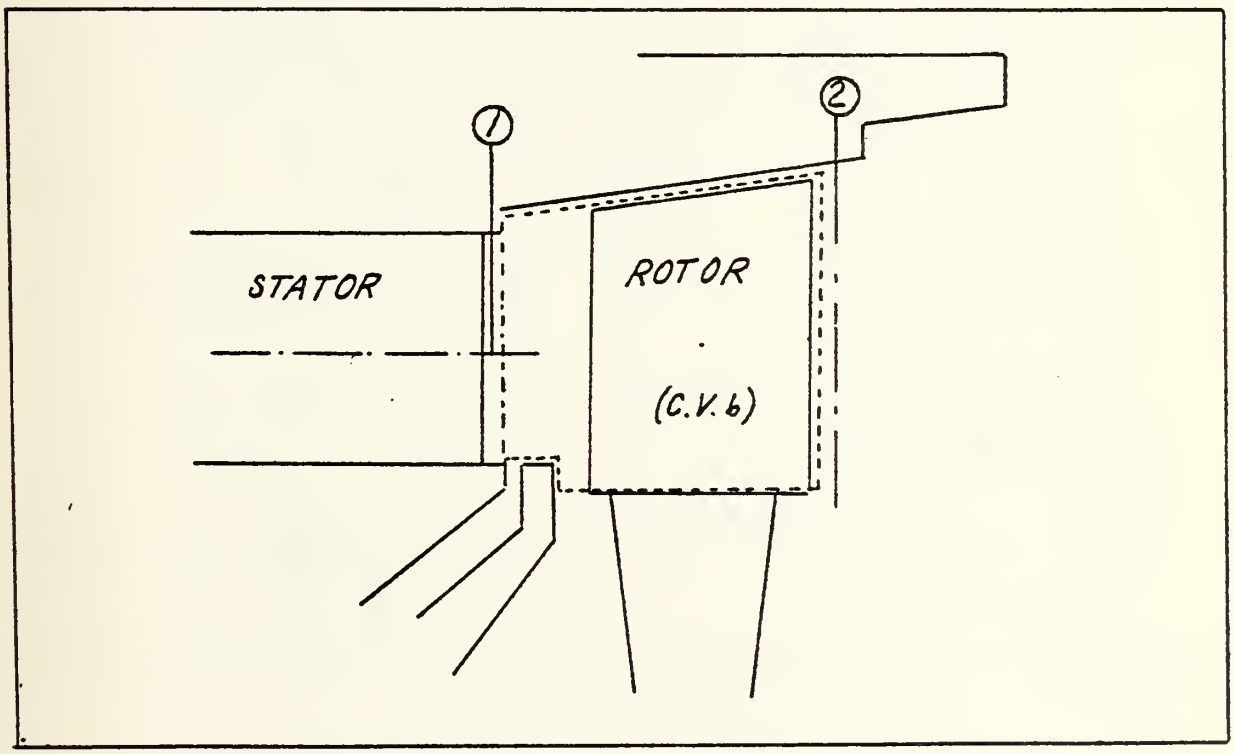

FIGURE B-3 CONTROL VOLUME b

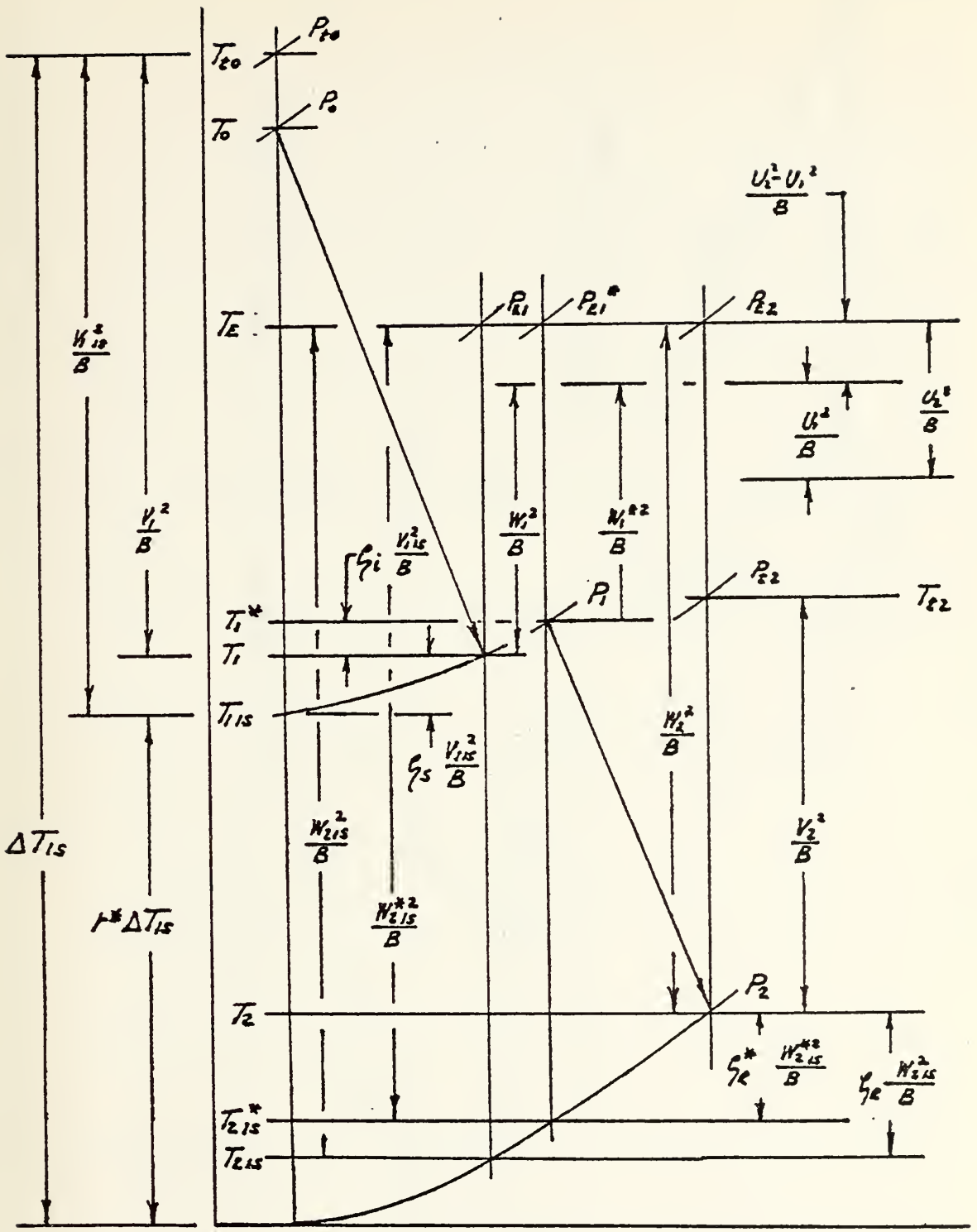

FIGURE B-4 THERMODYNAMIC PROCESS OF FLUID IN AN AXIAL TURBINE STAGE

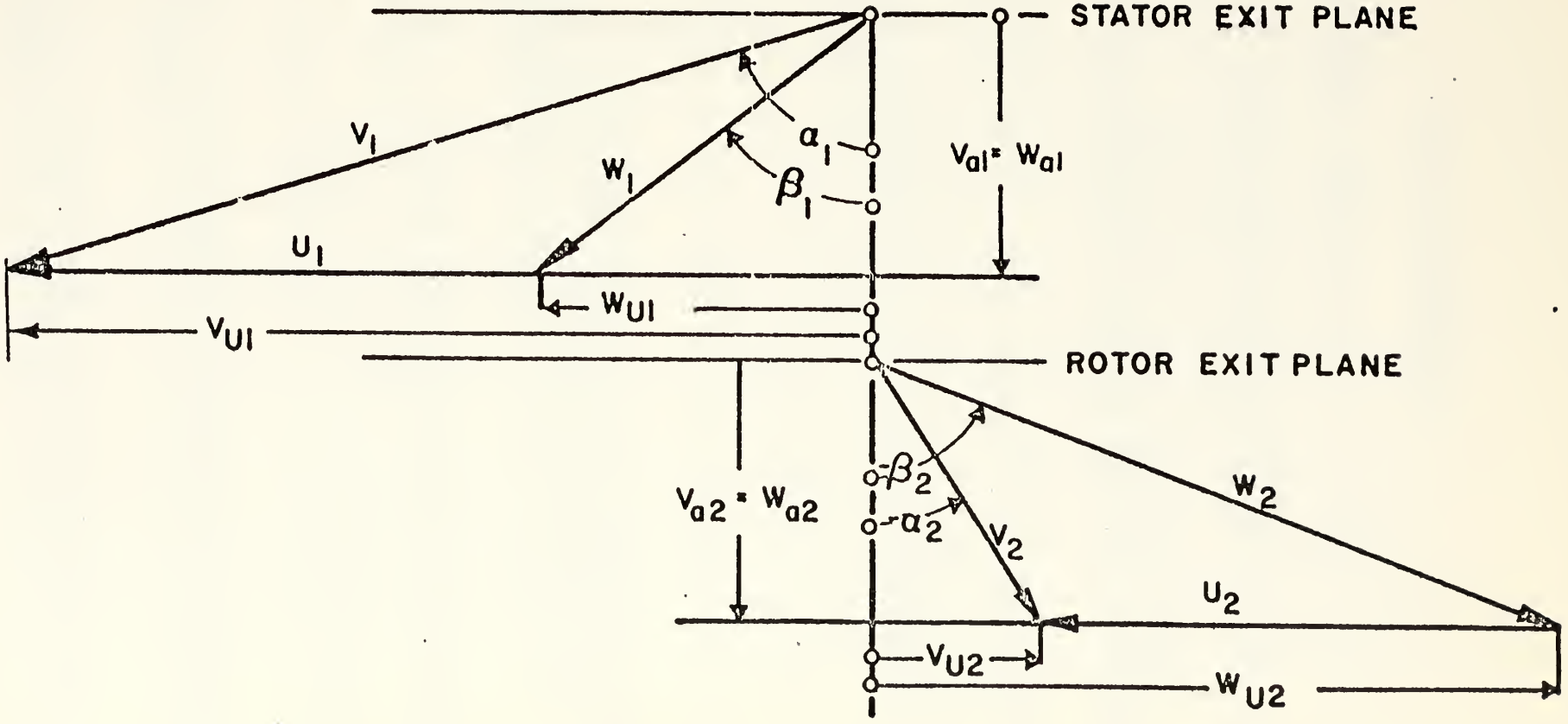

FIGURE B-5 VELOCITY DIAGRAM

LIST OF REFERENCES

1. Flow Measurement, Chapter 4, Part , Supplement to ASME Power Test Codes, ASME, 1959.

2. Naval Postgraduate School Report, NPS-57SF37071A, Calibration of Flow Nozzle Using Traversing Pitot-Static Probes, by R. P. Shreeve, July 1973.

3. Shreeve, R. P., Estimation of the Rotor-Face Inlet Conditions and Blockage Factor for the General Atomic Corp. Helium Compression. Memo GA-RPS7405-1, February 1973.

4. Hewlett-Packard 9830A, Model 30, Operating and Programming, Hewlett-Packard Part Number 09830-90001, January 1973.

5. Solms, W. R., Measurement of Stage and Blade Row Performances of Axial Turbines with Subsonic and Supersonic Stator Exit Condition, M. S. A. E. Thesis, Naval Postgraduate School, Monterey, California, 1975.

6. Schlichting, H., Boundary Layer Theory, P. 572-581, McGraw Hill, 1968.

7. General Electric, Duct System, Section 405.7, P. 1-15, October, 1973.

8. Commons, P.M., Instrumentation of the Transonic Turbine Test Rig To Determine The Performance of Turbine Inlet Guide Vanes by the Application of the Momentum and Moment of Momentum Equations, M.S.A.E. Thesis, Naval Postgraduate School, Monterey, California, 1967.

9. Lenzini, M. J., Calibration of Turbine Test Rig with Impulse Turbine at High Pressure Ratios, A.E. Thesis, Naval Postgraduate School, Monterey, California 1968.

10. Esdaile, S. G., An Investigation of a Transonic Turbine Test Rig, M.S.A.E. Thesis, Naval Postgraduate School, Monterey, California 1969.

11. DeThomas, J. B., On-Line Data Acquisition and Instrumentation Improvements for the Transonic Turbine Test Rig, M.S.A.E. Thesis, Naval Postgraduate School, Monterey, California 1972.

12. Donovan, S. J., Performance of a High Pressure Ratio Impulse Turbine With a Converging Nozzle, M.S.A.E. Thesis, Naval Postgraduate School, Monterey, California 1973.

13. Naval Postgraduate School Report, NPS-57Va72091A, A Description of the Turbopropulsion Laboratory in the Aeronautics Department at the Naval Postgraduate School, by M.H. Vavra and R.P. Shreeve, September 1972.

14. Stearns, R. F., and others, Flow Measurement with Orifice Meters, P. 65-212, D. Van Norstrand, 1951.

15. Andrews, J. and others, Turbine Test Rig Data, Naval Postgraduate School Turbopropulsion Laboratory, report submitted as partial fulfillment of the requirements for Course No. AE 4831, Monterey, California, March, 1974.

16. Vavra, M. H., Axial Turbine Design Data, Report 1174VA1, M.H. Vavra, (consultant), Pebble Beach, California, November, 1974.

17. Vavra, M. H., Aero-Thermodynamics and Flow in Turbomachines, Wiley, 1960.

18. Vavra, M. H., Estimated Performance of Main Circulator, Report GA-1074VA2, M.H. Vavra, (consultant), Pebble Beach, California, October, 1974.

19. Vavra, M.H., Axial Flow Turbines, Lecture Series 15, Von Karman Institute for Fluid Dynamics, Brussels, 1969.

INITIAL DISTRIBUTION LIST

		No. Copies
1.	Defense Documentation Center Cameron Station Alexandria, Virginia 22314	2
2.	Library, Code 0212 Naval Postgraduate School Monterey, California 93940	2
3.	Chairman, Department of Aeronautics Naval Postgraduate School Monterey, California 93940	1
4.	Associate Professor R.P. Shreeve, Code 57Sf Department of Aeronautics Naval Postgraduate School Monterey, California 93940	1
5.	Mr. J. E. Hammer, Code 57 Department of Aeronautics Naval Postgraduate School Monterey, California 93940	1
6.	Turbopropulsion Laboratory Department of Aeronautics Naval Postgraduate School Monterey, California 93940	12
7.	Lt. E. F. Robbins, USN VQ-2 NAVSTA ROTA Rota, Spain F.P.O. New York 09540	1

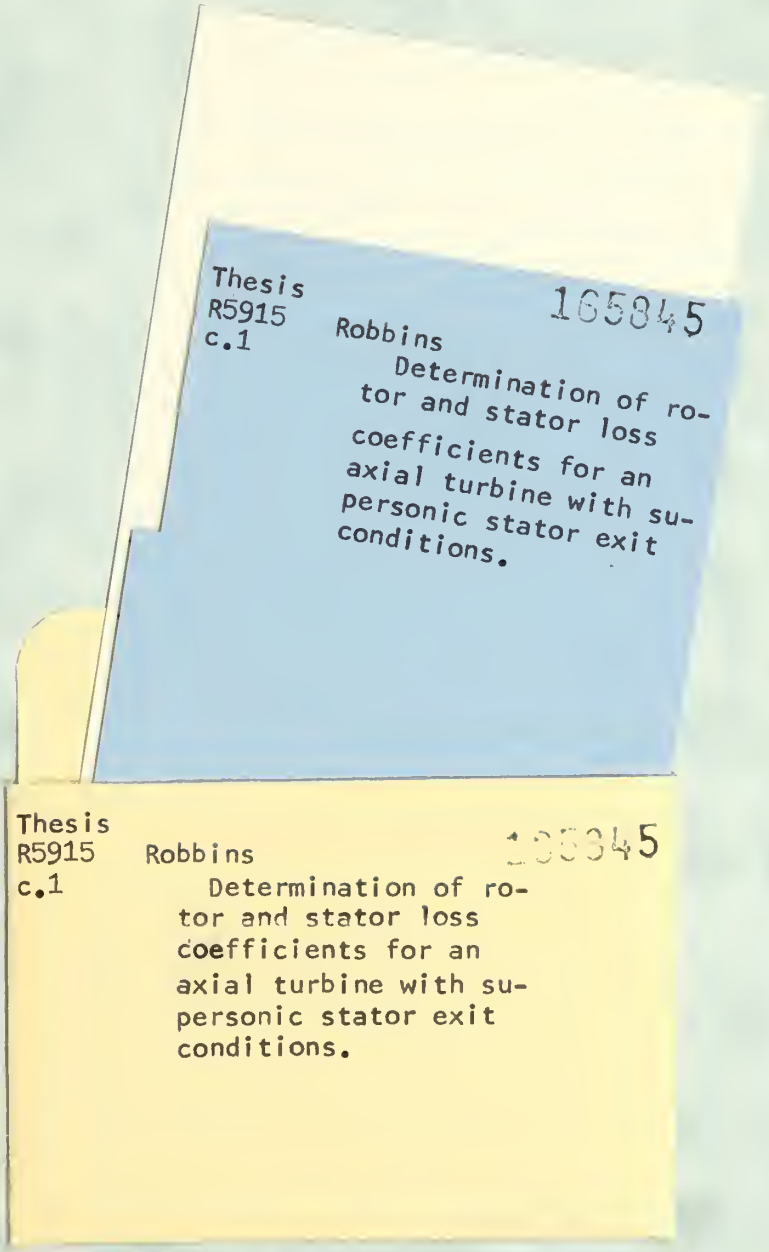

Thesis
R5915
c.1
Robbins
Determination of rotor and stator loss coefficients for an axial turbine with supersonic stator exit conditions.
165845